

Brno University of Technology
Faculty of Chemistry

Plasma diagnostics
during thin films depositions

Dissertation thesis

Acknowledgements:

I would like to thank to Dr. František Krčma, Associated Professor at the Faculty of Chemistry, Brno University of Technology, who was the tutor of my thesis, for the great guidance and patience, and, I thank to the Czech Science Foundation (contract No. 202/03/H162) and Ministry of Education (contract No. 2003/0895) for the financial support of my work in the investigated branch.

I thank to Dr Radek Přikryl and Jan Vaněk for the co-operation and for their kind advice.

I expres my gratitude to the whole group of scientists at the Department of Physical Electronics. My thanks belong especially to Dr Vilma Buršíková and to Dr Vít Kudrle, for their advice, suggestions and comments.

Furthermore, I would like to thank to prof. Nader Sadeghi from LSP UJF in Grenoble for his useful advice in the field of optical emission spectroscopy.

I also wish to thank to my friends and colleagues for their psychical support.

Contents

1	Introduction	9
2	Experimental	13
2.1	Plasma reactors	13
2.1.1	Inductively coupled RF reactor	13
2.1.2	Microwave model experimental set up	16
2.1.3	Planar capacitively coupled RF reactor	18
2.2	Optical emission spectroscopy	19
2.3	Liquid nitrogen trap	21
2.4	Experimental data treatment	22
2.4.1	Calculation of the rotational, vibrational and electron temperatures	22
2.4.2	The determination of electron density	24
2.4.3	Actinometry	25
3	Results and discussion	27
3.1	Analysis by infrared (FTIR) spectroscopy	27
3.1.1	Hexamethyldisiloxane	27
3.1.2	Vinyltriethoxysilane	28
3.1.3	Tetravinylsilane	29
3.2	Analysis by mass spectrometry	31
3.3	Analysis by gas-chromatography - mass spectrometry	35
3.4	Analysis by optical emission spectroscopy	39
3.4.1	Atomic lines and molecular bands	39
3.4.2	The deposition using hexamethyldisiloxane	42
3.4.3	The deposition using vinyltriethoxysilane	47
3.4.4	The deposition using tetravinylsilane	49
3.4.5	The rotational, vibrational and electron temperature	53
3.4.6	Electron concentration	58
3.4.7	Results from actinometric measurements	60
3.4.8	Influence of oxygen addition	64
3.5	Results from OES and thin film properties	68
4	Kinetics of the deposition processes	75
4.1	Hexamethyldisiloxane	79
4.2	Vinyltriethoxysilane	81
4.3	Tetravinylsilane	83
4.4	Structure of plasma polymers	85
5	Conclusion	89
	References	93
	Appendices	99

Abstract

This work deals with the plasma diagnostics during the deposition of the polymer thin films based on organosilicons. We were focused on the characterisation of the deposition processes using hexamethyldisiloxane (HMDSO), vinyltriethoxysilane (VTEO) and tetravinylsilane (TVS) as monomers. Experiments were carried out dominantly in the RF inductively coupled discharge in the reactor which was constructed at the Institute of Material Science at Faculty of Chemistry, Brno University of Technology. The mass spectrometry, optical emission spectroscopy and gas chromatography with mass spectrometry were used for plasma diagnostics. The Fourier transform infrared spectroscopy (FTIR) was used for the thin film diagnostics. The results were completed with the others from ellipsometric and contact angle measurements. Moreover, elemental composition and chemical structure were studied by Rutherford backscattering spectroscopy (RBS) and with Elastic recoil detection analysis (ERDA).

The work is focused mainly on the depositions which were carried out in a pulse mode. The pulse duration was changed from 1:1 to 1:999 (discharge on of 50 W was always 1 ms, discharge off was varied from 1 to 999 ms), and thus the effective power was changed from 25 to 0.5 W. The mass spectra and optical emission spectra were recorded during the depositions at various different effective powers for the all monomers. The oxygen addition was tried to obtain the optimum deposition conditions. It was found that oxygen plays an important role in plasma chemistry but its flow rate is not the most important parameter during the deposition. Various radiative particles (atomic, diatomic and some larger species) were identified in the optical spectra. Relative densities of the selected particles that were the most intensive in the spectra (it means in the gas phase) were plotted as a function of the effective power and/or oxygen or monomer flow rate.

The elemental composition of the plasma polymer films was studied as a function of effective power, too. The results from the gas-phase diagnostics were confronted with the results obtained by thin layer diagnostics. Based on this comparison a models of probable fragmentation and deposition mechanisms were suggested for each monomer. Finally, the probable plasma polymer structures were drawn out for all monomers.

It was found that it is possible to accomplish the optimum conditions for the polymerisation of required thin films that can be used as interphase for the composite materials. It could be done mainly by changing the effective power and monomer flow rate. It was found that the most important parameter in our case is the effective power. With increasing effective power, the density of small particles such as H, O, H₂, C₂, CO, CH, etc... increases in the volume while in the layers the concentration of these particles decreases. Mainly the bonds such as Si–O–Si, Si–Si, Si–H are created in the layer. Furthermore, it was found the range of effective power where the significant changes occur in the spectra character as well as in the layer properties. This effective power range and the deposition conditions improvement are the objective of further studies. Simultaneously, the research will be carried out also in the field of the kinetics of monomer fragmentation and consequent polymerisation as well as of the created polymer structures.

Souhrn

Tato práce se zabývá diagnostikou plazmatu během depozic tenkých vrstev polymerů na bázi organokřemičitanů. Je zaměřena na charakterizaci procesů probíhajících během depozic, k nimž byly jako monomery použity hexametyldisiloxan (HMDSO), vinyltrietylsilan (VTEO) a tetravinylsilan (TVS). Experimenty byly prováděny především v radiofrekvenčním (RF) induktivně vázaném výboji v depoziční aparatuře, která byla sestavena na Ústavu materiálů Fakulty chemické VUT v Brně. Pro diagnostiku procesů bylo využito kombinace metod hmotnostní spektrometrie, optické emisní spektroskopie a také plynové chromatografie s hmotnostním spektrometrem. K lepší představě o polymeračním procesu v plazmatu bylo nutné výsledky diagnostiky plynné fáze srovnat s výsledky získanými diagnostikou deponovaných vrstev. Pro tu bylo využito infračervené spektroskopie (FTIR), dále pak měření kontaktního úhlu, metod Rutherford backscattering spectroscopy (RBS) a Elastic recoil detection analysis (ERDA).

Hlavní část práce je zaměřena na procesy depozic probíhajících v pulzním režimu, přičemž efektivní výkon byl měněn od 0.5 W do 25 W a délka pulzu od 1:999 do 1:1 (doba aktivního výboje o 50 W byla vždy 1 ms a doba bez výboje se měnila od 999 do 1 ms). Při všech těchto výkonech aplikovaných při depozicích a také při různých průtocích monomeru a kyslíku byla měřena hmotnostní spektra a optická emisní spektra. Ze spekter pak byly vypočítány relativní hustoty vybraných částic v plynné fázi a byly vyneseny závislosti hustot a relativních intenzit na efektivním výkonu, na průtoku monomeru nebo na průtoku kyslíku. Dále byly pro srovnání vyneseny závislosti obsahu jednotlivých prvků v plazmovém polymeru na efektivním výkonu. Na základě všech těchto výsledků byl pak vytvořen model pravděpodobné fragmentace monomeru během procesů a model pravděpodobných struktur plazmových polymerů vzniklých při různých efektivních výkonech.

Bylo zjištěno, že strukturu polymeru a tím i jeho fyzikálně chemické vlastnosti lze ovlivňovat především změnou efektivního výkonu. Takto je možné vytvořit polymer, který má vlastnosti vhodné k tomu, aby se dal využít jako mezifáze v kompozitních materiálech. Bylo zjištěno, že se vzrůstajícím efektivním výkonem roste stupeň fragmentace monomerů, jsou tvořeny menší částice a největší koncentraci v plazmatu mají H, O, H₂, C₂, CO a CH, zatímco koncentrace těchto částic v plazmovém polymeru s rostoucím efektivním výkonem klesá. Dochází pak většímu stupni síťování a bylo detekováno větší množství vazeb Si–O–Si, Si–H, Si–Si. Dále bylo zjištěno, že přes významnou roli kyslíku při plazmochemických procesech, není jeho průtok zdaleka nejdůležitějším parametrem. Byla nalezena oblast efektivního výkonu 1.66 - 5 W, kde se charakter spekter podstatně mění a v důsledku toho byly vrstvy připravené při těchto výkonech studovány podrobněji. Dále se zjistilo, že TVS je velmi slibným monomerem, co se týče vlastností připravených polymerů, proto bude charakterizace procesů depozic s využitím tohoto monomeru předmětem dalšího výzkumu. Pozornost bude zaměřena především na oblast efektivního výkonu, při které byly pozorovány největší změny v charakteru spekter a vlastností vrstev. Zároveň bude důležité se zabývat kinetikou fragmentace monomeru a následující polymerace a také studiem struktury vzniklého polymeru.

1 Introduction

In recent years, most materials used in the high technology applications have a composite character. They have a near-surface region with properties differing from those of the bulk materials. This near-surface region is produced by deposition of a coating. Examples of depositing techniques include the following:

- Physical vapour deposition (ion implantation, magnetron sputtering).
- Electron bombardment and electrodeless deposition.
- Chemical vapour deposition and plasma chemical vapour deposition.
- Plasma spraying.

At the present industrial practice, the films are deposited mainly by various plasma chemical vapour deposition methods (PCVD). In the literature, the terms such as Plasma Enhanced CVD (PECVD), Plasma Assisted CVD (PACVD), Atmospheric Pressure CVD (AP CVD) and Hot Filament CVD (HF CVD) are mentioned [21, 24, 57].

CVD is a process whereby a solid material is deposited from a vapour by a chemical reaction as well occurring on or in the vicinity of a normally heated substrate surface. The solid material is obtained as a coating, powder or crystals. By varying the deposition process conditions, such as substrate material, substrate temperature, composition of the reaction gas mixture, gas flows, etc... films with different properties can be grown [52].

PECVD also involves forming solid deposits by initiating the chemical reactions in a gaseous discharge. The major advantage of PECVD is its lower temperature capability compared to thermal driven CVD. For example, deposition temperatures of 700 - 800°C are required to deposit silicon nitride films by CVD, while only 250 to 350°C are sufficient to deposit similar film by PECVD [54]. This method was investigated as a potential technique for the deposition of crystalline films such as polycrystalline silicon, epitaxial silicon, epitaxial gallium arsenide and refractory metal and silicide films. The deposition of diamond-like films has also received a great deal of attention. PECVD operates with various low pressure discharges (glow discharges) sustained mainly by radiofrequency (RF) and microwave (MW) sources.

Glow discharge can be defined as a partially ionised gas containing equal volume concentration of positive and negative charged particles and different concentrations of ground state and excited species.

Spatially homogeneous discharge with a high electron energy is required for the PECVD techniques. At low pressures (low collision frequencies), the electrons can accumulate sufficient kinetic energy to have a high probability of producing an excitation or ionisation during collisions with heavy particles. The reactive and charged particles are created without raising the gas temperature. The reactive species produced in the plasma have a lower energy barrier to physical and chemical reactions [40]. The reaction rate is directly proportional to the collision frequency. Reactions taking place in the plasma volume lead to the forming of molecular fragments, free radicals, etc..., that can condensate directly on the substrate, migrate or react to form compounds or precursors of the polymer species.

Depending on the materials (monomers) used for deposition, the plasma polymers (pp) can be divided into several groups:

- **Hydrocarbons** – the arbitrary hydrocarbons including methane can be the precursors for the pp creation. A long chain containing the double or triple bounds as well as complex cyclic structures can be created by plasma polymerisation. The polymers with good adhesivity are created.
- **Hydrocarbons with polar groups** – the reactivity and hydrophility depend on the content of polar groups in the polymer.
- **Hydrocarbons containing fluorine or other halogens** – those are commercially very important products, especially because of their low free energy and friction coefficient, chemical resistance and low wettability.
- **Organosilicons** – organic compounds containing H, C, Si, O and eventually N are used as precursors and SiO₂-like thin films are created. These polymers are used for thermophilic layers.
- **Organo-metal compounds** – compounds such as trimethylgallium or AsH₅ can be used as a monomer and the created polymers can be used mainly in microelectronic applications [24, 40].

During the deposition process, the gasses that do not take part in polymerisation (oxygen, nitrogen and inert gasses) are very useful for the processes in the plasma volume.

The application of coatings in current technology can be classed into the following areas:

- **Optically functional** - reflective and antireflective coatings, selective solar absorbers.
- **Microelectronically functional** - electronic circuits, insulating layers, solar cells, patterns and dry resists for X-ray and electron lithography.
- **Macroelectronically functional** - capacitors with dielectric polymer layer between two metals.
- **Physicochemically functional** - wear and corrosion resistant coatings, permeable or impermeable membranes for wrapping materials, protective coatings against corrosion and humidity, films with modified wettability and biocompatibility, and many others... [53].

Plasma enhanced chemical vapour deposition (PECVD) is commonly spread in the technological fields where amorphous and microcrystalline thin films such as Si:H, SiO_x-like or C_xH_xO₂ thin films are employed (for example for fabrication of integrated circuits). Properties like small size, enhanced chemical activity, chemical resistance etc. are useful for the fabrication of hard coatings, solar cells and also for packing materials, biomaterials or corrosion protective layers.

SiO₂ is one of the most important and studied materials in the field of microelectronics. The primary application of SiO₂-like films is an electronically passivation film for Si based electronic devices. Other important functions are the fabrication of the electrical isolation between devices on a densely integrated chip, the masking film for the lithography, for metal contact/line insulation, and for packing.

Plasma source	gas pressure [Pa]	T_{e^-} [eV]	e^- density [el/m ³]
DC parallel electrodes	6.6 - 133	2-4	$10^{15} - 10^{16}$
RF parallel electrodes	6.6 - 133	3-6	$10^{16} - 10^{17}$
Magnetron sputtering	0.133 - 26.6	2-4	$10^{14} - 10^{16}$
Epitaxy	0.01 - 2.6	2 - 5	$10^{14} - 10^{15}$
DC arc jet	$10^3 - 10^5$	1-2	$10^{18} - 10^{21}$
Inductively coupled RF	$10^{-2} - 10^2$	1 - 10	$10^{15} - 5 \times 10^{18}$
MW ECR	$10^{-3} - 2.6$	5 - 15	$10^{16} - 10^{18}$
MW	0.1 - 100	5 - 15	$10^{14} - 10^{17}$

Table 1: *Typical parameters of plasma sources used for thin film depositions [54].*

A specific modern kind of the Si based layers are organosilicons. It is possible to tune and control the degree of their organic/inorganic character that allows the changing of the physical-chemical properties of coating (density, refractive index, dielectric constant, surface energy, internal stress, hardness...). Parameters such as power, gas flow rate, gas pressure, etc. strongly influence the chemistry in the plasma and consequently the character of the deposited films. The adhesivity, wettability, hardness, density etc. are changed depending on the plasma polymerisation conditions [40]. The polymerisation process is based on the electron collisions with the monomer, especially organic (in our case organosilicon) molecule.

This work deals with the characterisation of plasma processes during the deposition of thin films by PE CVD, especially in RF discharges, on the flat substrates (glass plates, IR-transparent silica wafers, polyester foils) and glass fibres. The thesis is connected to the previous works [49, 66]. The subject of these studies was the material diagnostics of the thin films and the creation of the suitable interphase in the composite materials. This work is focused on the gas phase diagnostic and the infrared spectroscopy of various deposited thin films.

The plasma phase reactions and the species responsible for the deposition process form a very complicated system and there is more or less impossible to create a complete model (kinetic scheme) of the deposition process. Various excited fragments and many different free radicals are created. These particles are adsorbed on the substrate surface forming a thin film. The complicated fragmentation of the monomer causes the difficulties with identification of the polymer structure. The detection of particle formation, understanding how they grow and the deposition mechanism are needed to develop more efficient surface processing techniques.

In our work, hexamethyldisiloxane (HMDSO), vinyltriethoxysilane (VTEO) and tetravinylsilane (TVS) have been used as organosilicon monomers for the plasma polymerisation. A correlation between the results obtained by the emission spectroscopy (OES) with optical actinometry, mass spectroscopy (MS) and gas chromatography-mass spectrometry (GC-MS) were investigated. OES allows the determination of the light emitting species in the plasma, whereas, mass spectrometry allows the determination of heavy and light neutral and ionic species. Thus, the simultaneous use of these methods allows a complex view on the plasma composition during the deposition process.

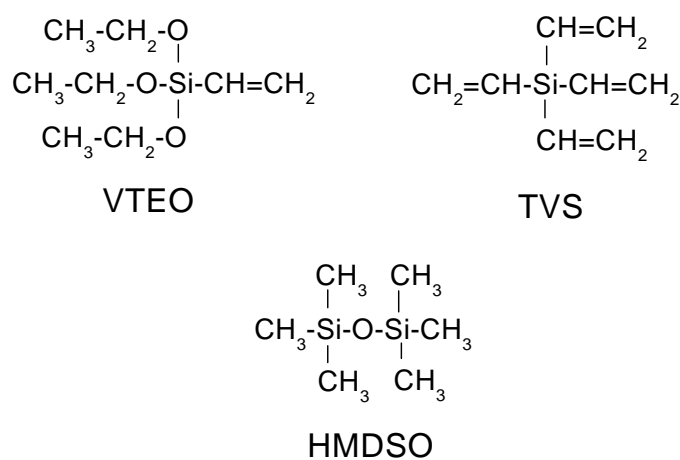


Figure 1: *Vinyltriethoxysilane (VTEO), tetravinylsilane (TVS), hexamethyldisiloxane (HMDSO)*

2 Experimental

In our work, we decided to compare the thin layer properties and the process mechanism during the depositions in different types of the plasma reactors. For this study, typical kinds of discharges used in industrial practice were chosen. In this section, the reactors used for our experiments are introduced. The deposition process conditions and diagnostic techniques are mentioned. Moreover, we are talking about the optical emission spectroscopy measurements, and about the experimental data treatment in detail.

2.1 Plasma reactors

The deposition processes that were studied in this work were carried out in several different reactors, at two laboratories.

- Inductively coupled RF discharge was used as the plasma source for the main set of experiments.
- MW device was used for another part of experiments.
- Capacitively coupled discharge with large plate parallel electrodes was used for comparative measurements.

2.1.1 Inductively coupled RF reactor

The photo and the scheme of the reactor are given in Figs. 3 and 2. The RF device was projected in relation to the PECVD deposition on the flat substrates as well as on the glass fibres. The device consists of the cylindrical Simax (Pyrex) glass reactor (40×400 mm) with the volume of 5.9 dm^3 .

The RF generators PG50 (13.56 MHz, 0 – 50 W) and PG503 (13.56 MHz, 10 – 500 W) were used as a plasma source. The discharge is coupled by the inductor (made of copper) with 6 turns. Effective power during the deposition was up to 50 W. The rotary oil pump ($16 \text{ m}^3/\text{h}$) and diffusion pump ($110 \text{ dm}^3/\text{s}$) were used to obtain the working pressure of about 1 Pa. The pressure was measured by Pirani and Penning vacuum gauges and by Capacitron DM41.

The depositions were carried out in two modes, continuous and pulsed.

- **Continuous mode** - vinyltriethoxysilane (VTEO or also VTES) and hexamethyldisiloxane (HMDSO) were used as monomers and supplied power was changed from 10 to 100 W to find the optimum power for the depositions. The gas pressure during the deposition processes was about 1 Pa. The monomer flow rate was kept between 0.5 and 1 sccm, ($1 \text{ sccm} \cdot 1.69 \cdot 10^{-3} = \text{Pa m}^3\text{s}^{-1}$).
- **Pulse mode** - the VTEO, HMDSO and vinyltriethoxysilane (TVS) were used as monomers. The duty cycle was 0.1 - 50%,

$$\text{duty cycle} = \frac{t_{\text{on}}}{t_{\text{off}} + t_{\text{on}}} \cdot 100\%.$$

Total supplied power W_{total} was 50 W, and t_{on} and t_{off} are the times in ms where the discharge is on or off (plasma on or plasma off). Plasma on period was always

1 ms and plasma off period was changed from 999 to 1 ms. Therefore, the effective power W_{eff} was changed from 0.05 to 25 W.

$$W_{\text{eff}} = W_{\text{total}} \cdot \frac{t_{\text{on}}}{t_{\text{off}} + t_{\text{on}}}$$

The corresponding density of the effective power was $8 \cdot 10^{-4} - 1 \cdot 10^{-1} \text{ W cm}^{-3}$, basic p 10^{-3} Pa , and working 10^{-3} Pa ; pressure was 1 l; rate was varied l; rate was 0.5 or 0.6 s

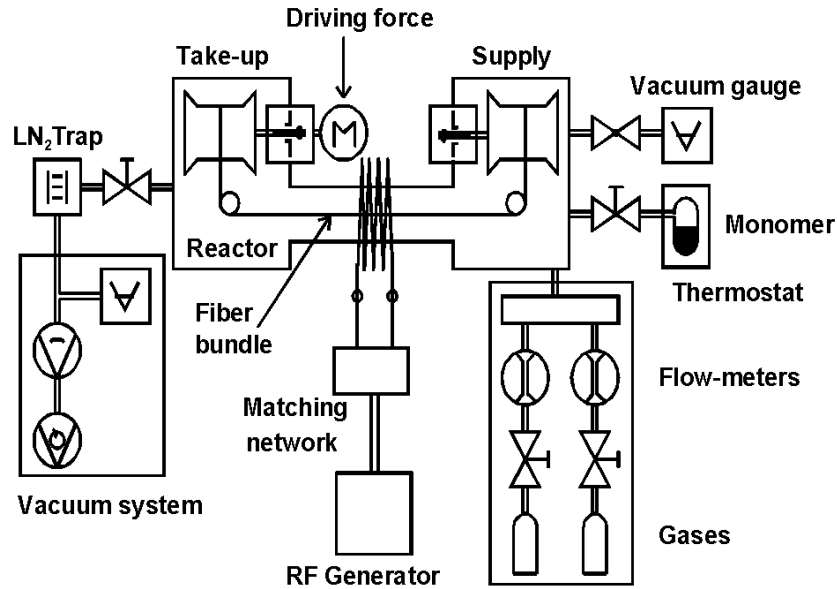


Figure 2: Scheme of the reactor used for the plasma deposition on the glass fibres [49].

The Monomer dosing was provided by a needle valve in the first case and in the second case by using a mass flow controller. Monomer is kept in the thermostat box that enable obtaining defined monomer pressure and thus keep the flow rate constant. Pressure of the monomer vapour is controlled by additional pressure gauge.

Besides the monomer, argon and oxygen lines are connected to the device. Argon is used for cleaning of the reactor and as an actinometer for the optical emission actinometric determination of the selected particle concentrations. After the deposition, argon was fed into the reactor to limit the polymer contamination by residual monomer.

It is well known that oxygen has very important role in the plasma chemistry, so, oxygen was added to monomer, too. Partial pressure of oxygen was measured by mass spectrometry (MS) or estimated from the leakage into the reactor.

The silicon and also glass plate or the slides (Si-wafers, $10 \times 10 \text{ mm}$, roughness of 10^1 nm) were used as substrates for the organosilicon layers deposition.

The Fig. 2 shows the device used for a plasma treatment of the silicon fibres. For the depositions on the plate substrates, similar reactor was used. The reactor that is shown in the picture differs from the other one by two cylindrical chambers. The length of one chamber is 250 mm and diameter is 100 mm. There are the take-up reels inside the chambers that allows its advance motion of the fibre through plasma.

In general, the **deposition process** considers:

- recipient pumping up to the pressure 10^{-3} Pa
- reactor cleaning by argon (10 sccm)
- substrate placing
- pumping and substrate cleaning by argon flow (10 sccm, 10 min at the pressure 10 Pa)
- monomer dosing
- deposition condition setting
- deposition process
- argon flow (10 sccm, 30 min) and residual monomer removal

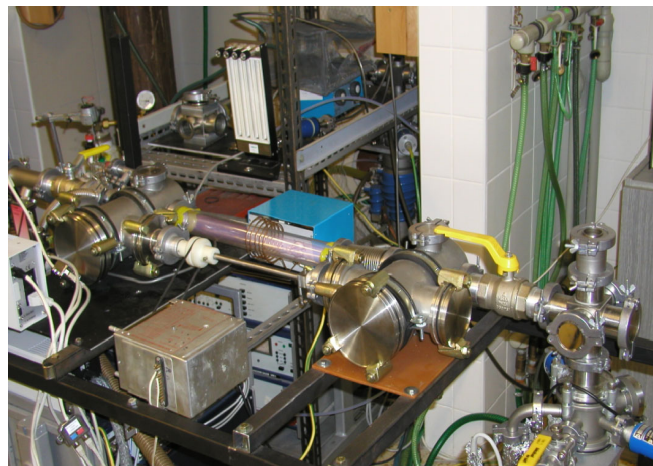


Figure 3: *Photo of the reactor used for the plasma deposition.*

The mass spectrometer HIDEN Analytical was used for obtaining information about ions that are present in the plasma reactor. It was connected to the reactor in the second set of experiment after the experiments with the fibre treatment. Thus, it is not marked in the scheme of the reactor in Fig. 2.

First, the MS was used for leak testing, only. Then, according to the intensity of the ion signal, the deposition conditions were fixed. MS is connected to the device by means of the bellows and electromagnetic valve. Ionising electron energy can be changed from 6 to 70 eV, usually was applied ionising energy of 50 eV.

2.1.2 Microwave model experimental set up

The microwave experimental testing device was constructed, see Fig.4. It concerned the first trial, only. For the plasma depositions, the HMDSO was used as monomer because we had good experience with this monomer using. Besides, the properties of the plasma polymer layers created by using HMDSO are well known, too.

The microwave frequency was 2.45 GHz. The effective power absorbed by plasma was estimated at 100 W. It was difficult to measure exact value of the effective power because of big depletion of the supplied power. The gas pressure was 5 Pa and monomer flow rate during all depositions was 0.4 sccm. Argon has the same role like in the case of the deposition in RF inductively coupled discharge.

Initially, there were the problems with overheating of the reactor quartz tube. The tube pass through across the waveguide that was parallel with the intensity of the electric field. Its length is 30 cm and inner diameter is 1.2 cm. The small diameter was chosen to obtain homogeneous discharge easy way.

The first idea was installation of the strong airflow as a cooling system directly into the waveguide. But it was found insufficient. It was necessary to built the pad that can reduce the output energy. The scheme of this water cooled attenuator is given in Fig. 5.

During the experiments, it was found that it is necessary to cool the discharge tube by strong air flow, in addition.

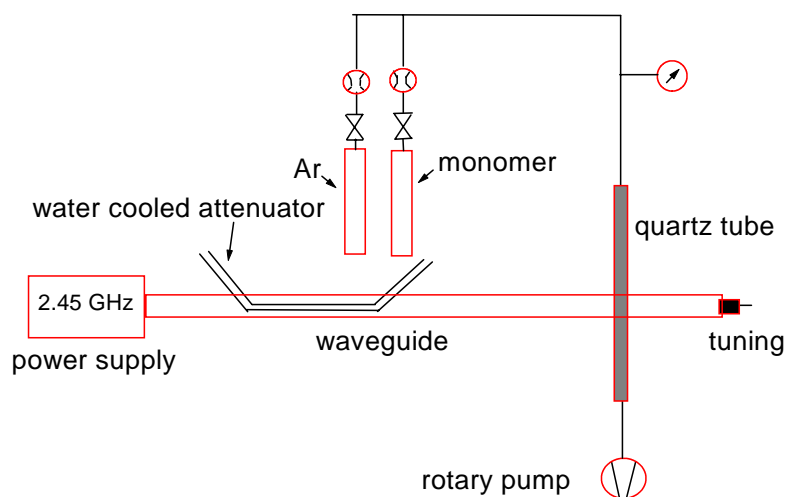


Figure 4: Scheme of the MW device used for deposition.

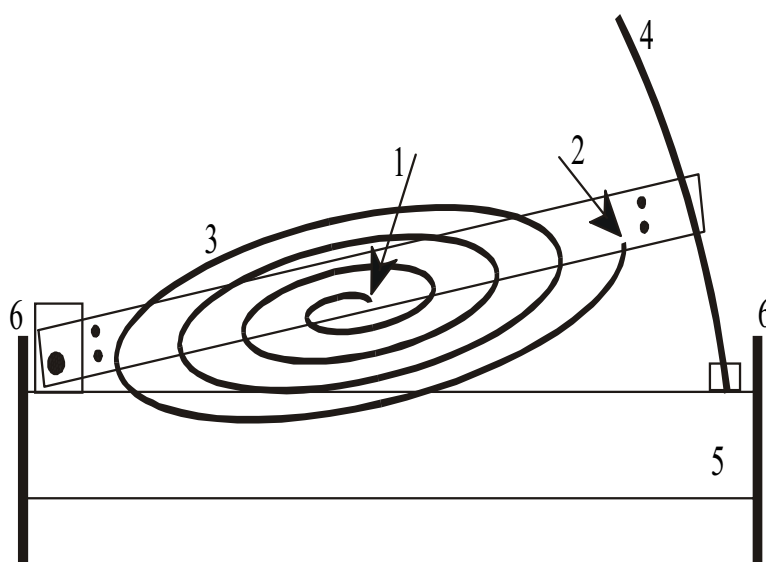


Figure 5: Scheme of the attenuator for MW device. 1 - water inflow, 2 - water outflow, 3 - cooling spiral made of PE, 4 - positioning, 5 - waveguide, 6 - waveguide flanges.

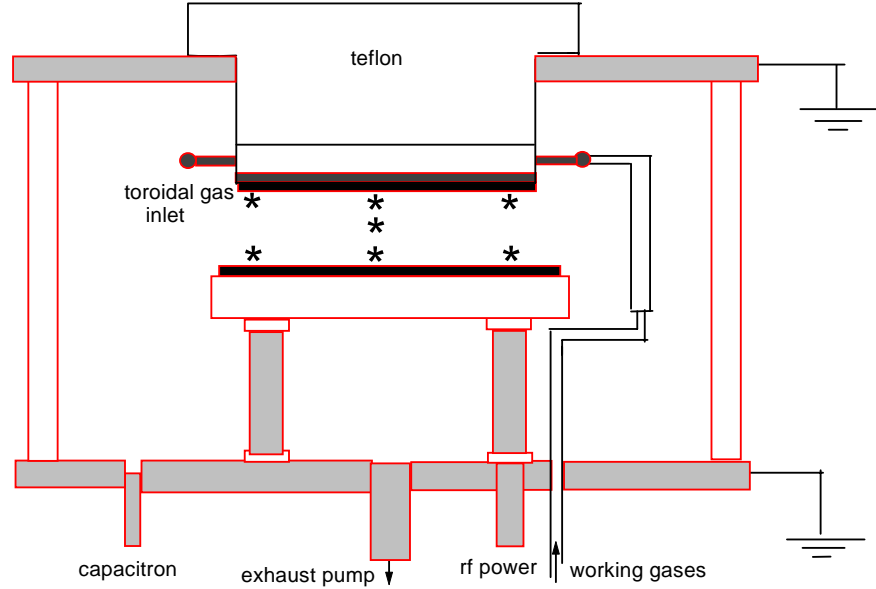


Figure 6: Scheme of the reactor used for the plasma deposition at the Department of Physical Electronics, Faculty of Science of MU, * - points of spectroscopic measurements.

2.1.3 Planar capacitively coupled RF reactor

The comparative measurements were carried out during the deposition using HMDSO in the different experimental setup at Department of Physical Electronics, Masaryk University in Brno. In this case, HMDSO was used for deposition of diamond-like carbon (DLC) films as a hard coating [46]. Films were deposited in a reactor with parallel plate electrodes. This reactor consists of glass cylindrical chamber (274 mm in the inner diameter, height is 190 mm), closed by stainless steel flanges. Schematic drawing of this reactor you can see in Fig. 6. The bottom electrode was connected to the RF generator (13.56 MHz), the second one was grounded. The distance between electrodes was 55 mm.

This deposition was provided only in a continuous mode. The monomer flow rate was changed from 0.31 to 0.53 sccm, methane (2.56 sccm) and hydrogen (0.35 sccm) were added. The power supplied into the plasma was 50 W, and DC bias was varied between 345 and 420 V. The working pressure was about 13 Pa. The optical emission spectra were measured in seven different positions: at the three points near to top, at the three points near to bottom electrode, and between electrodes, it means in the plasma centre, see Fig. 6. It was not possible to measure spectra in pulse mode because of strong signal noise. These measurements were carried out only to compare the character of spectra during the deposition in different kind of reactor (different kind of RF discharge) using the same monomer.

2.2 Optical emission spectroscopy

For optical emission spectra measurements a spectrometer Jobin Yvon Triax 550 with liquid nitrogen cooled CCD detector (1024×128 pixels) was used. The light resolution is provided by gratings with 300, 1200 and 3600 lines per mm.

During the deposition processes, after specification of the substrate position the spectra was measured 2 - 3 cm from the centre of the discharge, it means 1 cm from the coil. In Fig. 8, the point of measurements corresponds to the value 15 cm. The substrate was often placed in the discharge centre. In case of using the quartz tube, it was possible to measure directly in the centre of the discharge, it means that the tube was placed between coil turns. In the picture, this point corresponds to the value 19 cm. The quartz tube was connected to the optic fibre, its size was 25 cm and its diameter was 1 cm. This tube enabled to reduce the RF disturbance.

The position of substrate has an effect on the thin film properties. Thus, the spectra were measured at the different position along the plasma tube, and all points of measurements are marked in the Fig. 8. Moreover, from the front side of the reactor, through the UV transparent quartz window some measurements were provided. The quartz window was extra installed for this purpose.

The OE spectra were measured in the range from 200 to 900 nm. The slits were set at 0.02 nm and integrating time was changed depending on the intensity of spectra and deposition time. So, integration time was varied from 1 to 50 s. The highest time was used to reduce the signal noise. In all cases, the three accumulation were used.

The response curve of the spectrometer is given in literature [29]. The experimental response curve for the monochromator is possible to calculate from the black body radiation. But in our case, it was calculated according to the integral intensities of the transitions from different vibrational states at the different wavelength and transition probabilities, see Fig. 7. In this figure, two equations are marked. The first one is valid for the region from 200 to 500 nm, the second one for the region from 500 to 800 nm. The points R_i for the response curve calculation were obtained from the relation:

$$R_i = \frac{N_1}{N_2} = \frac{S_1/A_1}{S_2/A_2},$$

where S_1 , S_2 are integral intensities of the vibrational transitions, N_1 and N_2 are relative populations of the vibrational states and A_1 , A_2 are corresponding Einstein coefficients.

The calculation of the experimental set up real spectral sensitivity is more or less impossible due to the fact that the transmission of the window on the plasma reactor decreased with time due to films deposited from the plasma. The depositions were carried out from the lowest plasma off period (highest effective power) to the highest off period. Therefore, the higher integration time was applied during the spectra scanning in later part of the depositions. For the calculation, the spectral intensity of chosen (significant) bands were related to the intensity of the whole spectrum (or to argon line intensities for an actinometric calculations).

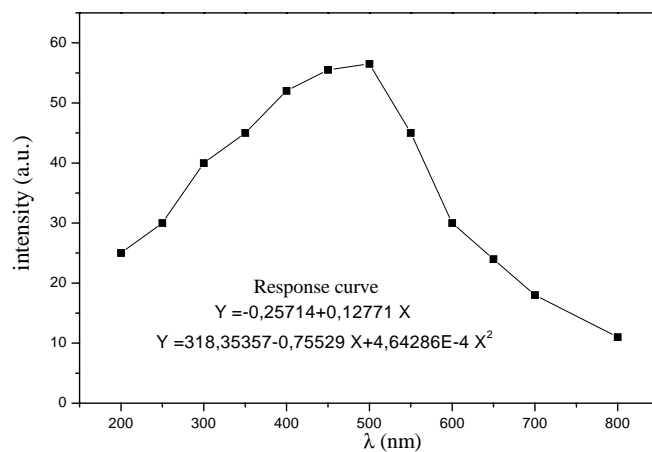


Figure 7: *The response curve of the monochromator, the first equation is valid for the region from 200 to 500 nm, the second one for the region from 500 to 800 nm.*

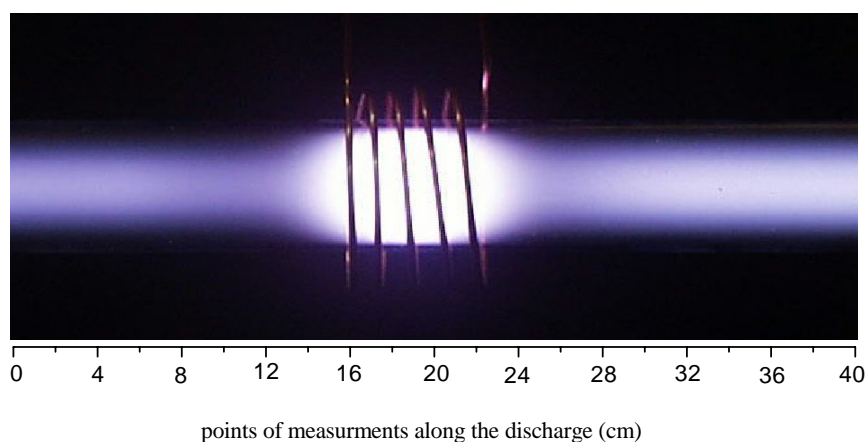


Figure 8: *The discharge range of the measurements along the tube. The real size of the reactor is 40 cm, the measurements were done from the point 0 or in some cases from the point corresponding to 2 cm in the scale. The most of spectroscopic measurements were provided in the point corresponding to 15 cm in the scale.*

2.3 Liquid nitrogen trap

In the part of experiments, the idea to identify formed plasma polymer due to its fragments detection was tested. We tried to catch and freeze out the molecules coming from the plasma during the deposition. We expected that the chemical structure of the condensate in the "cold trap" could be very similar to the chemical structure of plasma polymer on the substrate. Samples for GC-MS (gas chromatography - mass spectrometry) analysis were obtained by means of liquid nitrogen trap that was connected to the apparatus by rapid fastening clamp and vacuum valve. Exhaust gas was sampled at the liquid nitrogen temperature (77 K) for 20 minutes.

Before dosing to the gas-chromatograph, the cold trap was heated at laboratory temperature what produce the reaction of fragments. We suppose that the fragments are identical or similar to the fragments in the plasma during the deposition process. The chromatographic column is made of SiO₂-like polymer, so, the fragments from the liquid nitrogen trap could react with the walls of this polymer column. It is not sure if it occurred because the column was not changed.

After the trap heating, the condensate was dissolved in 1 ml of isooctane (dosing was 2 μ l). The analysis was performed with 2 sccm of helium as carrier gas, column temperature was programmed at 70°C. Separated products were analysed with quadrupole mass-spectrometer at ionising electron energy of 50 eV. In this case, the depositions were carried out in the pulse modes from 1:4 to 1:99 (time on $t_{\text{on}} = 1$ ms, time off $t_{\text{off}} = 4 - 99$ ms), it means that effective power W_{eff} was changed from 0.5 to 10 W. Monomer flow rate was kept constant at 0.6 sccm. The fragmentation of monomer and dimer of TVS was estimated by using GC-MS.

2.4 Experimental data treatment

The data recorded by OES were used for various calculations. To obtain the correct values for all calculations, the data were treated. First, the background was subtracted and then the spectral intensities were divided by the suitable factor to obtain the same integration time in the all cases. Then, the correction according to the response curve (see above) of monochromator was applied.

For some calculations, the line or band intensities were related to the total spectral intensity. The relative particle density was also obtained. In general, by the formula:

$$N \sim \frac{I_{rel}}{A_{v'v''}},$$

where $A_{v'v''}$ is probability of transition.

When the measurements were carried out in the discharge center by means of the quartz tube, the spectrum intensity was corrected according to the measurements provided without the quartz tube. It means that the influence of this tube was subtracted.

2.4.1 Calculation of the rotational, vibrational and electron temperatures

The CH and nitrogen spectra were simulated to determine vibrational and rotational distribution. The CH $A^2\Delta - X^2\Pi$ emission spectrum consists of overlapping 0-0, 1-1, and 2-2 bands [34, 23]. It was found that meaningful temperature simulation of CH requires inclusion of both the predissociation and quenching rates of the transitions 1-1 and 2-2 [58, 55]. It is necessary to know how much the other bands contribute to the main band that was used for the calculations.

Besides calculation from CH spectrum, the rotational temperature were also calculated using the simulations of the first and second positive system of nitrogen. The vibrational transitions are listed bellow.

N ₂ (C ³ Π _u) – (B ³ Π _g)	
transition	λ [nm]
0 - 1	357.6
1 - 2	353.6
2 - 3	349.9
0 - 2	380.4
1 - 3	375.4
2 - 4	370.9

N ₂ (B ³ Π _g) – (A ³ Σ _u ⁺)	
transition	λ [nm]
4 - 1	678.8
5 - 2	670.5
6 - 3	662.4

The dispersion was 0.7 Å/pixel, full width at half maximum (FWHM) that corresponds to the Doppler broadening set in the program was 9.2 - 9.9 and width $\delta_{1/2}$ was 1.52 - 0.9 nm.

$$\text{FWHM} = \left(\frac{2\sqrt{\ln 2}}{\lambda_0} \right) \sqrt{\frac{k_B T}{\pi}},$$

where k_B is Boltzmann constant and λ_0 is the central wavelength of the line. At higher temperatures, the Doppler broadening increases. The programs RotSimul358 [61] and

Specter1.4 were used for these calculations. The second one was created under the co-operation with Nader Sadeghi and Michael Nejbauer at Laboratoire Spectrometrie Physique in Grenoble. Temperatures obtained from the both programs were compared. The main difference between the both programs is that the one version of the program Specter1.4 considers experimental constants (Franck-Condon factor, rotational constant, etc...), thus, the spectra simulated by using the program Specter 1.4 fit better to the experimental spectra.

The rotational temperature was possible to calculate from the intensity of the Q - branch rotational lines of the molecular hydrogen Fulcher transition ($3d^3\Pi_u^- - 2a^3\Sigma_g^+$). It is possible to determine the concentration of molecules at different vibrational level of the electron state $3d^3\Pi_u^-$, too.

The spectral intensity is given by relation

$$\frac{I_{rel}}{A_{v'v''}} \sim \sum_v Q_x N_{xv},$$

where Q_x is a Franck-Condon factor of the transition from the ground state $X^1\Sigma_g^+$ to $d^3\Pi_u^-$ and N_{xv} is the concentration of molecule in the ground state.

The vibrational temperature can be calculate from the relation:

$$\ln \left(\frac{I_{rel}}{A_i v_i g_i} \right) = \frac{-E_v}{k_B T_v} + const.$$

E_v is the higher vibrational level energy of the transition, the v_i is frequency of the band head. The rotational temperature from for example molecular hydrogen bands, according to the relation:

$$\ln \left(\frac{I_{rel}}{v^4 g(2J+1)} \right) = \frac{-E_{rot}}{k_B T_{rot}} + const.$$

Molecular hydrogen was used only for comparative calculations and in the case when the nitrogen spectra were not available. We used the vibrational transition 0 - 0 for this calculations. The Franck-Condon factor for this transition is 0.0995 [36].

Electron temperature T_e is commonly measured by Langmuir probes [10] but in many plasma systems, this measurement is difficult or impossible. In commercial plasma reactors, the walls are coated with insulating materials so that it is difficult to obtain a good return path for the probe current. With regard to contamination, in some cases it is undesirable to insert a probe into the plasma. The problem with the probe measurement could be solved by using the triple probe [63]. But the obtained results seemed to be not very reproducible. After the first set of experiments, the probe was removed from the device.

For determination of the electron temperature, hydrogen lines $H^\alpha, H^\beta, H^\gamma, H^\delta$ were used. H^γ emission at 434 nm is often overlapped with the CH A-X emission, and therefore, relative excited state population of corresponding CH band is also included in our calculation. Intensity of H^α was saturated, so that it was not possible to calculate exact value of temperature. The Boltzmann plot was obtained according to the relation:

$$\ln \left(\frac{I_{mn}}{A_{mn} \nu_{mn} g_m} \right) = \ln K - \frac{E_m}{k_B T_e}$$

where I_{mn} , A_{mn} , ν_{mn} and g_m are relative intensity of hydrogen line, transition probability, frequency and statistical weight of the transition upper state. E_m , k_B , T_e , K are energy of the transition, Boltzmann constant, electron temperature and the constant equal $\frac{h m \alpha}{2}$.

If the argon lines are at disposal, the second method for determination of electron temperature is based on the equation:

$$y = \frac{h^4 c}{8\pi C_1 (2\pi m_e k)^{3/2}} \frac{g_m}{g_1} A_{mn} \frac{\lambda}{\Delta\lambda} \frac{\exp[(E_\infty - E_m)/kT_e]}{T_e \xi} \left(1 - \frac{\Delta E_\infty}{kT_e}\right)$$

h is Planck constant, c is light velocity, m_e is electron mass, g_1 is statistical weight of the fundamental level of ion (Ar II), E_∞ and ΔE_∞ are ionisation energies of the ground and excited state, $C_1 = 1.6310^{-43} \text{Jm}^4 \text{K}^{1/2} \text{s}^{-1} \text{st}^{-1}$ is the constant for all Ar (I) lines.

The calculation from Balmer hydrogen lines was preferred to our purpose.

2.4.2 The determination of electron density

Besides OES measurements, the Langmuir probe measurements can be used for the electron density determination. In our case, the triple probe is required. To obtain meaningful values, the construction of this set up is very complicated. So, the electron concentrations were calculated using the OES data. The first choice for the electron density determination in plasmas containing hydrogen should be H^β at 486.1 nm. It is a strong line, sufficiently broadened for precise measurements. Its self-absorption is relatively small. The other Balmer lines, H^α , H^γ are commonly used for determination of electron density, too. Balmer H^α line due to transition between principal quantum numbers ($n=3$, $n=2$) is the most prominent line. Measurements of the symmetrical profiles and widths in dependence on electron concentration were carried out and published in literature [19, 73]. In our case, H^γ is overlapped by its neighbours, mainly by CH band. H^α is often saturated and relatively narrow. And moreover, it has strong self-absorption.

Electron density is given by the Griem equation:

$$n_e = C \Delta \lambda_s^{3/2}$$

where λ_s is Stark broadening of the atomic line, and C is Griem coefficient [18].

The calculation is based on the theory of the Stark broadening which is caused by coulomb interactions. The measured line profile could be well-represented in terms of Voigt profiles, with Stark and Doppler profile. The Doppler broadening of the line is much simple than calculation of Stark broadening (the Maxwellian distribution is used to describe the velocity of radiating particle). For the Doppler broadening we can write:

$$\varphi_D(\omega) = 1/\beta\pi^{1/2} \exp[(\omega - \omega_0)^2/\beta^2]$$

$$\beta = 2k_B T / (M c^2) \omega^2,$$

where $k_B T$ is kinetic temperature in energy units, ω_0 is frequency of unperturbed transition, M is the particle mass, ω is frequency of emitted photon, and c is light velocity. Total line profile is given by [73].

$$I(\omega) = \int_{-\infty}^{\infty} \varphi_D(\omega - \omega_0) I_{Stark}(\omega') d\omega'$$

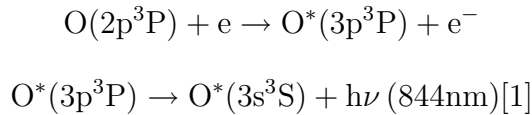
In our case, electron concentration was calculated from the H^β line at 486 nm by using program HBETA [33]. This program provides the deconvolution of the line-profile to the particular sections. According to the Griem's theory, it is possible to calculate electron concentrations in the range from 10^8 to 10^{16} cm^{-3} . Natural broadening of the H^β is 10^{-4} nm, thus, it is negligible. [18]. Simplified relations used for the electron density calculations are following:

$$\begin{aligned}\Delta\lambda_D &= (v/c)\lambda \\ v &= (2RT/\mu)^{1/2} \\ \Delta\lambda_{1/2} &= 2(\ln 2)\Delta\lambda_D = 1.665 \times \Delta\lambda_D = 1.1610^{-7}\lambda(T/\mu)^{1/2} \\ \Delta\lambda_L &= 0.3110^{12}v^2\lambda^2n_e^{-1} \\ \Delta\lambda_{1/2} &= 2.510^{-9}\alpha_{1/2}n_e^{3/2}\end{aligned}$$

where $\alpha_{1/2}$ is half-width, $\Delta\lambda$ is the distance from the line centre, $\Delta\lambda_D$ is the Doppler broadening and $\Delta\lambda_L$ is the Lorentz broadening [18]. The detailed deduction of these equations used in the program HBETA can be found in literature [33].

2.4.3 Actinometry

Actinometry involves using of the optical emission intensity ratios to provide an estimation of the ground state species concentrations. The intensity emitted from the species is divided by the emission intensity from actinometer. The gas with a known spectrum and excitation and de-excitation rate constants is used as an actinometer. The actinometry technique depends upon the assumption that the emitting excited state atoms are produced by the electron impact upon the ground-state atoms. For example:



Considering the short lifetime of the excited state and low-pressure conditions, collisional deactivation of the emitting atoms could be negligible.

In our case, argon was used and it was added to the plasma in a small quantity without any modification of the discharge properties. Strong argon lines are present in the spectrum between 680 and 900 nm.

The atomic oxygen line at 844.6 nm, CH bands at 431 nm, hydrogen H^α line at 656.2 nm were monitored to obtain the actinometric signal in our experiments. The argon line at 750.4 nm was used as actinometer for the calculation of atomic oxygen concentration, and argon line at 696.5 nm was used for the calculation of hydrogen and CH concentrations.

The absolute density of Ar was determined from its partial pressure and from the calculated temperature of the gas mixture.

The absolute density of the atoms in the ground state N_1 could be determined from the corresponding spectral bands ratio I_1/I_2 and from the absolute density of the actinometer N_2 .

$$N_1 = k \frac{I_1}{I_2} N_2$$

$$k = \frac{\sigma_2 A_2 t_2 \nu_2}{\sigma_1 A_1 t_1 \nu_1},$$

where σ_i is the maximum value of the direct electron impact excitation cross section of the excited state, A_i is emission Einstein coefficient, t_i is lifetime of excited state, ν_i is the transition wavenumber.

For example, the expression of the oxygen actinometric signal I_O/I_{Ar} is given by

$$\frac{I_O}{I_{Ar}} = \frac{k_{exc}^O [O]}{k_{exc}^{Ar} [Ar]} + \frac{k_{diss}^{O_2} [O_2]}{k_{exc}^{Ar} [Ar]}.$$

$$\left[\frac{[O_2]}{[Ar]} \right]_{feed} = \left[\frac{2[O_2] + [O]}{2[Ar]} \right]_{plasma}.$$

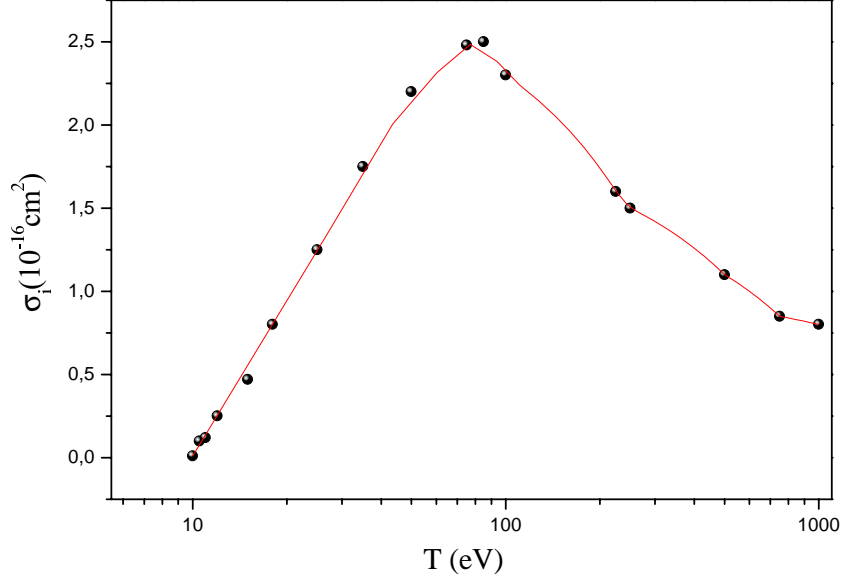


Figure 9: *The electron excitation cross section coefficient for CH to the $A^2\Delta$ state as a function of electron energy [26].*

In the literature, the actinometric calculations are provided mostly from atomic line intensities. But under certain conditions, it is possible to apply the actinometric calculation to the molecular spectral bands, too. The good example is CH band at 431 nm [8, 44]. The approximately same population of the all rotational levels is required.

We can obtain concentration values from the actinometric calculations. However, this method is estimative. Furthermore, actinometric measurements allow to calculate dissociation degree. To calculate the excitation rate, the cross section coefficient is necessary to know. Emission coefficient of the CH (A-X) transition is $1.8 \times 10^6 \text{ s}^{-1}$ and direct impact cross section coefficient can be found in [9]. The dependence of cross section coefficient on the electron energy is shown in Fig. 9. Due to the uncertainty of the electron temperature, the calculations of reaction rates were not provided.

3 Results and discussion

The detailed characterisation of thin films prepared from HMDSO, VTEO and TVS is described in [2, 66, 49]. Various analytical methods, such as RBS, ERDA, AFM, SEM, measurements of the contact angle and of the mechanical properties were used. In this study, the species in the gas phase were detected and these measurements are compared with the results recently published in the literature [64, 66]. In order to characterise the processes in the plasma during the deposition, the several diagnostics were provided: GC-MS, MS, FTIR and OES. Many authors have pointed out that the gas temperature is one of the critical parameters for polymer formation [13, 32, 57]. Thus, the particle content in the gas phase was observed mainly as a function of the effective power. The other very important parameter is the reaction gas mixture composition, mainly the content of oxygen. Following section about FTIR spectroscopy shows the results of Jan Vaněk [66]. They are important for the comprehension of further results and conclusions.

3.1 Analysis by infrared (FTIR) spectroscopy

The chemical structure of plasma polymers was investigated in the range from 4000 to 400 cm^{-1} . The layers were measured without the protective atmosphere with resolution of 0.96 cm^{-1} . By reason of an elimination of the Si-substrate spectral influence (interference, absorption), the absorption subtract technique was used.

First, the monomer and polymers arising from monomer by the polycondensation were analysed. Then, the spectra were compared with the spectra of plasma polymers. Drops of the monomer were spread on the KBr crystal and polymers were deposited on the polished silicon plate. This substrate shows out the bands of Si at 610 cm^{-1} and bands of SiO_2 at 1103 cm^{-1} . In general, we can say that spectra from monomer and polycondensated polymer have more or less the same FTIR spectrum and it differs from the spectra of plasma polymer (pp), an example is given in Fig. 10. The work [66] deals with the FTIR of TVS and VTEO in detail.

Some published interpretation of the IR bands at different wavenumbers and corresponding bonds are given in the table 2 [48, 35].

3.1.1 Hexamethyldisiloxane

In case of the HMDSO monomer, the Si – O – Si at 1280 - 1240 cm^{-1} , Si – CH_3 at 870 – 820 cm^{-1} and CH vibration of CH_3 group at 2980 - 2880 cm^{-1} belong among the most intensive absorption bands. On the other hand, in ppHMDSO, vibration of the Si – O – Si is moved to other wave numbers, comparing to the spectrum of classical polymer and monomer. It means that these bands are bounded up with the part of a longer chain. We can suppose Si – O – Si – O – or –O – Si – $(\text{CH}_2)_2$ – O – main structure. Si – C bands are present at 820 – 790 cm^{-1} .

Depositions with the HMDSO were carried out mainly in the continuous mode. In this mode, the intensities of peaks that belong to Si – O – Si and Si – O – C bonds decrease, with increasing power. But the SiH intensity increases. In a pulse mode, with increasing effective power, the intensity of Si – C bands also increases. In the plasma polymer

wavenumber [cm^{-1}]	bond	in the structure	vibration
622	Si – C		stretching
680 - 690	Si – C		asym. stretching
791-922	Si – H	SiH _x	stretching
804 - 857	Si – C	Si(CH ₃) _x	rocking
1015, 1040	Si – C	Si – CH ₂ – Si	wagging
1100	Si – O	Si – O – Si	asym. stretching
1430	Si – C _{arom}	Si-phenyl	valence-vibr.
1480	C – H	–CH ₂ –	scissor
2850 - 2930	C – H	CH ₂ , CH ₃	stretching
2971	C – H	CH ₃	sym. valence
2998	C – H	CH ₃	asym. valence

Table 2: Examples of the bonds in different geometry in infrared spectra.

prepared in the pulse mode, the SiH bonds were also detected. On the contrary, the intensity of SiH at 2100 cm^{-1} decreases.

It was also possible to identify (R)₂HSiO band due to vibration of hydrogen bounded to the Si atom.

3.1.2 Vinyltriethoxysilane

In Fig. 11 the infrared spectra of pure VTEO (marked as VTES) and the spectra of pp-films deposited at different conditions, are presented.

In case of the ppVTEO, vinyl group at 3030 , 1600 and 1008 cm^{-1} disappeared, while in the spectra of monomer or polymer formed by polycondensation, the vinyl groups were observed. Comparing to the monomer or the classical polymer, we can observe some new bands at 3600 and 1710 cm^{-1} , which correspond to the OH and CO bands. CO bands appeared also at 1700 cm^{-1} . The new chemical bonds were also identified at 880 cm^{-1} (SiH, SiOH). The cage-like vibration of the Si – O – Si group also disappeared while in the spectrum of monomer it was relatively strong. But we can observe the vibration of Si – O – Si at 1072 cm^{-1} .

The Si – CH₃ and Si – CH₂ groups are visible at 1440 and 1380 cm^{-1} in both cases. Very weak bands of Si – O – C₂H₅ appeared in the spectrum, too.

The appearance and wave number of these vibrations are dependent on the substituents. In the layers prepared with $W_{\text{eff}} = 0.05 \text{ W}$, the –SiC₂H₅ and Si – O – Si bands can be recognised, see Fig. 11. These bands are overlapped or unidentified with increasing the effective power. We can suppose that Si – O – Si group is present in ppVTEO as a siloxane with various substituents on the Si atom.

You can see, that pp thin films differs from the polycondensated VTEO. With increasing effective power, the content of CO groups increase in the layer, while the Si – O – Si bonds appears mainly in pp prepared at the lowest effective power. Besides, the SiH

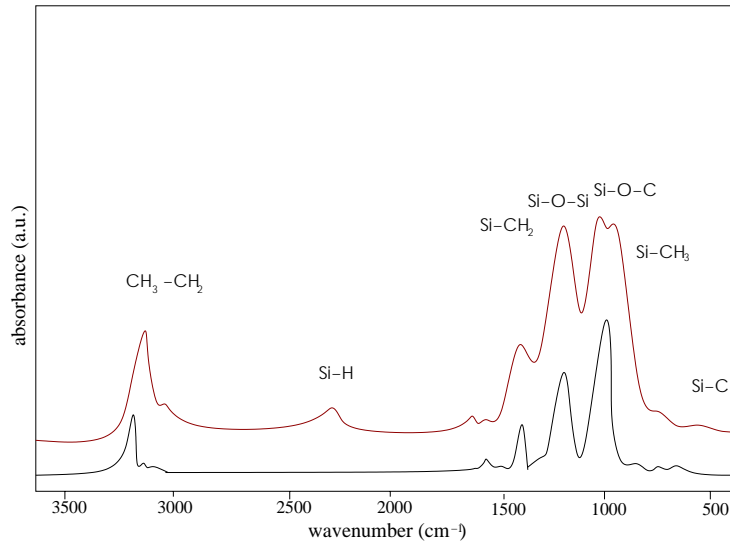


Figure 10: An example of the infrared spectrum of the HMDSO monomer and pp layer based on HMDSO (red one), power was 40 W [49].

groups appear in the pp prepared at effective power 0.05 W and also in the polycondensated VTEO.

3.1.3 Tetravinylsilane

An example of the infrared spectra of the thin films prepared at selected effective powers is shown in Fig. 12. The CH bending and CH stretching vibration of the CH₃ and CH₂ group appeared at 1375 and 1460 cm⁻¹. Some cyclic structures can be present in the polymer structure, therefore we can expect sp³ and sp² vibrations of the CH₂ groups at 1445 cm⁻¹ and vibration of the clusters at 1600 cm⁻¹. At 1650 cm⁻¹ we can see stretching vibrations of C = C and the CH = CH in phase vibration are present between 611 and 682 cm⁻¹. There is also CH wagging vibration and weak bands of R - (CH₂)_n = CH₂ in the region of finger print. In contrast to the polymers formed from VTEO, the vibration of vinyl group appears in the spectrum (mainly antisymmetric rocking at 1404 cm⁻¹). The C = C - CH₃ group is another possible interpretation of this peak. We can also suppose that the CH₂ group vibrations are present in the spectrum. Between 1470 and 1435 we can find O - CH₃, O - CH, and O - CH₂ - CH₃ groups. These groups change their positions according to the character of their substituents. The oxiran structures or other cyclic groups are very probable, too.

It is evident, that with the effective power decreasing, the content of CO, SiH bonds and double vinyl group increase in the layer. This is the main difference between IR spectra of ppVTEO and ppTVS. The peaks that belong to SiC, CH - CH and OH groups can be seen in the relatively constant intensity.

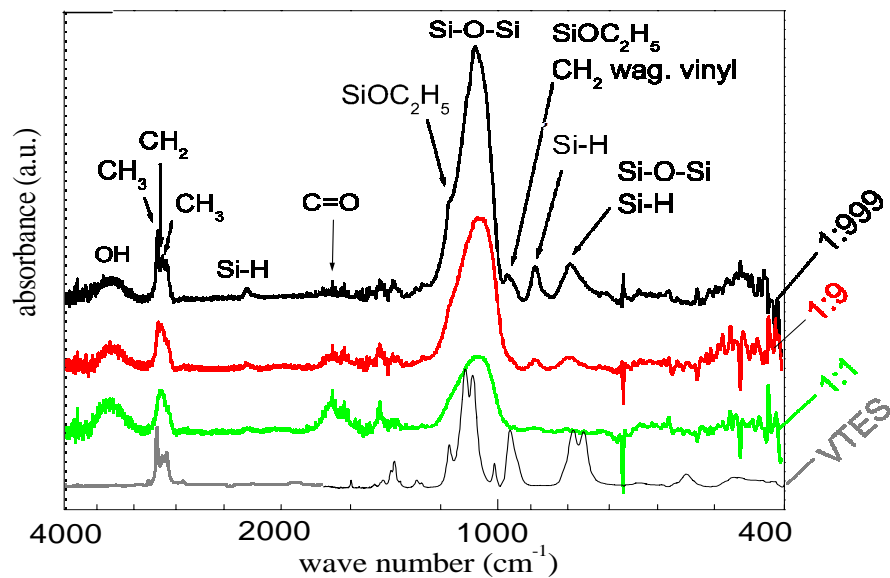


Figure 11: An example of the infrared spectrum of the layer formed from VTEO, [66].

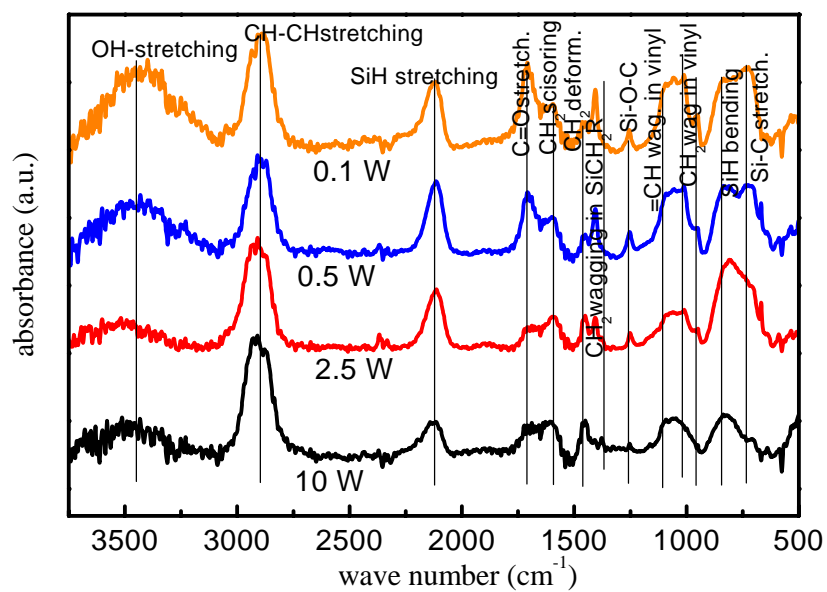


Figure 12: An example of the infrared spectrum of the layer formed from TVS, [6].

3.2 Analysis by mass spectrometry

A mass spectrometer was connected to the device when the experiments with HMDSO were ending, thus, there are only a few available data from MS for this monomer. At the beginning, the mass spectrometer was used only for leak detection. After, the monomer flow rate was kept constant and the effective power was changed from 0.05 to 25 W (with pulses 1:999 to 1:1). It was found that in the case of the lower effective power we could observe bigger fragments of monomer in the plasma. The most important is vinyl group that could enable to improve adhesion of polymer to the composite material matrix. On the basis of the results from MS (later completed with the results from OES), we can suppose that the monomer is completely fragmented when the pulse duration 1:9 is applied.

In case of HMDSO, a big amount of CO^+ and CO_2^+ fragments appeared in the mass spectrum and it was possible to observe also $\text{H}(\text{CH}_3)_2\text{Si}^+$ fragments. These particles could be the building units of the created plasma polymer. Probable fragmentation of the monomers and pp creation will be discussed later in the section *Kinetics of deposition processes*.

m/z	formula	parent molecule
2	H_2^+	H_2
15	CH_3^+	$\text{CH}_3, \text{CH}_4^+$
26	C_2H_2^+	C_2H_2
28	$\text{CO}^+, \text{C}_2\text{H}_4^+$	$\text{CO}, \text{C}_2\text{H}_4, \text{C}_2\text{H}_6$
31	CH_3O^+	CH_3OH
32	CH_3OH^+	$\text{CH}_3\text{CH}_2\text{OH}$
33	$\text{H}_2\text{O}^+, \text{CH}_3 \cdot \text{H}_2\text{O}^+$	$\text{CH}_3\text{CH}_2\text{OH}$
44	$\text{CO}_2^+, \text{CH}_3\text{CH}_2\text{O}^+$	$\text{CO}_2, \text{CH}_3\text{CHO}$
163	$\text{SiO}_3\text{C}_6\text{H}_{15}^+$	VTEO

Table 3: Examples of a possible attribution of the different ions to their parent molecules. These particles were found in the MS spectra during the deposition using VTEO.

Using HMDSO or VTEO for the deposition, first, it was not clear if Si – C or Si – O bonds are created preferentially. This problem was solved by MS spectra measurements during the deposition using VTEO. Mass spectra were measured also during the process without discharge. The intensive peaks at $m/z = 147$ and 73 were identified. Those correspond to $[\text{Si}_2\text{O}(\text{CH}_3)_5]^+$ and $\text{Si}^+(\text{CH}_3)_3$. They correspond to the neutral species $\text{Si}(\text{CH}_3)_4$ or to the radical $\text{Si}(\text{CH}_3)_3$. The 73 to 147 peak ratio was plotted as a function of deposition time (with plasma on) and as a function of the time with plasma off, too (see Fig. 16). The ratio during plasma off process should be constant. The fluctuation of the values are in the interval of acceptable error. The results suggest that Si – O bonds are created in the polymer film, on the other hand, the Si – C bond is unstable under electron collision. The MS measurements with HMDSO were done additionally with the simulated deposition conditions.

The main peaks detected in the mass spectrum of VTEO you can see in the Figs. 13, 14.

At lower effective power, the peaks with $m/z = 190$, 162 , 157 and 129 were relatively intensive. These peaks belong probably to $VTEO^+$, $SiO_4C_6H_{16}^+$, $SiO_2C_7H_{13}^+$ and $SiO_2C_5H_9^+$.

At higher effective power, we identified the peaks with $m/z = 2$, 18 , 26 , 28 , 32 , 33 and 44 . The correlation of the observed ions with the corresponding neutral molecules is given in table 3.

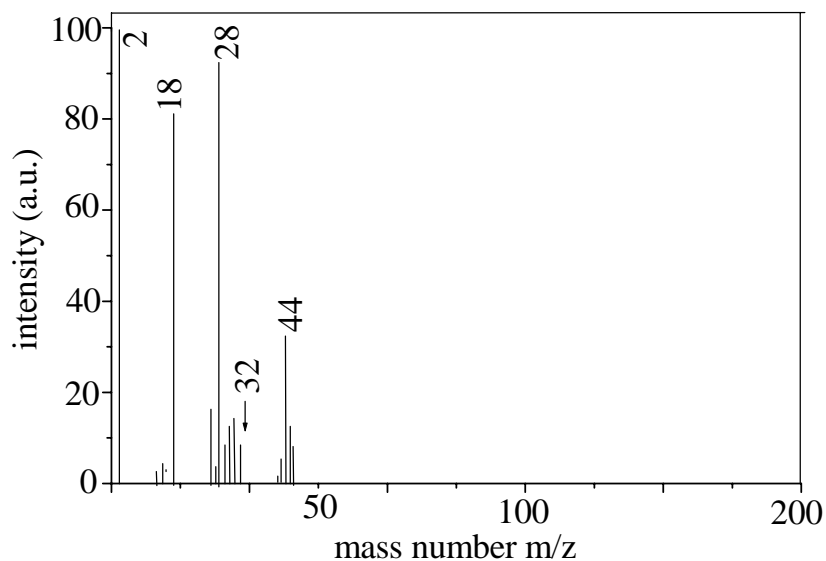


Figure 13: *Mass spectrum measured during the deposition with VTEO, $W_{\text{eff}} = 25$ W, $Q_{VTEO} = 0.9$ sccm.*

In case of TVS with higher effective power, it was possible to identify only groups that probably have not taken part in deposition (H_2 , $CH_2 = CH_2$, $CH - CH$). With lower effective power we can find larger fragments of monomer. Scheme of fragmentation will be discussed later and it is shown in the Fig. 70. Mass spectra were measured for pulsed plasma at different effective power and compared with those without discharge, see Fig. 15. Identified peaks are summarised in Table 4.

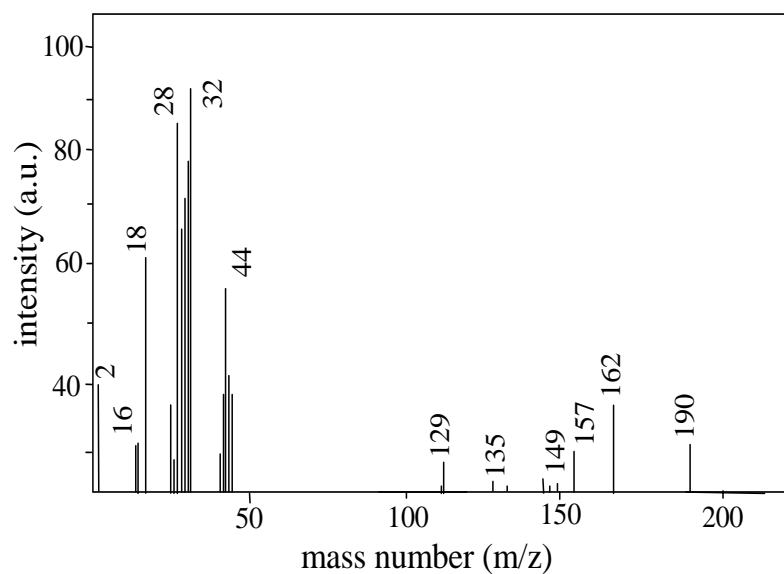


Figure 14: Mass spectrum measured during the deposition with VTEO, $W_{\text{eff}} = 2.5 \text{ W}$, $Q_{\text{VTEO}} = 0.9 \text{ sccm}$.

m/z	formula	parent molecule
2	H_2^+	H_2
24	C_2^+	C_2H_2 , C_2H_4 , vinyl
25	C_2H^+	C_2H_2 , vinyl
26	C_2H_2^+	vinyl
27	$\text{C}_2\text{H} = \text{CH}^+$	vinyl
28	CH_2CH_2^+	CH_3CH_2
40	SiC^+	$\text{SiCH}_2 = \text{CH}-$
53-58	$\text{SiCH} = \text{CH}_2^+$	TVS
80-84	$\text{Si}(\text{CH} = \text{CH}_2)_2^+$	TVS
106-110	$\text{Si}(\text{CH} = \text{CH}_2)_3^+$	TVS

Table 4: Examples of a possible attribution of the different ions to their parent molecules. These particles were found in the MS spectra during the deposition using TVS.

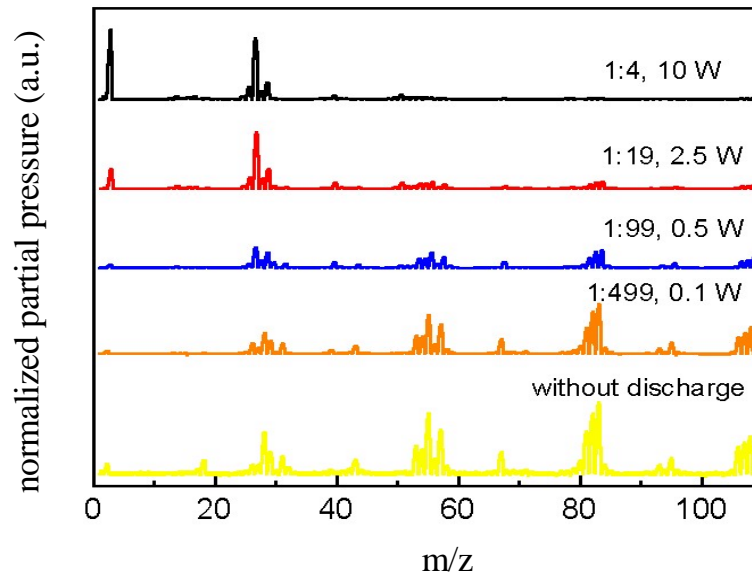


Figure 15: *The mass spectra measured at the different effective power and without discharge, $Q_{\text{TVS}} = 1 \text{ sccm}$ [6]*

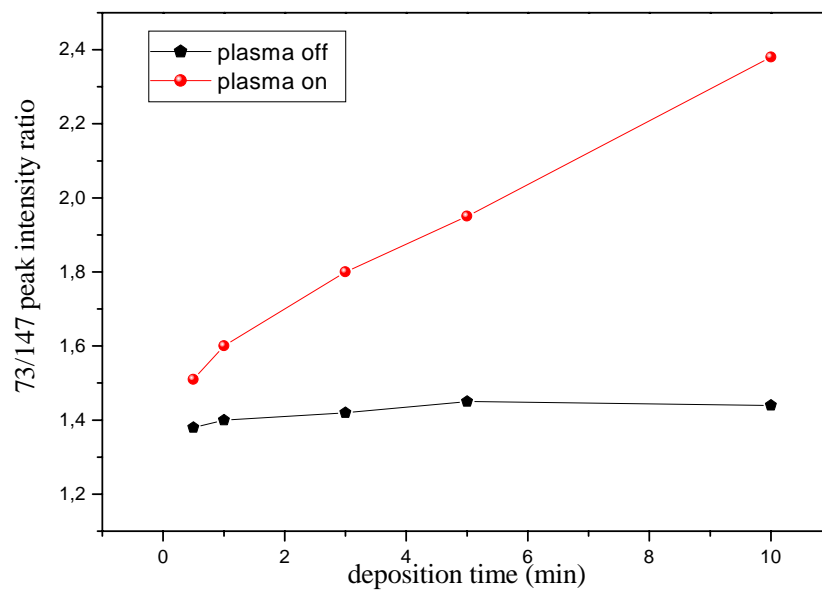


Figure 16: *The 73 to 147 peak intensity ratio as a function of deposition time, $Q_{\text{HMDSO}} = 1.5 \text{ sccm}$, $W_{\text{eff}} = 5 \text{ W}$.*

3.3 Analysis by gas-chromatography - mass spectrometry

First, we supposed that gas (monomers fragments) which are sampled by means of nitrogen cold trap could simulate the forming of plasma polymer. GC-MS was applied to better comprehension of this process. The analysis by GC-MS were carried out only during the deposition using TVS and the chromatographic spectra with their corresponding mass spectra are given in the appendix at the end of this work.

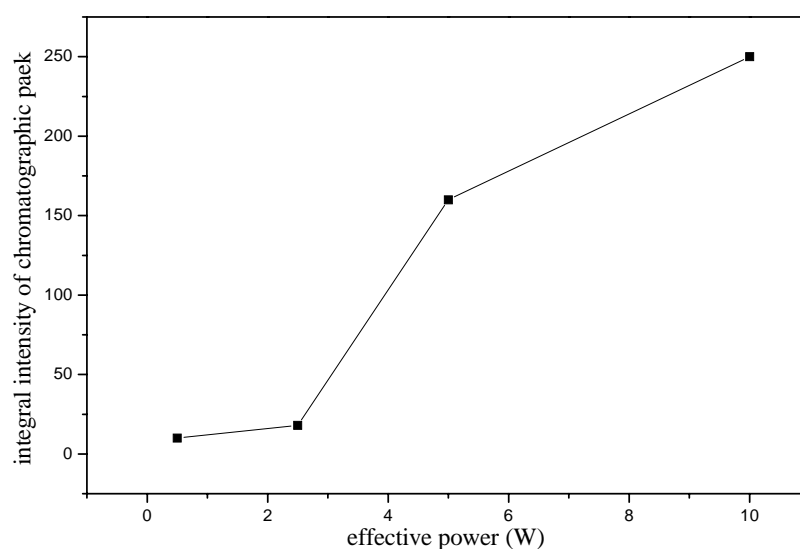


Figure 17: *Dependence of the chromatographic peak total intensity as a function of the effective power.*

We observed very intensive chromatographic peak at the retention time of 5.75 min. Intensity of this peak was plotted as a function of effective power, see Fig. 17. Its total intensity increases with the increasing effective power. This fact sustain the theory that many small particles are created with higher effective power. The particles flow out from the reactor easier than larger particles. Then, they can react and form the plasma polymer in the cold trap. It was difficult to identify this peak because corresponding MS spectrum is not described in databases or spectra-libraries. Thus, the interpretation of the mass spectrum originated by electron impact ionisation was provided. The peaks with 216 and 108 m/z value were the most intensive. From the pictures of mass spectra it is clear that at the effective power of 5 W (in a pulse mode 1:9), the character of the deposition process changes. It corresponds with the results from OES and FTIR. Between the pulse modes 1:4 and 1:19, the significant changes of optical emission end infrared spectra were observed, too.

We have tried to interpret the mass spectra. According to the following fragmentation we can consider that these peaks correspond to the molecular ion or ion-radical. In that case, we can expect the fragmentation schemes shown in Fig. 18 - 20.

Initially, the spectrum of pure TVS was found in the NIST database [26]. There is not molecular ion in this spectrum. The most intensive peak has m/z 108.

In our case, we can suppose the fragmentation $M^+ \rightarrow FR \cdot I^+$ in the ionic source. It is not sure if the peak 216 is molecular ion. Furthermore, the particles with m/z 83 and 133 were detected in the mass spectrum of TVS. Those can form the particle with m/z 216 and their intensity at an effective power of 5 W is the highest. The peak 121 is the most intensive in the mass spectrum. This particle should be relatively stable. The other intensive peaks have m/z 175 and 216. The first of probable fragmentation schemes is shown in Fig. 18. It is demonstrated that the ion-radical could be created and the peak 216 is not molecular ion.

As dissociation of double bond is not very probable in the ionic source, the peak 216 is supposed to be ion-radical. Thus, particle coming into the MS has higher M_r than 216. Exact process of fragmentation could be studied by MS-MS methods. Scheme of probable fragmentation way of molecular ion 216 is shown in Fig. 19.

It can be supposed that the oxygen from atmospheric impurity is built into the ion radical that is created from TVS. The structures similar to vinyltrimethoxysilane can be created. Fragmentation of this ion-radical is given in Fig. 20.

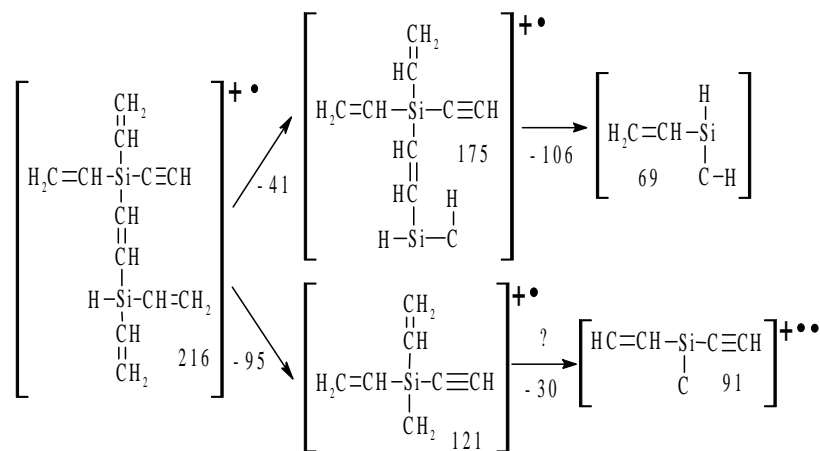


Figure 18: Scheme of a probable fragmentation of the ion-radical formed from TVS, provided that peak 216 is not molecular ion. Consequent ion-radical and one neutral molecule could be created.

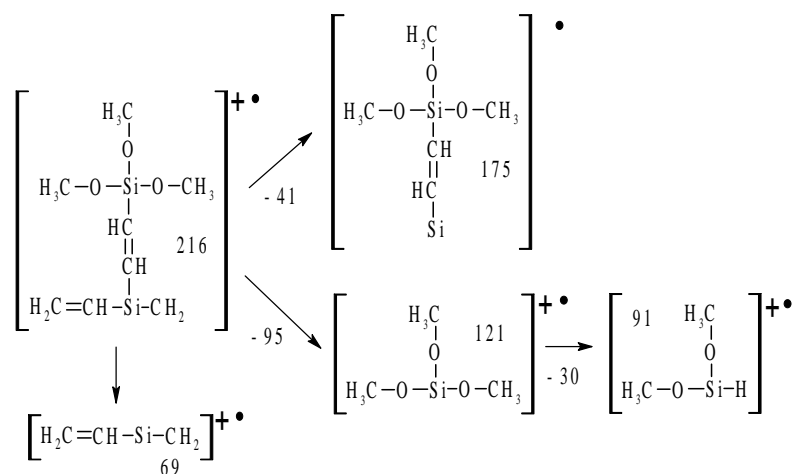


Figure 19: Scheme of a probable fragmentation of the molecular ion formed from TVS, provided that peak 216 is not a molecular ion, and oxygen is built into the structure.

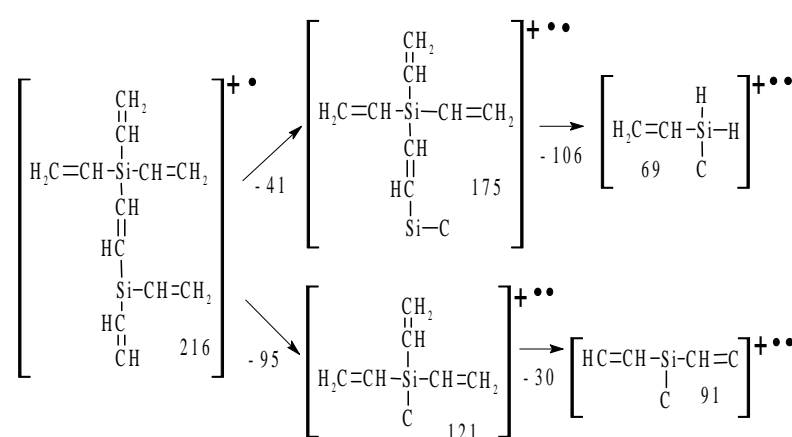


Figure 20: Scheme of a probable fragmentation of the ion-radical formed from TVS at the assumption that peak 216 is molecular ion. Two eventual ion-biradicals could be formed.

From the fragments created in the plasma by electron - monomer collision, the dimer or longer chains or cyclic compound could be formed in the cold trap. In addition, the fragments can react with oxygen and thus trimethoxyvinylsilane like molecules are created. Probable molecules formed on the cold trap walls are given in the Figs. 21 and 22.

It can be appreciated that organosilicon fragments undergoes conversion to many different linear and cyclic compounds. General formula of these compounds could be probably $\text{CH}_3 - (\text{CH}_2\text{SiO})_n - \text{Si}(\text{CH}_3)_3$. Furthermore, analysis by GC-MS confirms that with lower effective power the less number of small fragments is created.

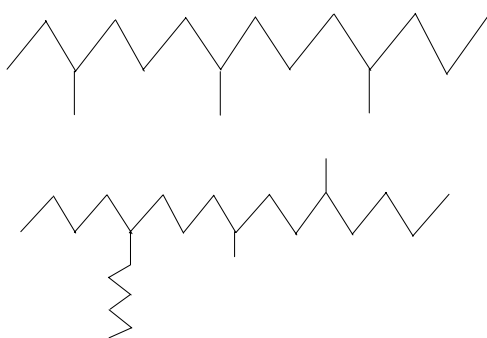


Figure 21: Long chain hydrocarbon identified by GC-MS, W_{eff} during the deposition using TVS was 10 W.

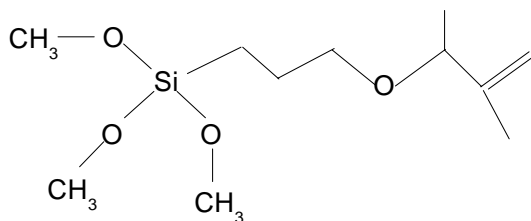


Figure 22: Molecule with the Si-O-Si bonds identified by GC-MS, W_{eff} during the deposition using was 5 W.

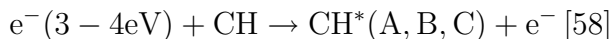
3.4 Analysis by optical emission spectroscopy

3.4.1 Atomic lines and molecular bands

The spectral bands dominating in the spectrum during the deposition processes with all monomers are presented in the table 5. The spectra identification was provided according to the literature [34, 47, 72]. The spectra were recorded mainly at the pulse mode, gas pressure was always about 1 Pa and monomer flow rate was changed from 0 to 2 sccm. Regarding our previous experience, the most preferred monomer flow rate was 0.5 or 0.6 sccm. So, the spectra presented in this section were recorded at these monomer flow rates. Presence of all expected emissions was difficult to distinguish due to mutual overlapping of the spectral bands. The examples of the spectra are presented in Figs. 25, 32 and 34. The radiation of hydrogen Balmer lines (H^α , H^β , H^γ) were observed in all cases. Molecular hydrogen appear in high intensity in the whole spectral range, too. The most intensive peaks appeared at 542, 601, 609, 612, 622, 725 and 835 nm. In general, Fulcher α structure in the range from 520 to 650 nm was very intensive in the spectra.

Besides hydrogen, the CH band of $A^2\Delta - X^2\Pi$ 0-0 vibrational transition strongly emitted at 431 nm in all cases. Furthermore, 0-0 vibration of the CH $B^2\Sigma - X^2\Pi$ system at 390 nm was observed in very low intensity. This band was almost completely overlapped with the 0-0 transition of the nitrogen first negative system $N_2^+(B^2\Sigma_u^+ - X^2\Sigma_g^+)$, in case of oxygen addition to the monomer. The nitrogen is present in the reactor as impurity in negligible amount with respect to the deposition process condition. When the oxygen is added, the excitation and ionisation of nitrogen is probable. Nitrogen appears in the spectrum only at the beginning of deposition process.

The CH bands were used for several calculations in our work. The upper state of CH can be populated from the ground state or by dissociative excitation of vinyl group or (in case of using HMDSO) from dissociative excitation of methyl group. These excitations are described by following reactions.



An example of measured CH band is given in Fig. 23.

We can see also remarkable emission from the C_2 Swan bands, ($d^3\Pi_g - a^3\Pi_u$) transition, $\Delta v = 1, 0, -1$. The most intensive is the band at 516 nm (0-0 transition) and 513 nm (1-1 transition), the bands at 474, 471, 469 nm (transitions 1-0, 2-1, 3-2) are slightly weaker. The C_2 bands emission was the most significant especially during the deposition with VTEO. The upper states of this emission can be populated from the dissociative excitation of vinyl group or from ground state of C_2 molecule by collisions with electrons.

In some cases, C_3 emission at 405 nm was identified. The OH radical (Schuler band, $B^2\Sigma^+ - A^2\Sigma^+$) was observed at 434 nm when some oxygen was present during the deposition. The emission of SiH band was identified at 414 nm only at low effective power and mainly at monomer flow rate higher than 0.9 sccm. Atomic Si lines were not identified and SiO at 241 nm was observed only in very low intensity with the highest integration time.

Moreover, the CO bands are very intensive in the spectra. The stability of the CO at high temperature account its activity as a carbon trap product. But according to the FTIR analysis, the CO takes not part in the polymer creation, the CO is not available

particle	transition	λ [nm]
H ₂	$d^3\Pi_u^- - a^3\Sigma_g^+$	407 - 835
CH	$A^2\Delta - X^2\Pi$ 0-0	431
CO	$B^1\Sigma - A^1\Pi$ 0-0 0-1 0-2 0-3	400 - 600 431 483 520 561
CO	$d^3\Delta - a^3\Pi$ 0-0 1-0 2-0	550 - 650 644 601 564
C ₂	Swan system ($d^3\Pi_g - a^3\Pi_u$) 1-0 2-1 3-2 0-0 1-1	460 - 520 471 489 468 516 513
OH	Schuler band $B^2\Sigma^+ - A^2\Sigma^+$ 0 - 5	434
CHO	Vaidya's hydrocarbon flame bands A ₀	279.6 294.7 311.5 329.8 350.1
CH ₂ O		395 424 435
SiH	$A^2\Delta - X^2\Pi$ 0 - 0	414
SiO	$A^1\Pi - X^1\Sigma$ 0-1	241

Table 5: *The most intensive molecular spectral bands appearing in the spectrum during the thin film deposition. These bands were identified using the HMDSO, VTEO and TVS with oxygen.*

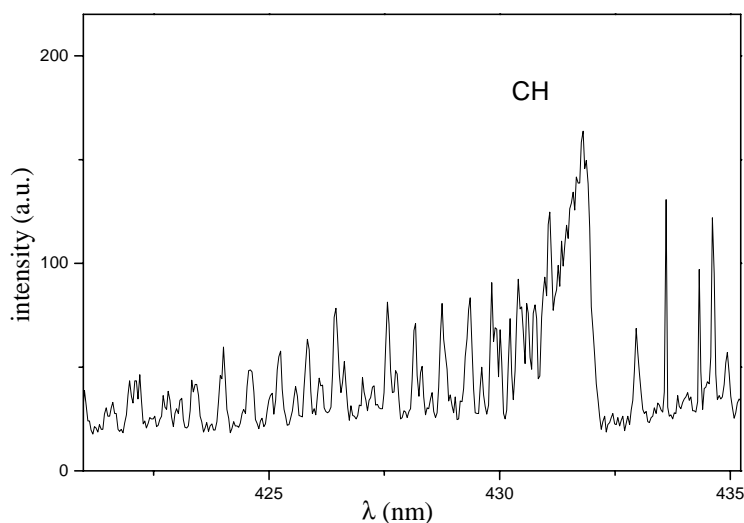
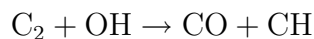
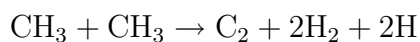


Figure 23: An example of the CH band measured during the deposition process.

for the deposition. Before, it was supposed that CO is not only side product. The main way to the production of the C₂ and CO species could be following [31]:



The CH₃ emission at 216.6 nm (B²A₁ – X²A₂ transition) was expected but it was not measurable in the spectra. The CH₃ as well as CH₂ or Si with SiO are present probably only in their ground state, or it could be lost in the noise because the MS analysis confirmed their presence. The density of these atoms and molecules could be calculated from LIF or UV broad band absorption spectroscopy but these methods are not actually accessible in our laboratory.

3.4.2 The deposition using hexamethyldisiloxane

HMDSO was initially used only for the fibre treatment and later it was applied also for the thin films deposition on the flat substrates. The main part of experiments was carried out in a continuous mode and RF power was changed from 20 to 100 W. Later, it was found that better thin films could be obtained by using lower RF powers or pulse mode. The spectroscopic measurements were provided during both modes. When the continuous mode was applied, the spectra were very complex and hardly identifiable, see Fig. 24. In a pulse mode, the effective power from 0.5 to 25 W was applied. The corresponding spectra are shown in Fig. 25 and in the detail in Fig. 26.

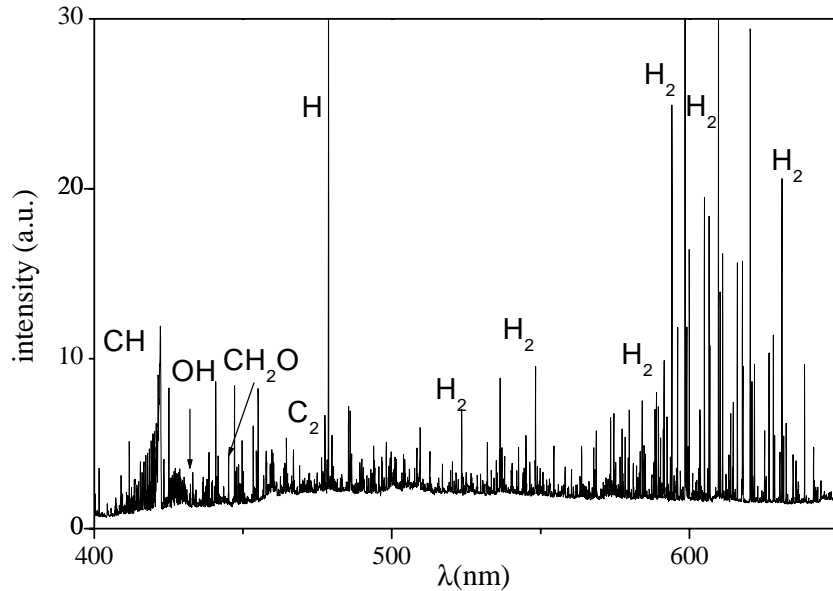


Figure 24: An example of the spectrum measured during the deposition with HMDSO in continuous mode, RF power was 50 W, $Q_{\text{HMDSO}} = 0.6 \text{ sccm}$.

The main difference between spectra obtained during the continuous mode and during the pulse mode was that we identified many CO^+ bands between 218 and 282 nm at pulse mode, especially with lower effective power. Additionally, the CO_2^+ bands at 289 and 288 nm were observed, too.

Regarding the usage of the different monomers, in case of the HMDSO using, the strongest change between spectrum measured during continuous regime and spectrum measured in pulse mode was observed. The CO^+ bands are the most dominant with increasing an effective power. With the effective power decreasing, the total intensity of the spectrum decreases but the emission of CO^+ bands was still relatively strong. The dependence of CO^+ band intensity on effective power is presented in Fig. 28. Its intensity decreases with the increasing effective power while the intensity of CO bands increases.

The CH band intensity decreases slowly with effective power increasing in comparison with the deposition using TVS or VTEO. At effective power reaching the value higher than 5 W, the CH band intensity is more or less constant or we can note its small decrease.

The H^α intensity compared with the intensity of the whole spectrum is plotted in the Fig. 27 as a function of HMDSO flow rate. The H^α intensity increases with a monomer flow rate. With increasing monomer flow rate, the larger fragments appear in the spectrum but in very low intensity. Thus, the total intensity of the spectrum is lower.

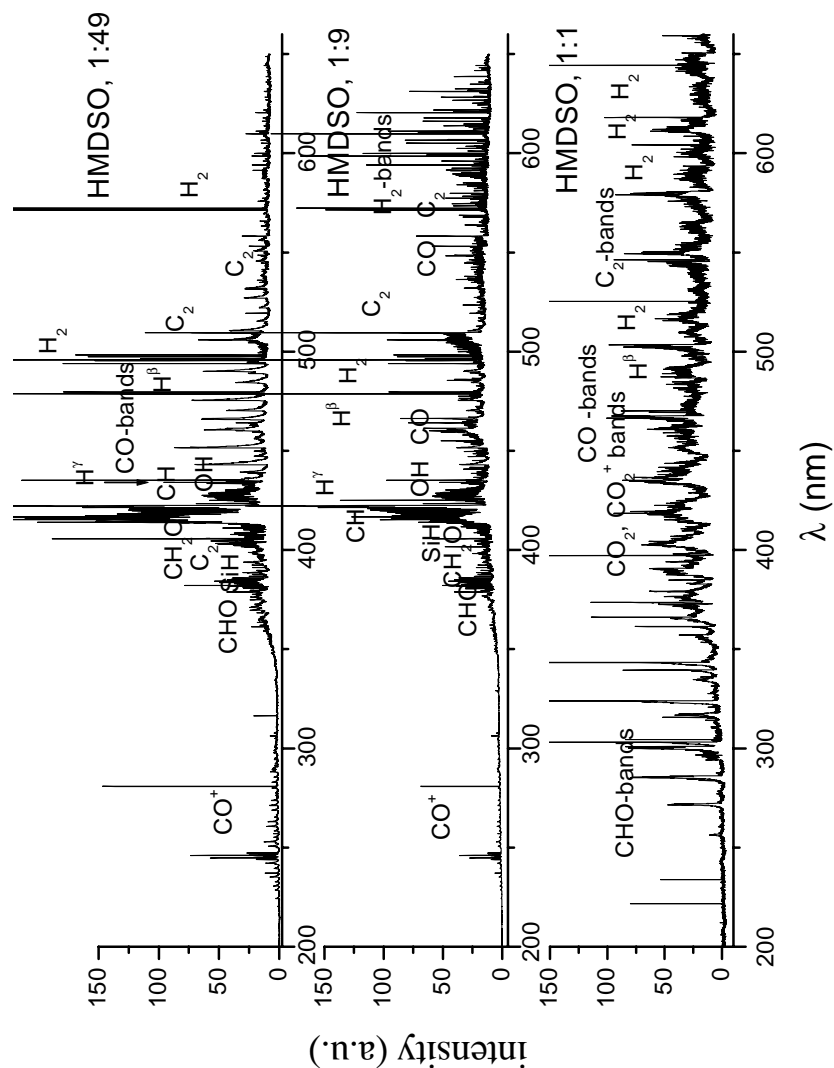


Figure 25: An example of the OE spectrum measured during the deposition with HMDSO at three different effective powers $W_{\text{eff}} = 1 \text{ W}$, 5 W and 25 W , $Q_{\text{HMDSO}} = 0.65 \text{ sccm}$.

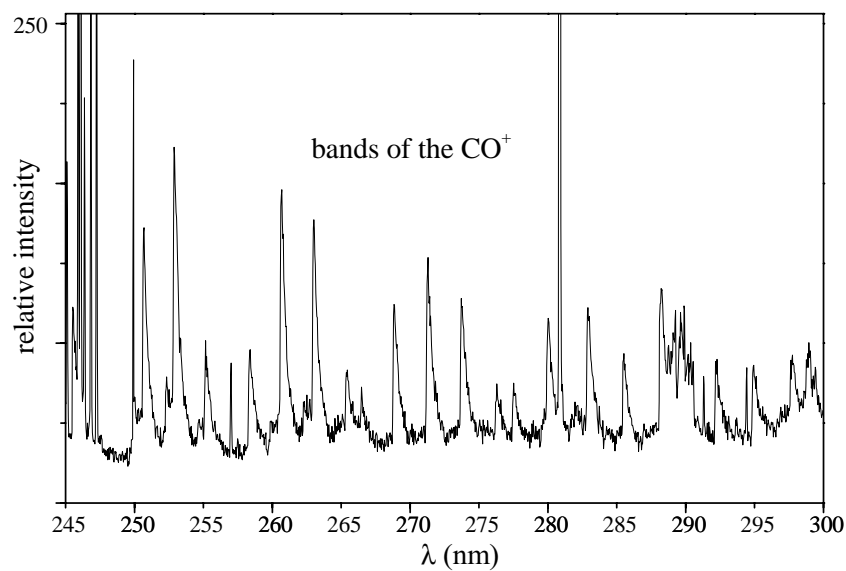


Figure 26: An example of CO^+ bands, $W_{\text{eff}} = 2.5 W$, $Q_{\text{HMDSO}} = 0.6 \text{ sccm}$.

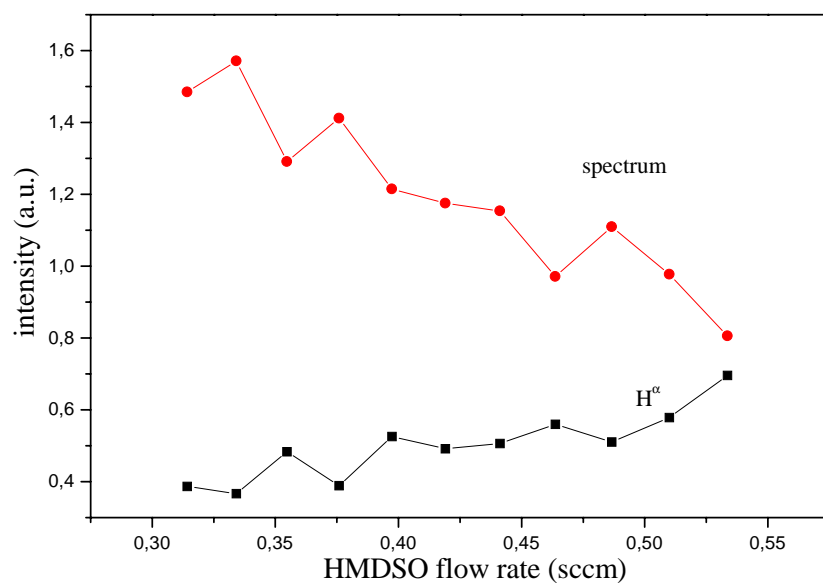


Figure 27: Spectrum integral intensity in the range from 300 to 700 nm and the H^α line intensity as a function of the monomer flow rate. The whole spectrum intensity is divided by factor 10 and intensity of hydrogen line is related to the whole spectrum intensity.

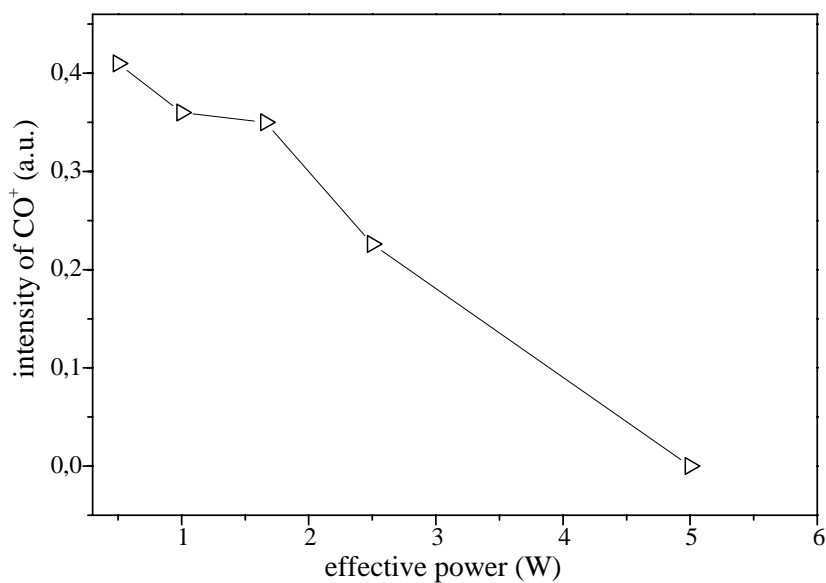


Figure 28: Intensity of the CO⁺ bands as a function of the effective power, $Q_{\text{HMDSO}} = 0.65 \text{ sccm}$.

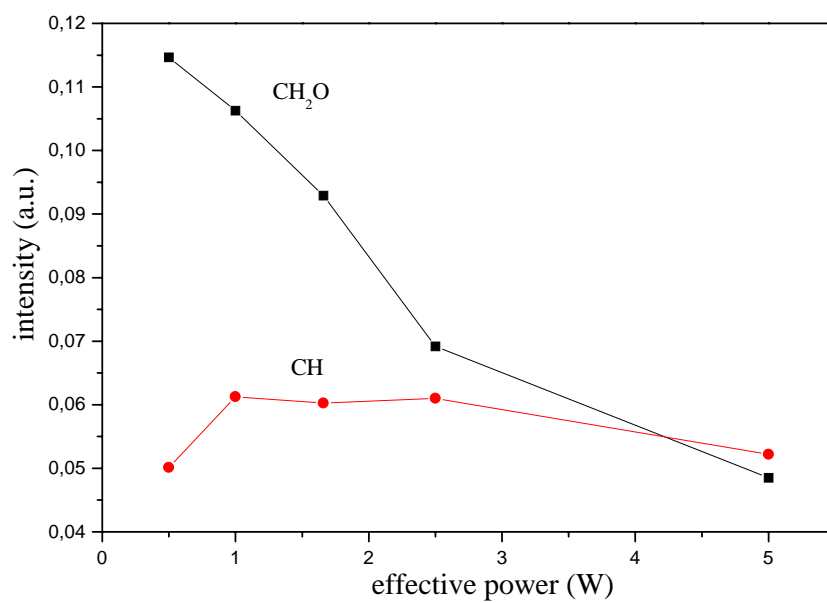


Figure 29: Relative intensity of the CH and CH₂O spectral bands as a function of the effective power $Q_{\text{HMDSO}} = 0.65 \text{ sccm}$.

Bands and lines observed during the deposition in microwave plasma

In the next part, the film deposition in a microwave discharge was investigated. After the problem solving with the overheating of the MW device, it was possible to record the spectra during the deposition process using HMDSO as a monomer. The deposition time was fixed at 3 minutes. The increasing of the power leads to an enhancement of the electron density and to increasing of deposition rate. However, we have not managed to protect the device from the impurity, thus, many bands of nitrogen were observed in the spectrum. The overlapping by nitrogen bands complicate the other bands identification, see Fig.30. In comparison with the measurements during the deposition in RF-inductively coupled plasma, the OH at 306 nm and SiO bands at 230 nm were observed in UV region and at 525 and 536 nm the bands of O_2^+ appeared. CN bands also appeared in the spectrum at 388, 419 and 457 nm.

In the microwave plasma, the electron energy is quite high. On the other hand, the ion energy is not sufficient for ion-bombardment of the substrate surface, which is very important for the deposition of thin films with desired properties. Degree of the dissociation is very high, thus, there are the missing spectra of larger molecules. The properties of thin films prepared in MW discharge will be a subject of further studies. It is well known that oxygen and O_2^+ can be responsible for the plasma etching of C and H from the layers, even if high power seems to slightly improve the quality of the layers [32]. It is necessary to improve the control the deposition condition in MW plasma.

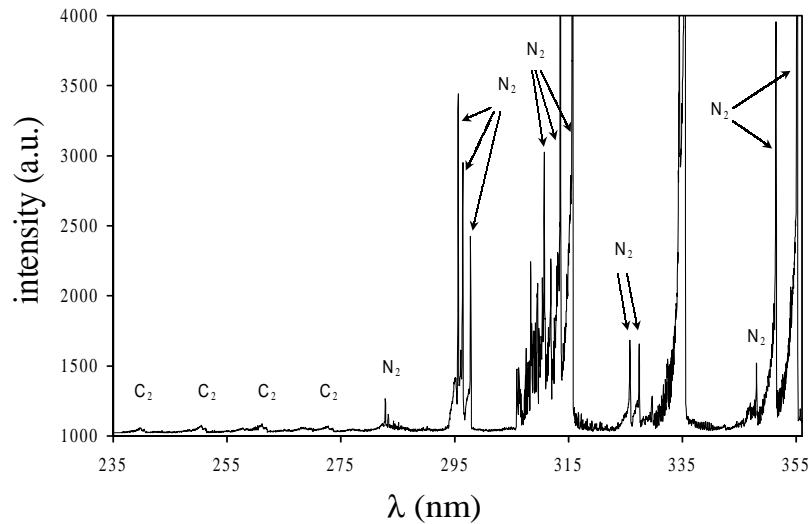


Figure 30: An example of the spectrum obtained during the deposition in MW plasma, $W_{\text{eff}} = 100W$, $Q_{\text{HMDSO}} = 2 \text{ sccm}$, [4].

The comparative measurements using the HMDSO monomer that were done during the deposition in the capacitively coupled plasma at the Department of Physical Electronics shows that the $H_2 - \text{Fulcher } \alpha$ structure and CO bands are dominant in the spectrum.

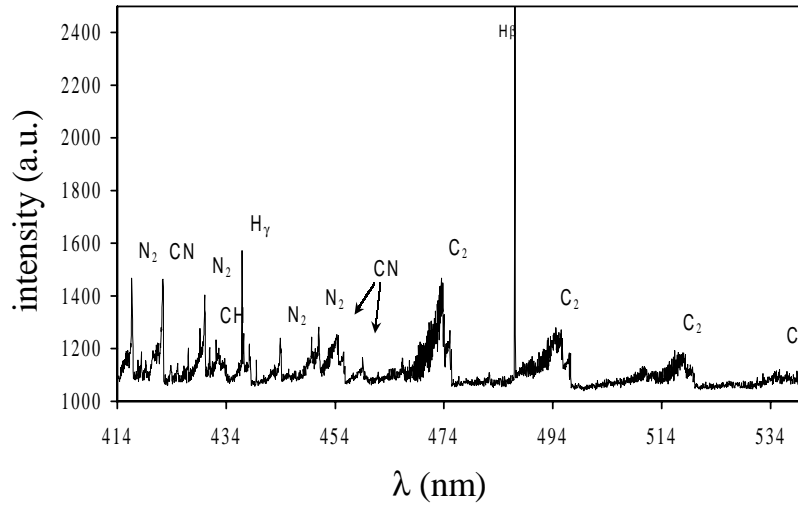


Figure 31: An example of the spectrum obtained during the deposition in MW plasma, $W_{\text{eff}} = 100\text{W}$, $Q_{\text{HMDSO}} = 2\text{ sccm}$, [4].

On the contrary, it was difficult to distinguish the CH bands. When the oxygen was added, the strong emission of O at 777 and 840 nm and OH at 306 nm were observed. For the lowest oxygen flow rate (2 sccm) and long integration time, the Si and SiO bands were determined. In general, it was confirmed what we supposed. By OES measurements, it is possible to estimate the deposition mechanism directly during the depositions. The detailed analysis of the spectroscopic measurements as well as the Langmuir probe measurements and this discharge type characterisations are described in [10].

3.4.3 The deposition using vinyltriethoxysilane

When the VTEO was used, it was possible to control an amount of disappearing oxygen. The oxygen from ethoxy group was forming CO molecule. At higher effective power, whole CH_2O group appeared in the spectrum. But these larger molecules are expected at lower effective power and their presence at higher effective power is rather surprising. The CH_2O group is probably built into the polymer film at lower effective power. The SiO bands were possible to identify at low effective power (the most visible they are under 2.5 W) and with high monomer flow rate of about 1 sccm. Spectra had to be recorded with very high integration time (50 s). In Fig. 32 are presented the examples of spectra obtained during the deposition. The spectrum recorded at the highest effective power is similar to the HMDSO spectrum measured at the same discharge conditions. With changing the effective power, the great step in character of the spectra occurs at the pulse mode 1:19 (2.5 W) while for other monomers it happen at pulse mode 1:9 (5 W). That is why we presented the spectrum measured at this effective power. Between pulses 1:19 and 1:49, only negligible changes were observed in the spectra. At the pulse mode 1:99 (0.5 W), we identified additionally the SiC_2 , relatively intensive SiO, Si_2 , C_2 and CH bands. The intensity of these bands was related to the whole spectrum intensity in the

range from 350 to 600 nm and it was higher than the band intensities obtained from the spectra measured at higher effective powers.

The dependences of hydrogen line and CH band intensity on the effective power are shown in Fig. 33. Both intensities increase with increasing effective power. The evolution of CO intensity is similar like in the case of HMDSO using. It means that with the effective power increasing, the intensity of the CH, hydrogen and CO bands increases and in the same time, a lot of these groups are lost from the prepared ppVTEO with the increasing effective power.

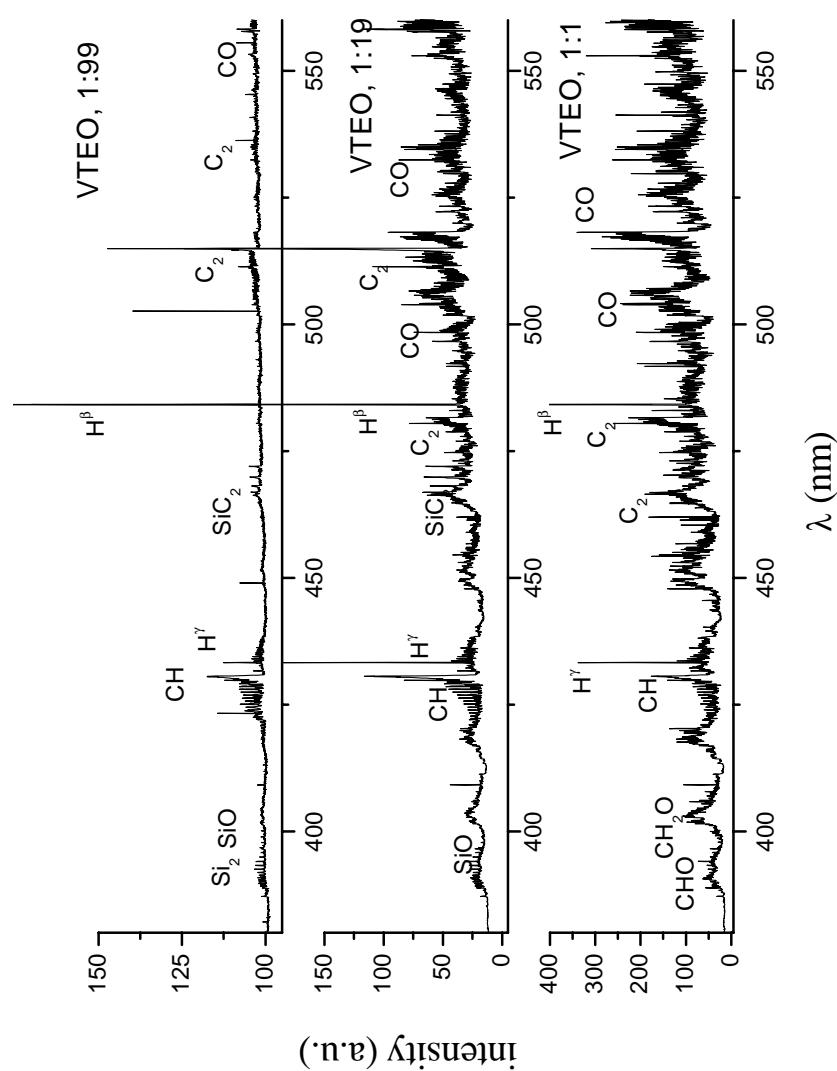


Figure 32: An example of the OE spectrum measured during the deposition with TVS, $W_{\text{eff}} = 25 \text{ W}$, 2.5 W and 0.5 W .

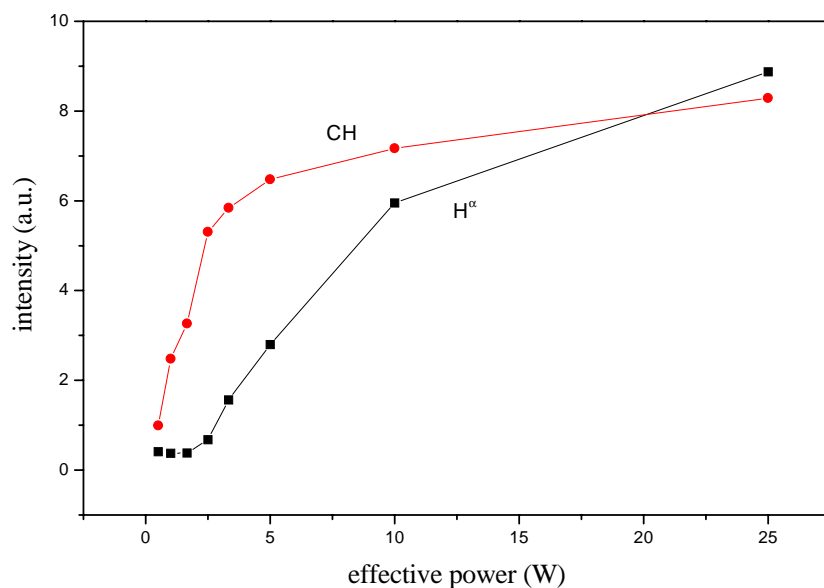


Figure 33: Dependence of the spectral band intensities on the effective power, $Q_{\text{VTEO}} = 0.7 \text{ sccm}$, $W_{\text{eff}} = 10 \text{ W}$ (pulse mode 1:4).

3.4.4 The deposition using tetravinylsilane

As the last monomer, the TVS was tried because of its interesting properties. It contains four vinyl groups, so, better adhesion to polymer matrix was expected. It was also possible to control oxygen amount in the layer by changing effective power and additional oxygen flow rate. Interesting changes in the spectra are visible during the deposition with TVS. The intensity and appearance of different bands are strongly depending on the pulse mode. The H_2 and CO bands appeared at the another wavelength. Furthermore, it was found that for the pulse duration 1:19 ($W_{\text{eff}} = 2.5 \text{ W}$), the fragments of monomer begin reaction with the residual oxygen that is present in the reactor from the leakage. Therefore, the $\text{C} = \text{O}$ and also $\text{Si} - \text{O}$ bounds are created and built in the plasma polymer on the substrate. But the CO bands have been not identified in the spectrum in that case. Using TVS with oxygen we observed CHO bands at 295, 311, 329 and 347 nm and also bands of second and first positive system of nitrogen and NH as impurities.

The examples of spectra measured during the deposition you can see in Fig. 34. The spectral band intensities in comparison with the thin film properties will be discussed later.

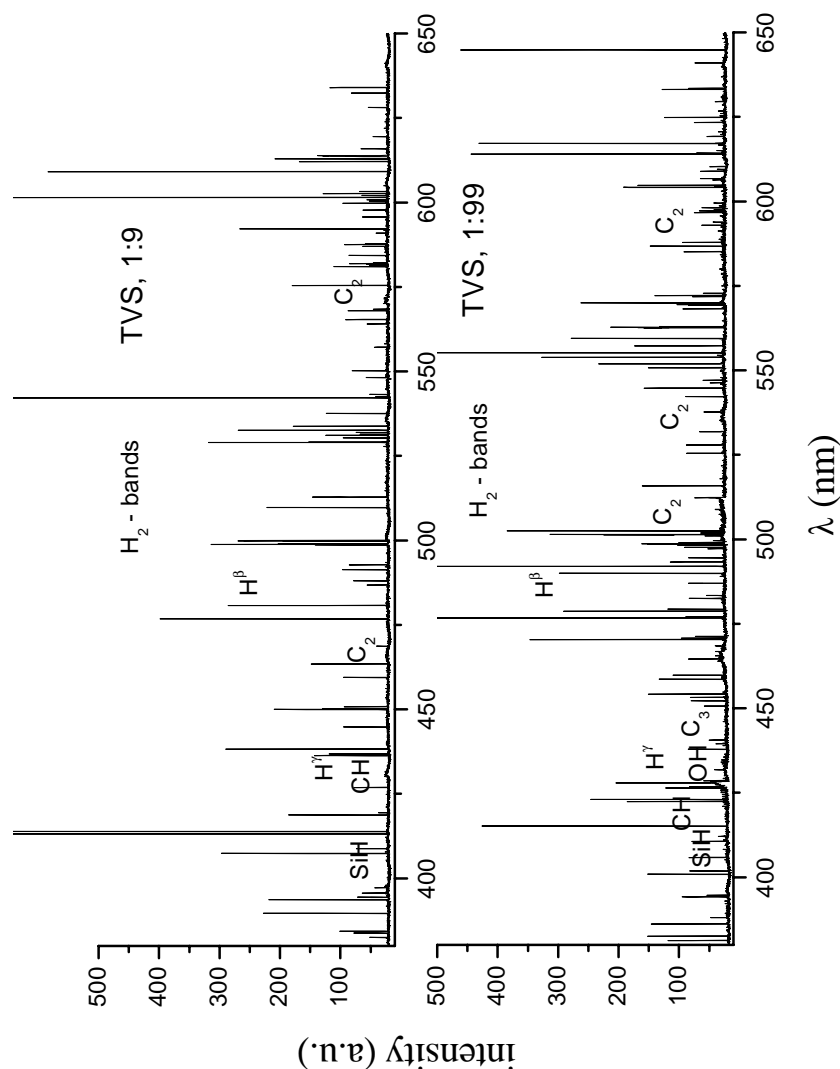


Figure 34: An example of the OE spectrum measured during the deposition with TVS, $W_{\text{eff}} = 5 \text{ W}$ and 0.5 W .

When very low effective power (0.1 W) was applied during the deposition, the emission of oxygen and CO_2^+ was observed, even when no oxygen was added to monomer. The molecular hydrogen lines are very intensive. Using effective power of 0.5 W, there are no peaks of oxygen, CH appears in very low intensity.

The dependence of CH band intensity as a function of effective power is given in the Fig. 35. At the effective power reaching the value higher than 5 W, The CH band intensity is more or less constant, only small decrease can be noted at the highest effective power.

As it is shown in Fig. 35, the SiC_2 band intensity decreases with effective power. Si – C bond is stable only at lower effective powers, thus, this decrease can be caused by bond dissociation and by oxidising reaction in plasma volume.

The absence of Si lines in the spectrum suggest that the molecule of monomer is not

completely dissociated. But the results from MS and FTIR show that the monomer was probably completely dissociated in the case of the highest effective power. Therefore, it is possible that Si undergo directly to the reactions on the substrate or on the reactor walls. They can also form the SiC_2 or SiH which are visible mainly at the lowest effective power.

Using TVS as monomer, the best substrate position was looking for. Therefore, the variation of the relative density and intensity of spectral bands along the plasma discharge during the deposition using TVS was monitored. The effective power was 10 W, with pulses 1:4. The points of measurements are shown in the experimental part. The dependences are given in Figs. 36 and 37. These pictures show the dependencies of the most intensive bands on the position read and also very important SiH band intensity is plotted there. Regarding the thin film properties, the Si content is very important. The picture show that SiH and CH band intensities are the lowest in the centre of the discharge. These particles probably undergo the reactions on the substrate surface, they could be built into the polymer structure. It is also possible that CH depletes for CO molecule creation. The intensity of CO is relatively strong in the discharge centre.

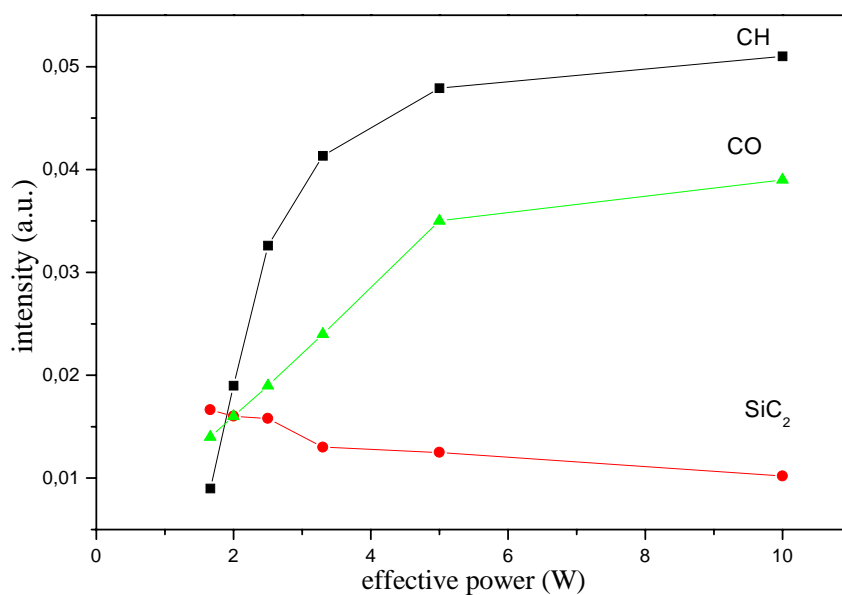


Figure 35: Dependence of the selected spectral band intensities on the effective power, $Q_{\text{TVS}} = 0.7 \text{ sccm}$.

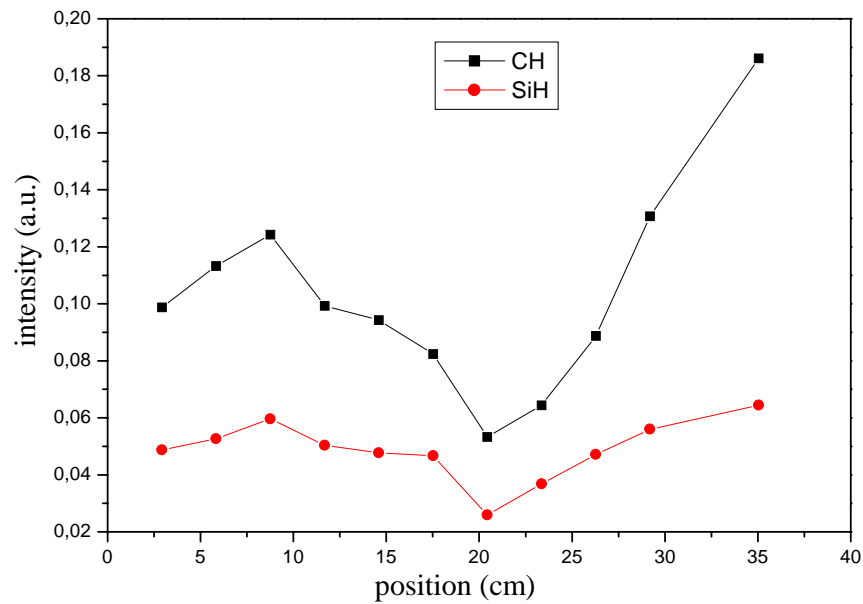


Figure 36: *Relative intensity of the CH and SiH bands evolution along the plasma discharge, $W_{\text{eff}} = 10 \text{ W}$, $Q_{\text{TVS}} = 0.5 \text{ sccm}$. The discharge centre is between 14 and 24 cm in the x-axis.*

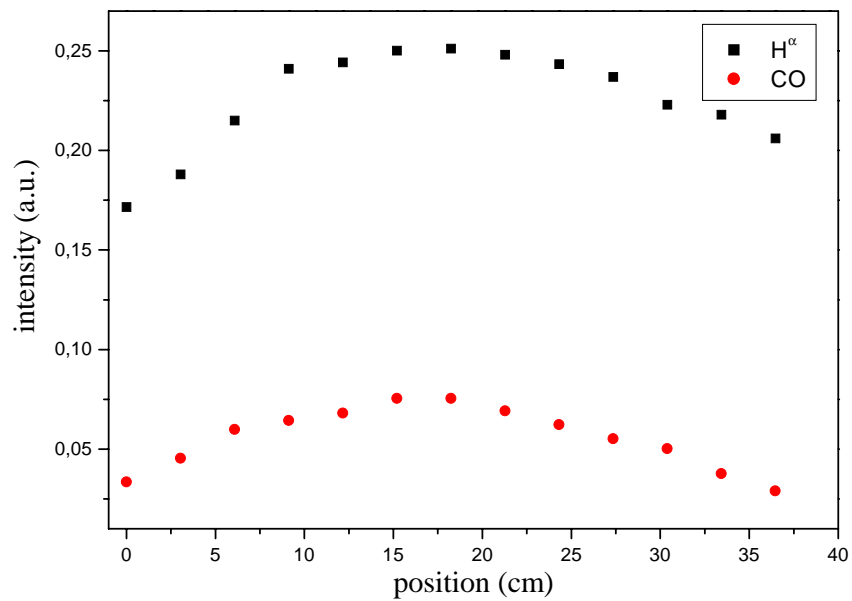


Figure 37: *Relative intensity evolution along the plasma discharge, $W_{\text{eff}} = 10 \text{ W}$, $Q_{\text{TVS}} = 0.5 \text{ sccm}$. The discharge centre is between the points 14 and 24 in the x-axis.*

3.4.5 The rotational, vibrational and electron temperature

For CH (A state) we found the rotational temperature T_{rot} from 300 to 550 K and vibrational temperature T_{vib} changed from 2800 to 5000 K, depending on the point of measurement along the reactor. From the simulation of nitrogen, lower temperatures were determined, as it is shown in Fig. 39. The rotational temperature calculated from the simulation of CH molecules was always little higher than the temperature calculated from the simulation of nitrogen transition by using the program Simul1.4. An example of the comparison of the experimental and simulated spectrum is plotted in the Fig. 38. The evolution of the rotational and vibrational temperatures along the plasma discharge are presented in Fig. 40 and 41. In the Fig. 40 you can see the evolution of the rotational temperature of several vibrational transition of the first and second positive system of nitrogen. Effective power during these measurements was 10 W, the T_{rot} varies from 280 to 540 K. The same evolution shapes were obtained also for the vibrational and electron temperatures as show Figs. 41 and 44.

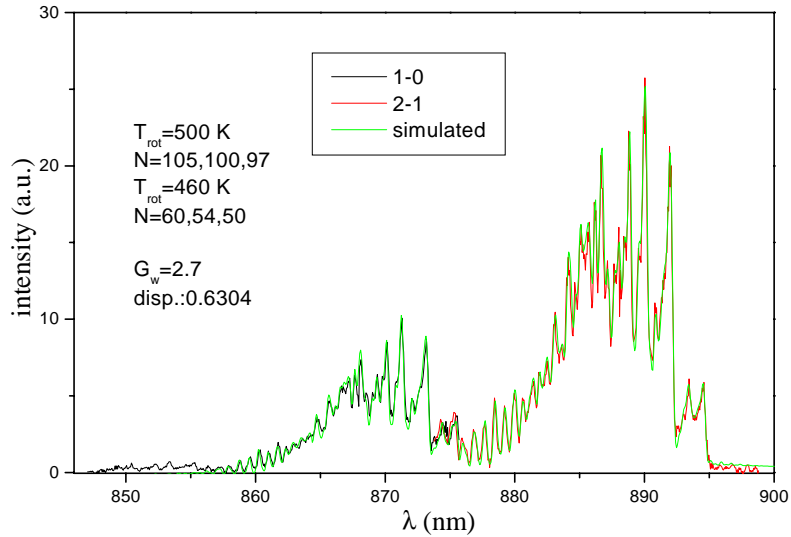


Figure 38: An example of the measured and simulated spectrum of nitrogen first positive system, $B^3\Pi_g - A^3\Sigma_u^+$, $W_{eff} = 10$ W, $Q_{TVS} = 0.5$ sccm, the error of measurement is ± 50 K.

The disadvantage of the temperatures determination from the optical emission spectra is that the temperatures from the excited state emission are substantially higher than those determined from the ground state population. The ground states are not removed by quenching but only by chemical reactions which have slower rates. Therefore, they have rotational and vibrational state distribution which corresponds better to the real gas temperature.

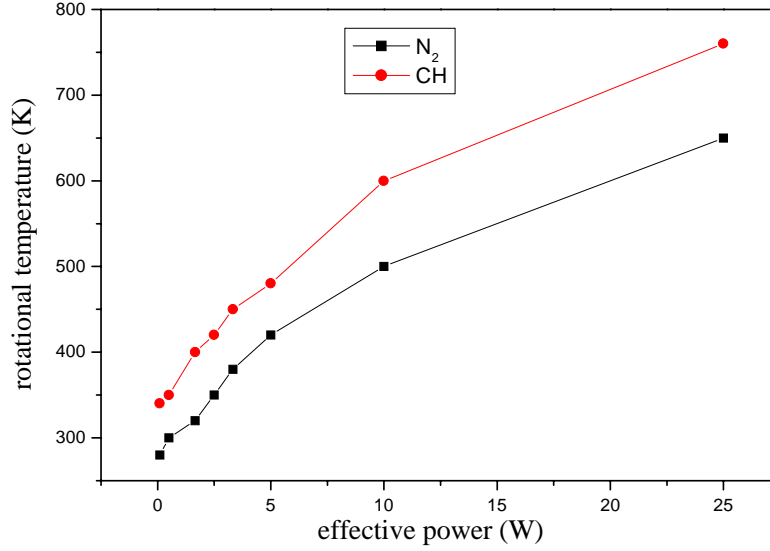


Figure 39: Comparison of the rotational temperature evolution calculated from the simulation of the the CH and N₂, $Q_{\text{TVS}} = 0.6$ sccm, $W_{\text{eff}} = 10$ W. The measurements were provided near the discharge centre 15 cm from the point 0, see Fig. 8.

The temperatures increase with an effective power. Electron temperature decreases with increasing monomer flow rate, see Fig. 46. It is the highest during the deposition using VTEO when it varies from approximately 2 to 3 eV. For HMDSO and TVS, the electron temperatures are between 1 and 2.5 eV and T_e is higher in the case of HMDSO. The temperature increases with the increasing effective power, and at 2.5 W we can observe some "skip" in the plot. At this effective power, the changes in the character of spectra and in thin film properties are observed, too. Thus, this skip in the electron temperature value could relate to the different character of the deposition mechanism.

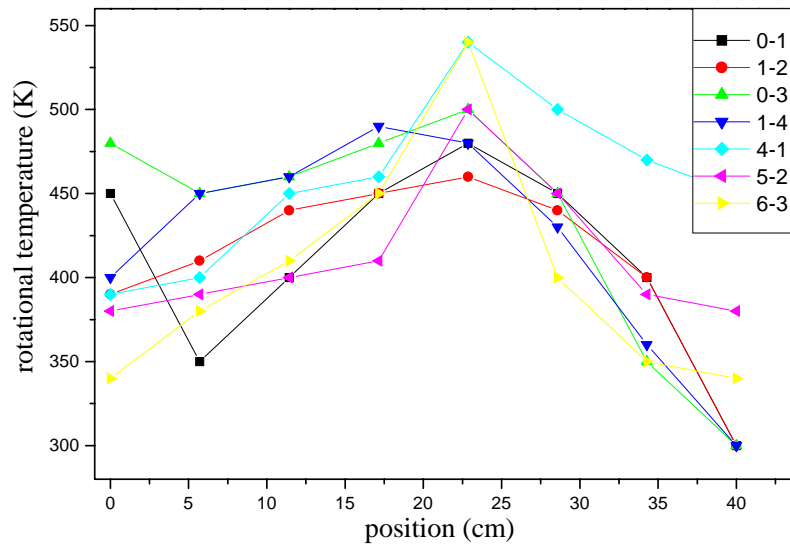


Figure 40: Rotational temperature as a function of position read, along the plasma discharge, $W_{\text{eff}} = 10 \text{ W}$, $Q_{\text{TVS}} = 0.5 \text{ sccm}$, the error of measurement is $\pm 50 \text{ K}$. The transitions 0-1, 1-2 and 2-3 were taken from the second positive system and the rest of the transitions belong to the first positive system of nitrogen, The discharge centre is between 14 and 24 cm in the x-axis.

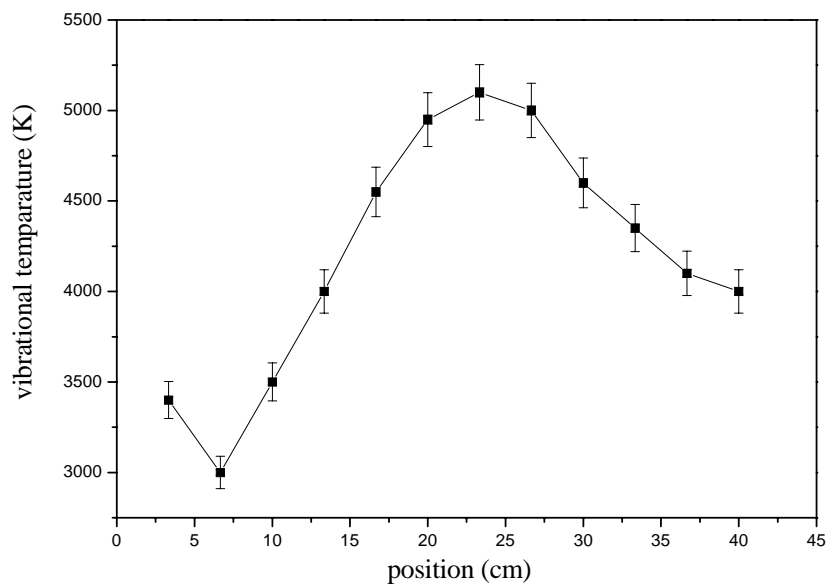


Figure 41: Vibrational temperature as a function of position read, $Q_{\text{TVS}} = 0.6 \text{ sccm}$, $W_{\text{eff}} = 10 \text{ W}$, The discharge centre is between 14 and 24 cm in the x-axis.

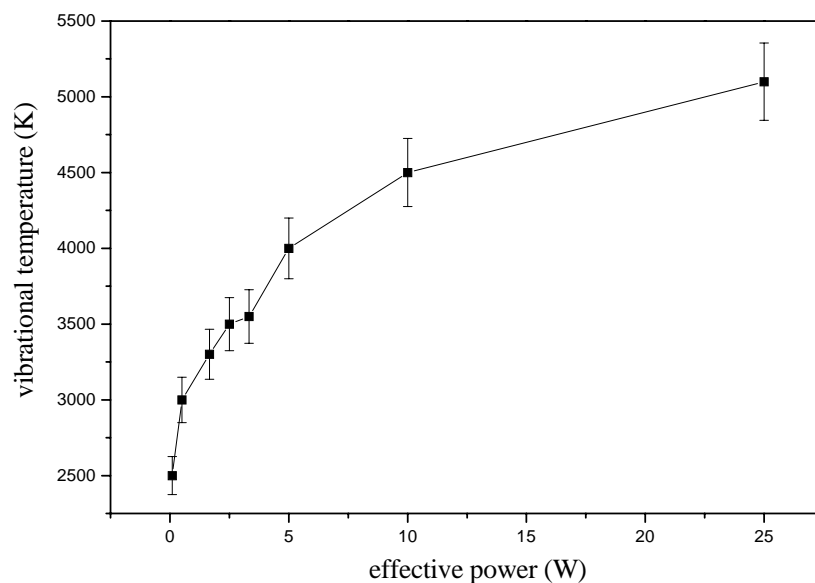


Figure 42: *Vibrational temperature as a function of effective power, $Q_{\text{TVS}} = 0.6$ sccm. The measurements were provided near the discharge centre 15 cm from the point 0, see Fig. 8.*

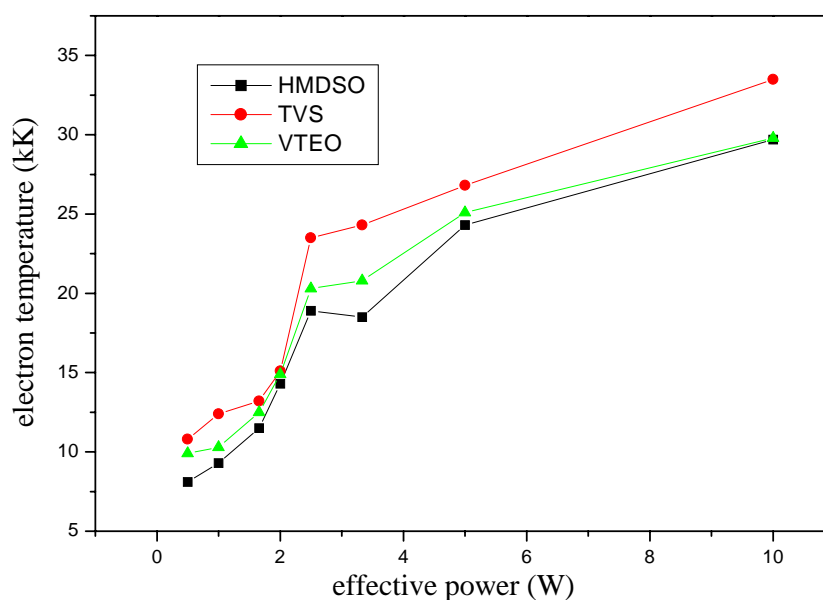


Figure 43: *Electron temperatures as a function of effective power, the monomer flow rate was 0.6 sccm. The measurements were provided near the discharge centre 15 cm from the point 0, see Fig. 8.*

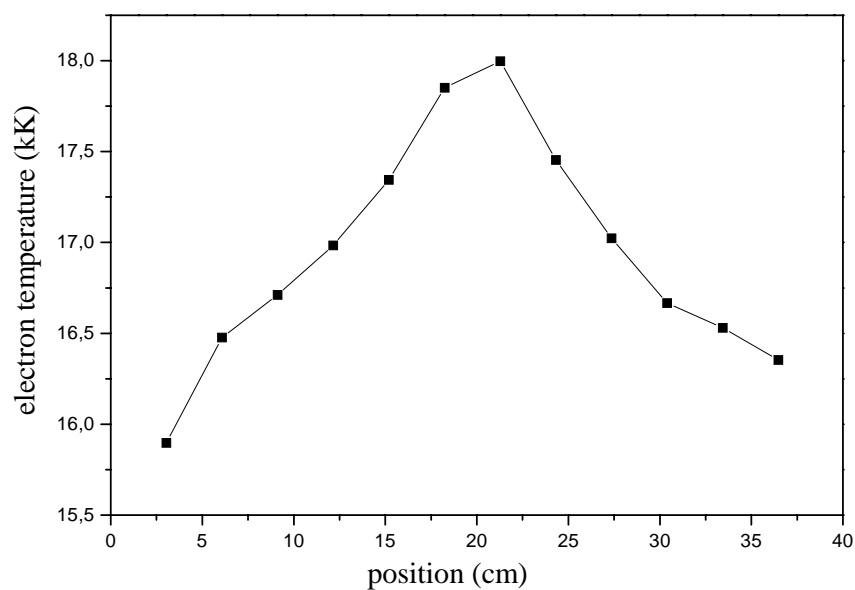


Figure 44: *Electron temperature evolution along the discharge, $Q_{\text{TVS}}=0.6\text{sccm}$, $W_{\text{eff}} = 10\text{ W}$, The discharge centre is between 14 and 24 cm in the x-axis.*

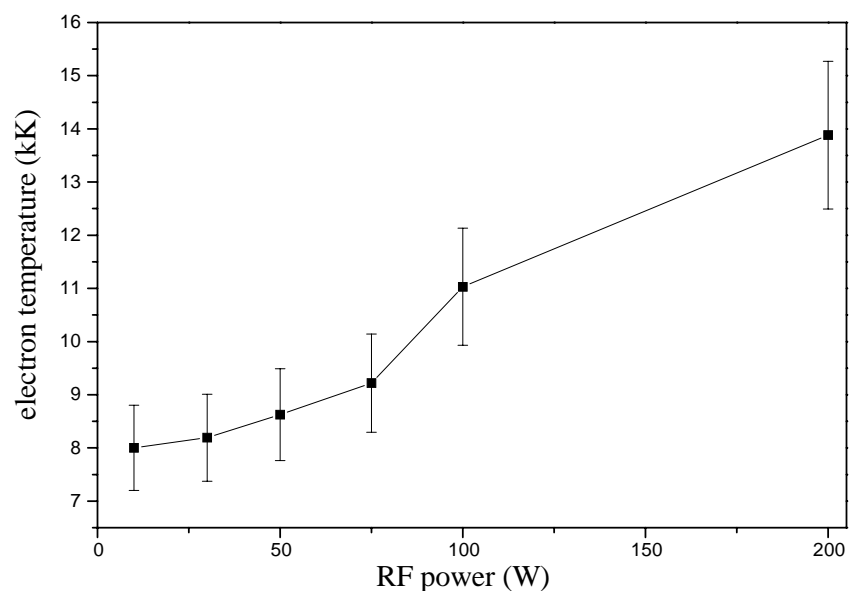


Figure 45: *Electron temperature as a function of total power in a continuous mode, $Q_{\text{VTEO}} = 0.6\text{sccm}$. The measurements were provided near the discharge centre 15 cm from the point 0, see Fig. 8.*

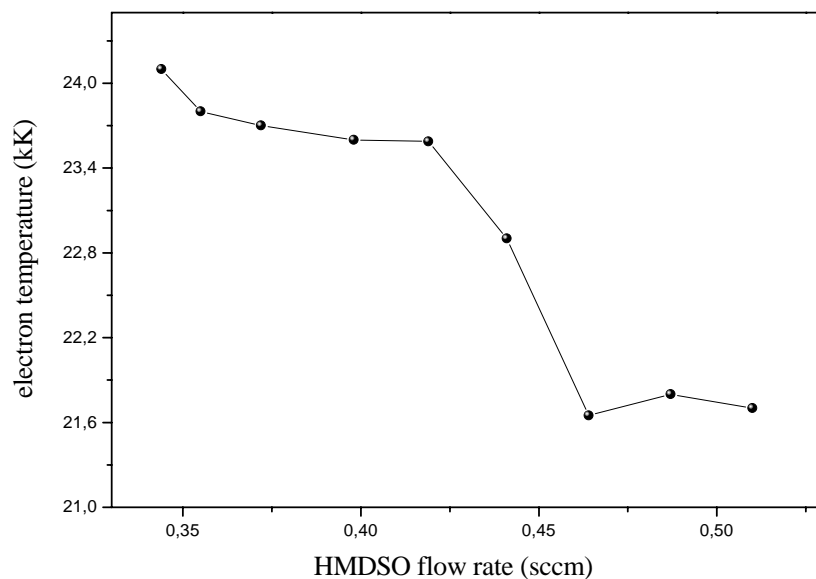


Figure 46: *Electron temperature as a function of monomer flow rate during the DLC films deposition in a continuous mode, total power was 25 W.*

3.4.6 Electron concentration

The Fig. 48 shows the dependence of electron concentration on the position read along the discharge during the deposition. The electron density decreases between the points 3 and 10 of the position read. This is probably caused by the presence of negative ions that are created near the discharge centre or large negatively charged particles or formation free ion-radicals by electron impact. Electrons could be repulsed by negative ions and attracted to the positively charged flange, thereby, the higher electron concentration on the down-stream of the discharge could be explained. The results show that density in the middle of the discharge varied from $1,31$ to $1,36 \cdot 10^{13} \text{ e}^{-}\text{cm}^{-3}$. The different evolution was found for the electron temperature, see Fig. 44. It is the highest in the discharge centre.

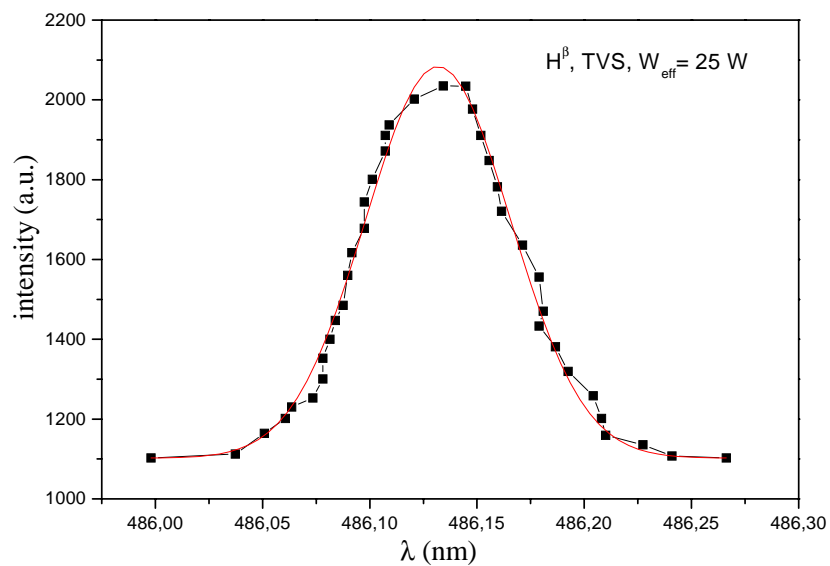


Figure 47: An example of the H^β line profile used for the calculation of electron concentration, $Q_{\text{TVS}} = 0.8 \text{ sccm}$, $W_{\text{eff}} = 25$ W.

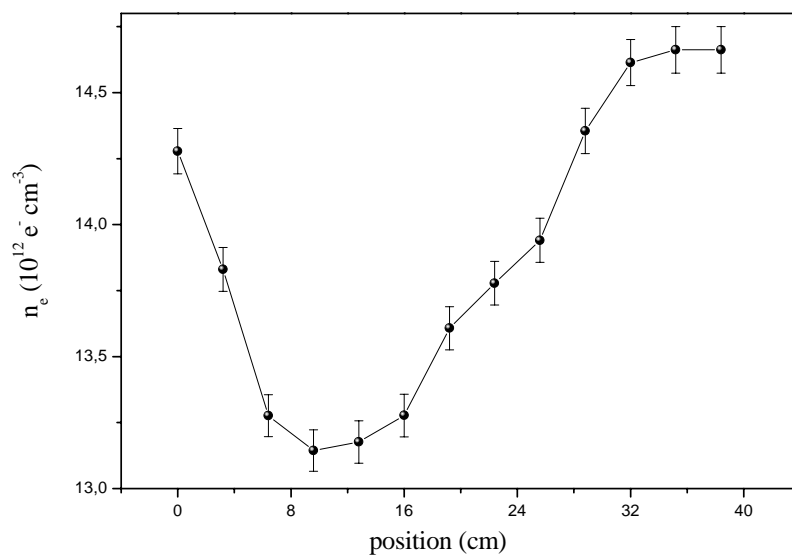


Figure 48: Electron density evolution along the discharge, $Q_{\text{TVS}} = 0.8 \text{ sccm}$, $W_{\text{eff}} = 25$ W, The discharge centre is between 14 and 24 cm in the axis-x.

3.4.7 Results from actinometric measurements

The VTEO and TVS were the most useful polymer precursors (more than HMDSO), in term of required properties of the created plasma polymers. Therefore, the variations of the actinometric signal in VTEO, TVS and TVS with oxygen plasmas were studied as a function of the effective power and monomer flow rate. Argon flow rate during the measurements was kept constant at 0.02 sccm and working total gas pressure was 0.9 Pa. As we expected, actinometric signals of the monitored particles mostly increase with the increasing effective power.

At higher VTEO flow rate, the concentration of atomic oxygen [O] decreases. The highest value of [O] was found for the monomer flow rate of 0.5 sccm while for the flow rate of 1.5 sccm it is relatively low. It could be caused by reduction of oxygen or by its consumption by a redox reactions near the substrate surface. Additionally, CO and CO₂ molecules are created, and thus the atomic concentration further decreases. When the oxygen was added, the sharp increase of I_O/I_{Ar} was observed while the I_{CH}/I_{Ar} ratio decreases. This decrease is probably caused by CO creation in the plasma.

It was found in previous studies [2] that the optimum monomer flow rate for the good-quality films is in the range 0.5 - 0.7 sccm. It is better when the oxygen amount takes only a few percent of the working gas mixture [64]. The dependence of the actinometric signal on the oxygen flow rate at different effective power is given in Fig. 51.

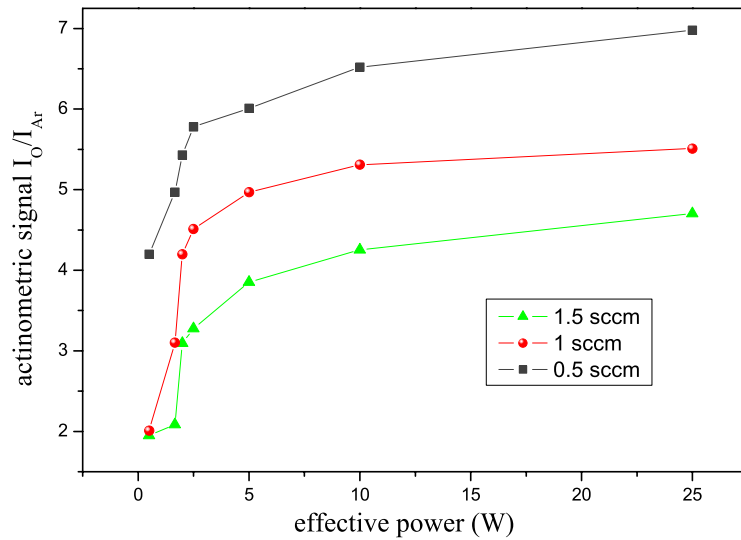


Figure 49: Actinometric signal (oxygen at 844 nm to argon at 750 nm intensity ratio) as a function of the monomer flow rate during the deposition with VTEO. The measurements begin at the monomer flow rate 0.5 sccm what is the optimum flow rate for the depositions.

Actinometric measurements were carried out also during the deposition using TVS and TVS with oxygen. In that case, we could have up to 10 % of oxygen in the gas

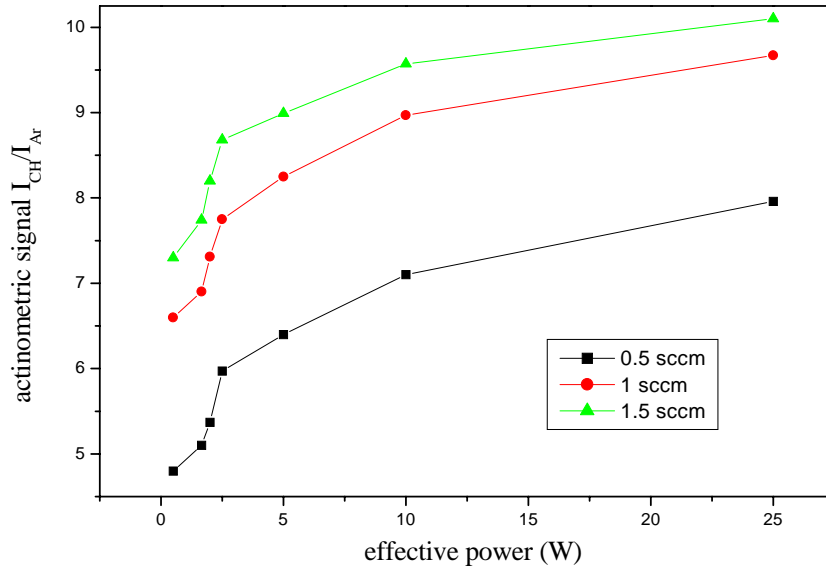


Figure 50: Actinometric signal of CH band at 431 nm (related to the Ar line at 697 nm) as a function of the monomer flow rate during the deposition with VTEO.

mixture to obtain required thin films. During these measurements, the similar results as in previous case (using VTEO) were found, as it is shown in Fig. 52. But the actinometric signal of oxygen decreases. It is probably built into the layer as Si – O – Si or Si – O – H groups, and simultaneously it could flow out through the CO or CO₂ that are created as in the case of the VTEO using. In the Fig. 53 we can see that the actinometric signal of CH, hence, its concentration is almost the same like in the case of TVS without oxygen. When the effective power reaches the value of 10 W, the shape of the dependence is less sharp than those in the case of the pure TVS. Actinometric signal of hydrogen is a little higher. If the energy is sufficiently high, the C – H bonds can be destroyed and thus the OH signal decreases and on the contrary, the CO emission significantly increases. Hydrogen probably comes from dissociated C – H bonds and we can suppose that it is also flown out like the CO. The second possible way of hydrogen removal is OH group creation. Anyway, as we will see later, oxygen content in the layer decreases with the increasing effective power. Therefore, in this case the OH species are not participating in the polymerisation.

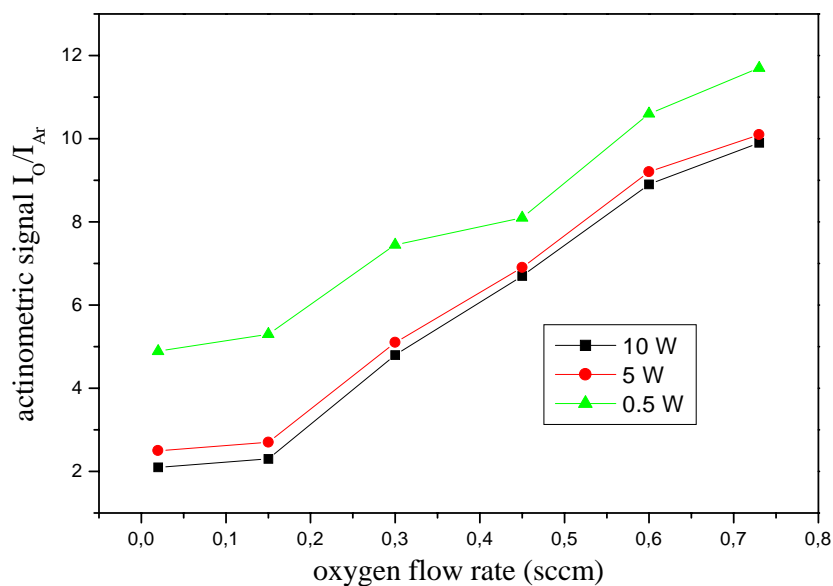


Figure 51: Actinometric signal as a function of the oxygen flow rate during the deposition using TVS with oxygen addition.

According to the calculations mentioned in the section *Experimental data treatment*, the oxygen concentration during the deposition at the standard conditions was estimated. The standard conditions mean that the measurements were done 4 cm downstream from the discharge centre at effective power 5 W and monomer flow rate of 0.5 sccm. [O] was estimated at $2.6 \cdot 10^{10} \text{ cm}^{-3}$, for the TVS as a monomer and 10% of oxygen addition. For the deposition using VTEO it was $3.9 \cdot 10^{10} \text{ cm}^{-3}$. Using HMDSO it was about $6 \cdot 10^{10} \text{ cm}^{-3}$, and in that case, the concentration stays almost constant with the increasing effective power. The concentration of hydrogen and CH were estimated too. The value about $1.4 \cdot 10^{11} \text{ cm}^{-3}$ was found for the deposition using the TVS, $9.8 \cdot 10^{10} \text{ cm}^{-3}$ for the deposition with the VTEO and $1.2 \cdot 10^{11} \text{ cm}^{-3}$ for the deposition with HMDSO.

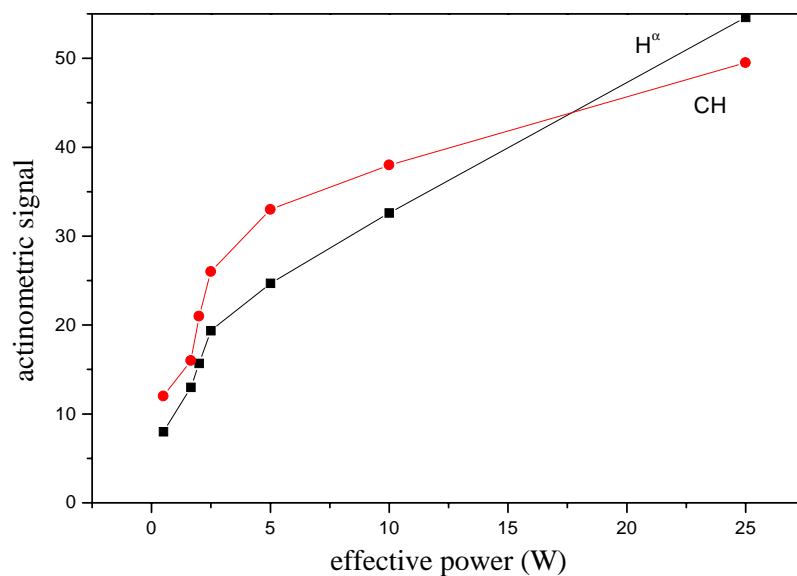


Figure 52: Actinometric signal (intensities of the hydrogen line at 656 nm and the CH band at 431 nm to argon line intensity ratio) as a function of the effective power during the deposition with TVS, $Q_{\text{TVS}} = 0.5$ sccm .

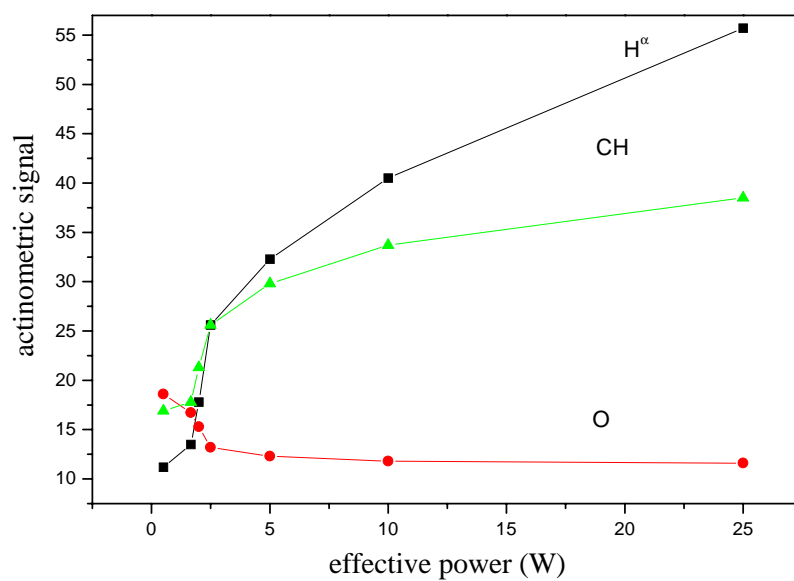


Figure 53: Actinometric signals as a function of the effective power during the deposition using TVS with oxygen addition, $Q_{\text{gas}} = 0.85$ sccm, $Q_{\text{O}_2} = 0.35$ sccm.

3.4.8 Influence of oxygen addition

F_{TVS} (sccm)	F_{O_2} (sccm)
0.44	0.05
0.38	0.12
0.32	0.21
0.25	0.31
0.18	0.38
0.12	0.46

Table 6: Monomer and oxygen flow rates during the deposition using TVS with oxygen addition. In the other cases, oxygen was added up to 10 % of the total gas flow rate.

The strong effect of oxygen addition on the character of spectra as well as on the thin films properties has been observed during the depositions.

When the VTEO or HMDSO were used as monomers, it was not surprising that more CO, CO⁺, CO₂, and CHO bands were identified in the spectra at different wavelengths. The oxygen promotes the fragmentation of monomer and CO or CHO are created very easy. With the increasing monomer flow rate, the initial decrease of the CO band intensities were observed, then, for $Q_{\text{O}_2} = 1$ sccm, the strong increase of the intensity started and more of CO triplet bands were observed. After getting over the 1.5 sccm of oxygen flow rate into VTEO or 2 sccm for HMDSO, the intensities stayed relatively independent on the further increase of the oxygen addition. Moreover, the decrease of CH and C₂ and C₄H₂ band intensities were recorded. For $Q_{\text{O}_2} = 2$ sccm, the decrease reaches the minimum and then we can see slow increase. Due to appearance of many CO bands, the other bands except C₂ were not measurable.

The effect of oxygen addition was studied especially during the deposition using TVS. The strongest influence on the layer properties was observed at the effective powers under 5 W. When low effective power is applied, the oxygen is built into the plasma polymer structure as we determined by RBS and FTIR measurements,. This structure with oxygen content is needed for its application as a suitable interphase between resin and glass fibre.

An example of the spectra recorded during the deposition using TVS with oxygen are shown in Figs. 54 and 55. The Figs. 56 - 58 show the dependencies of the relative spectral band intensities of the various species as a function of the oxygen flow rate.

Oxygen was added to raise the probability that the percentage of oxygen in the layer will be higher. The Si - OH and the Si - O - Si groups are responsible for the hydrophilic character of the layers. The detailed description of the contact angle measurements and results is given in [2, 66].

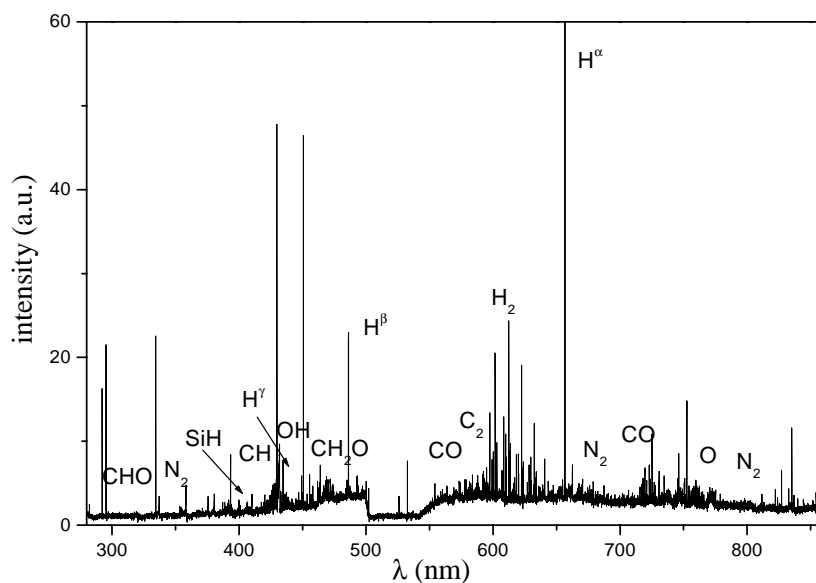


Figure 54: An example of the OE spectrum measured during the deposition using TVS with oxygen addition, $W_{\text{eff}} = 10 \text{ W}$, $Q_{\text{O}_2} = 0.6 \text{ sccm}$.

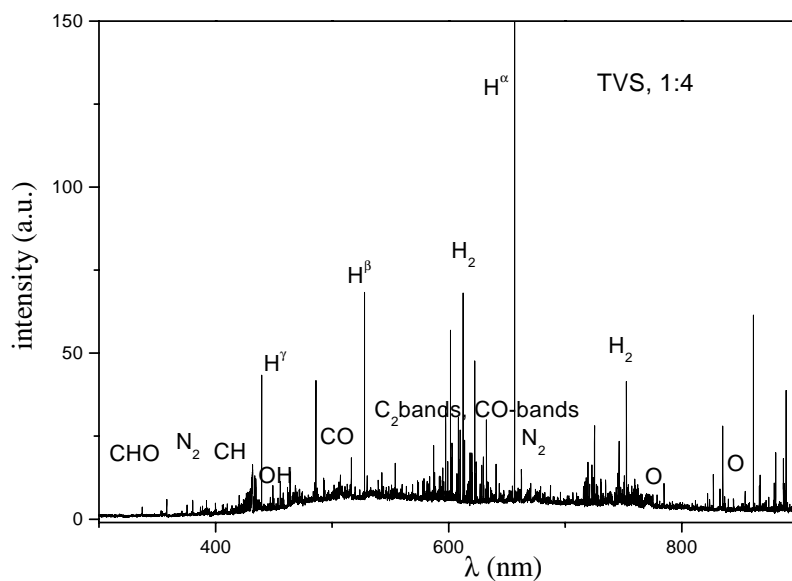


Figure 55: An example of the OE spectrum measured during the deposition using TVS with the oxygen addition, $W_{\text{eff}} = 10 \text{ W}$, $Q_{\text{O}_2} = 0.15 \text{ sccm}$.

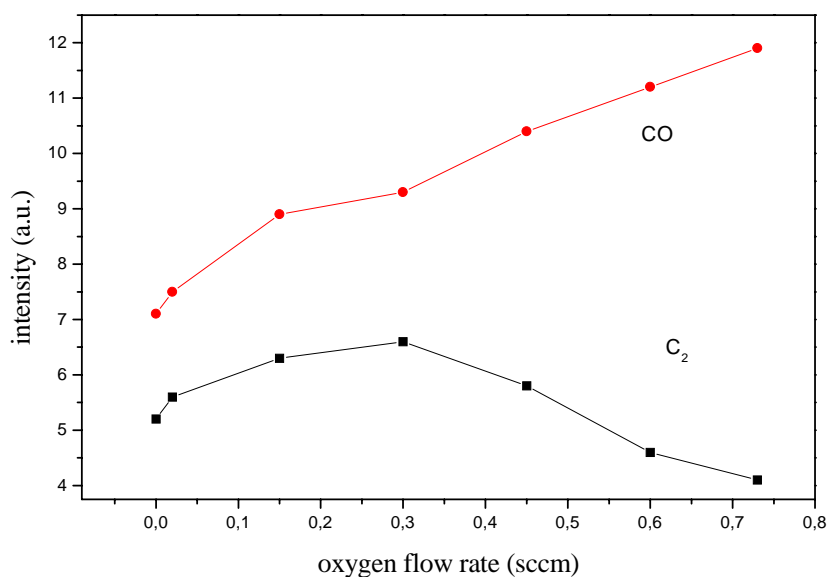


Figure 56: C_2 and CO band Intensities as a function of oxygen flow rate during the deposition using HMDSO, $W_{\text{eff}} = 5 \text{ W}$.

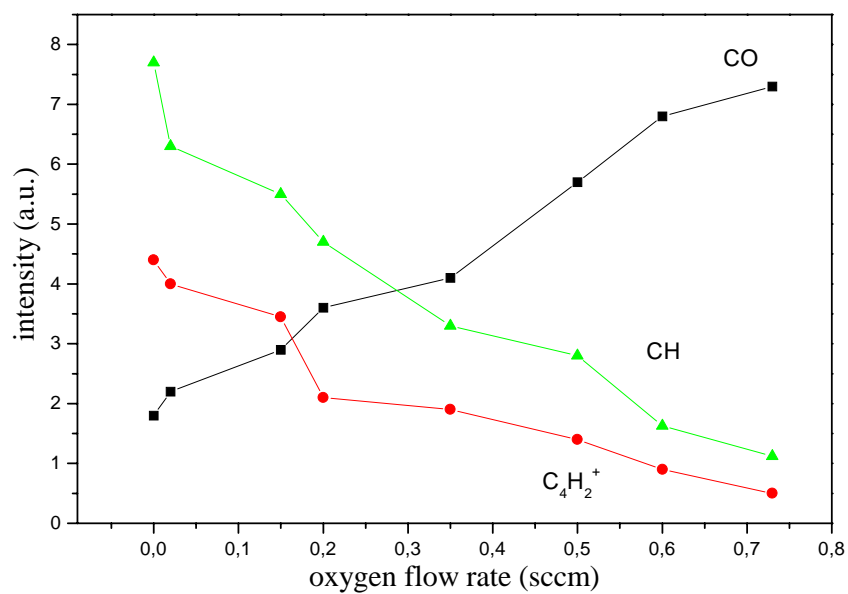


Figure 57: Intensity of spectral bands as a function of the oxygen flow rate during the deposition using VTEO, $W_{\text{eff}} = 5$ W.

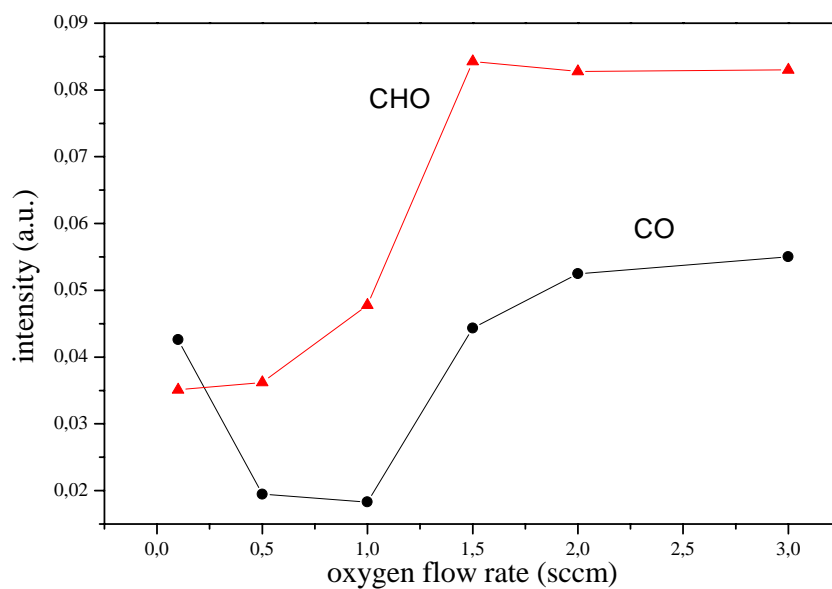


Figure 58: Intensity of spectral bands as a function of the oxygen flow rate during the deposition using TVS, $W_{\text{eff}} = 5$ W.

3.5 Results from OES and thin film properties

The surface morphology and chemistry of the created fibre coating play a very important role for the achieving good adhesion and strong bonding between the fibre and matrix in the composite materials. It is correlation between the changing of layer properties and changing of the optical emission spectra character. FTIR analyses show that in the case of VTEO and HMDSO, different plasma conditions have not great influence on the chemical structure of the prepared plasma polymers. Using the TVS as a monomer, the changes of FTIR spectra are indispensable with changing of the discharge conditions. But FTIR analysis is not sufficient for the pp model structure searching. By OES measurements, we have found a significant changes in the spectrum in the case of all monomers. Some results from thin layer diagnostics are presented in the following paragraphs. We have tried to compare these results with the results from the gas phase diagnostics by OES and MS. The combination of the results from various analyses could form a basis for the deposition mechanism model creation as well as for the creation of probable plasma polymer structures.

The effective power during the deposition has an important effect on the thin film properties. Applying effective power of about 25 W, the spectra as well as the thin film properties do not differ from the other recorded in continuous mode.

In comparison with the continuous regime, during the pulse mode 1:1, the relevant changes were not observed in the spectra. The significant changes in character of spectra and in thin film properties were observed when the effective power was lower than 10 W.

The optical emission spectrum strongly varied with effective power, too. The break in character of the spectra arose at $W_{\text{eff}} = 5$ W. The significant changes were observed at effective powers between 1.66 and 3.33 W (pulse 1:29 - 1:14).

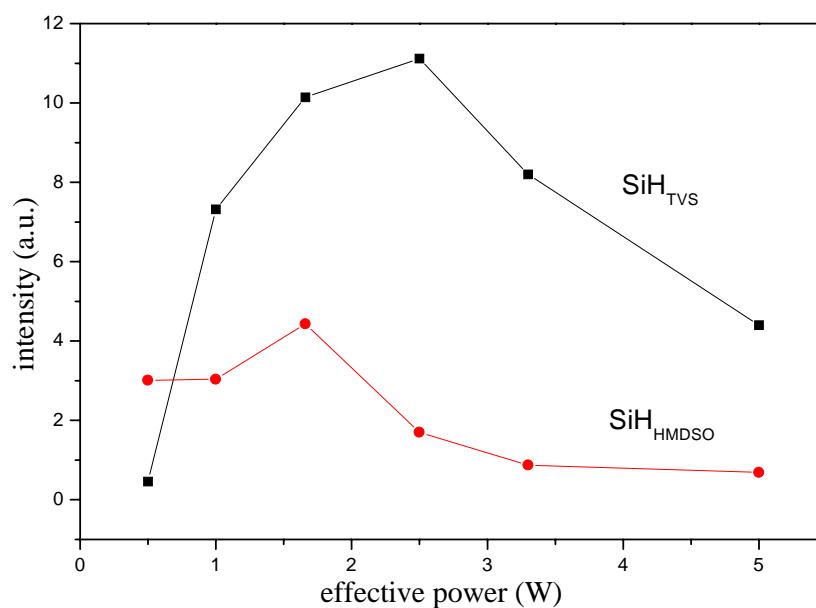


Figure 59: Dependence of the SiH intensity on the effective power, $Q_{\text{monomer}} = 0.5$ sccm.

Additionally, at low effective powers, it was possible to identify the SiH bands in OE spectrum. SiH groups are present also in the plasma polymer structure. It was found that by OES, generally, we were able to observe mainly the particles that are not taking part in the polymerisation process. In Fig. 59, the evolution of the SiH emission for the deposition using HMDSO and TVS at different effective powers is shown. First, the intensity of SiH increases and reaches the maximum value at 2.5 W. After, the intensity decreases. This effect can be explained by the silicon consumption during the deposition.

The Fig. 60 shows the dependence of the deposition rate as a function of effective power. Deposition rate was measured according to the thickness of the layer and deposition time. Deposition rate of 180 nm/min during the processes using TVS is higher than with using of VTEO and HMDSO where the deposition rate reach only 120 nm/mm [48].

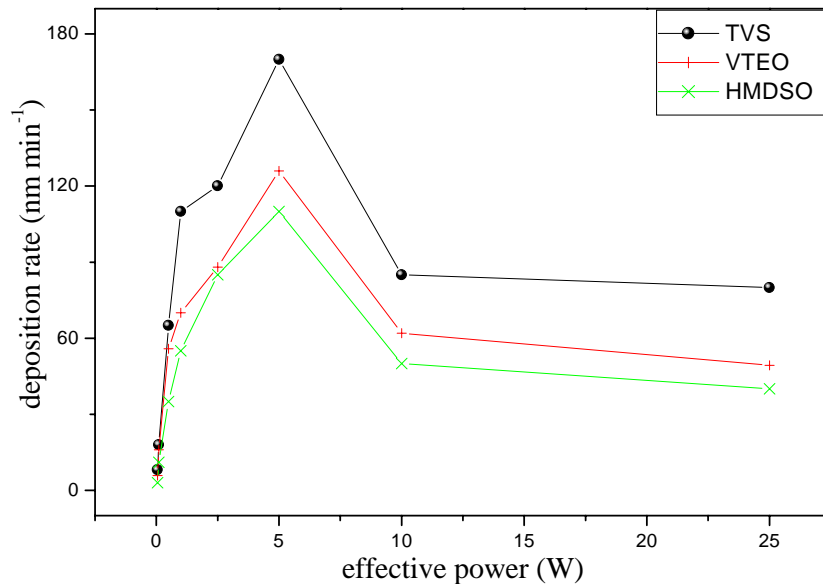


Figure 60: Deposition rate of TVS, VTEO and HMDSO as a function of effective power, $Q_{\text{monomer}} = 0.5 \text{ sccm}$.

It was found that the most of hydrogen is eliminated from the monomer during the deposition, and it is outflow from the device. Hydrogen is mostly eliminated at the high effective powers. In the OE spectra, molecular bands of hydrogen appear and the atomic hydrogen lines have higher intensity at higher effective powers. The hydrogen deficiency can cause crosslinking and creation of double bonds. Cross-linking degree increases with the increasing effective power, thus, module of elasticity increases, too [64].

RBS and ERDA analysis were carried out, too. The results from these analyses are presented in [49] and [66]. The hydrogen concentration in the layer decreases with the increasing effective power as well as oxygen is fitted into the layers with decreasing effective power. In Figs. 62 and 63 you can see the dependence of percentage content of O, H, Si and C in the thin film as a function of the pulse duration. The hydrogen is present in the layer, often as the SiH group.

The dependences of the ppTVS film elementary composition on the effective power is

given in Figs. 65 and 64. The graph of the elementary composition as a function of effective power for the ppTVS prepared using oxygen addition to the monomer is presented in Fig. 66. The oxygen amount decreases rapidly and thus the carbon atom content increase with the increasing effective power. The concentration of oxygen atoms decrease from 13 atomic % (at 0.05 W) to 1 at % (at 10 W), while carbon atom concentration rises from 27 % (at 0.05 W) to 42 % (at 10 W).

In case of using TVS for the plasma deposition, there is not a significant decrease of the hydrogen in pp thin film. On the contrary, the hydrogen to carbon ratio became higher with decreasing effective power.

In case of using HMDSO, content of carbon and hydrogen (or more precisely, content of the groups containing C and H) decreases with the increasing effective power. Better adhesion to the substrate was observed with lower deposition rates.

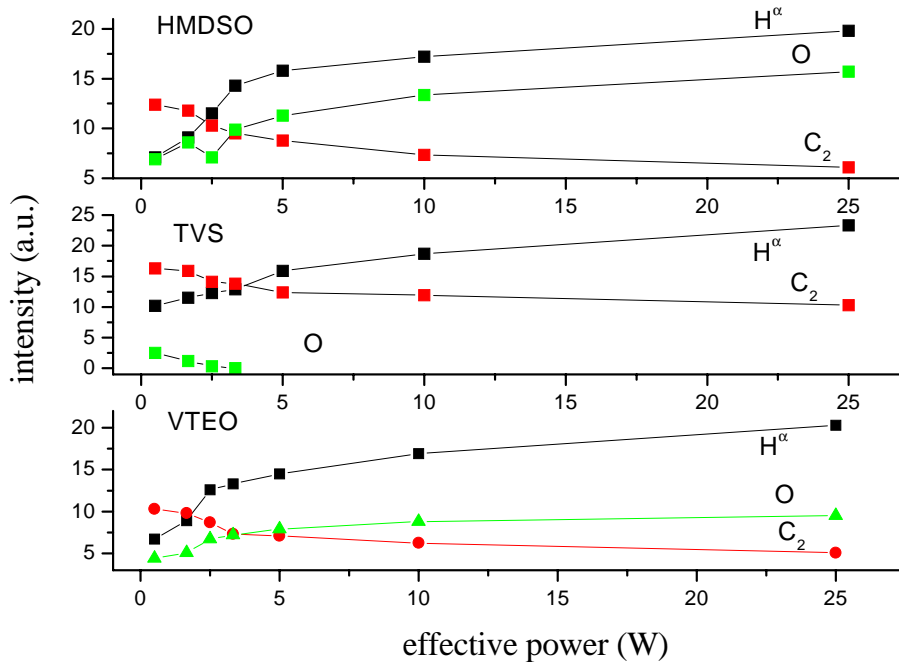


Figure 61: Dependences of the intensity of C_2 band, H^α at 656 nm and oxygen lines at 777 nm on the effective power for all monomers used for the deposition. Monomer flow rate was 0.5 sccm.

Moreover, the ellipsometric measurements were performed in order to determine the polymer film thickness and optical constant, refractive index and extinction coefficient. Detailed results and discussion which concern the ellipsometry are published in [6]. Ellipsometric measurements show that with increasing effective power also index of refraction increases. In case of the highest value of refraction index, the content of carbon is reaching the highest value too.

Furthermore, it was found that the Young module and hardness of the layers increase almost four times with enhanced power. Besides the crosslinking, this effect could be

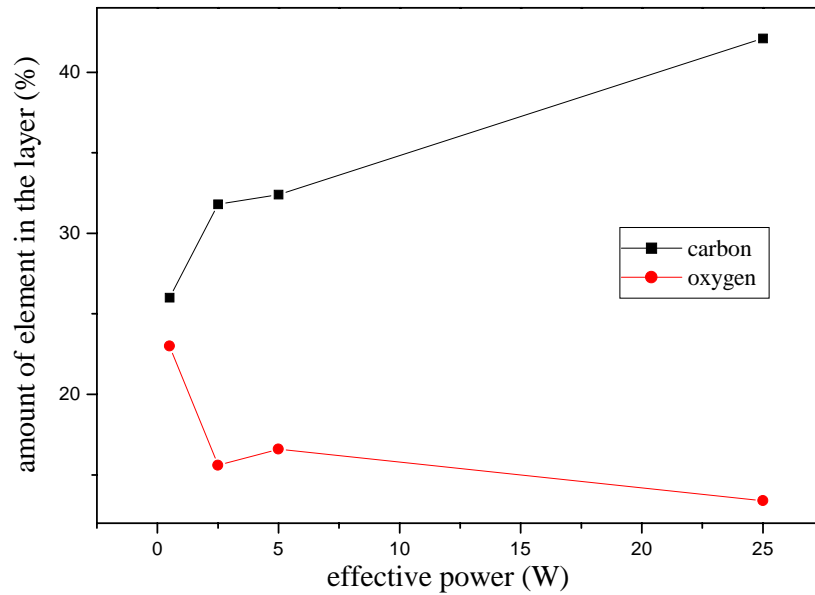


Figure 62: Content of the main significant elements in the pp layers as a function of the effective power, $Q_{\text{VTEO}} = 0.5 \text{ sccm}$.

caused by higher organic character of the layer [67].

As it was pointed above in Fig. 59, at first, the SiH intensity increases and after the reaching 2 W for HMDSO and 2.5 W for TVS it strongly decreases. From the RBS and ERDA analysis, it is clear that the silicon content in the layer is the highest between effective powers 1.66 and 2.5 W. After, we can observe the slow decrease and in the case of ppTVS, the silicon content is again higher at the effective power 25 W. So, we can suppose that when the decrease of SiH in the OE spectrum is observed, the silicon is built into the deposited layer structure. In the spectra obtained during the deposition with VTEO, the SiH bands were not very well distinguished, thus, their dependence on the effective power was not done for all three monomers. The dependences of the main significant band intensities are given in Fig. 61. Oxygen and hydrogen line intensities increase with increasing effective power. In the spectrum recorded during the deposition using TVS, the oxygen was observed only at the lowest effective powers. So, the intensity of oxygen lines decreases with respect to the whole spectrum. The intensity of C_2 bands was monitored, too. The atomic carbon lines were not identified. The C_2 band intensities decrease and at the effective power of 10 W, the intensity decreases were not very strong. By the thin film analysis was found that the content of carbon in the pp layer is higher at the higher effective powers.

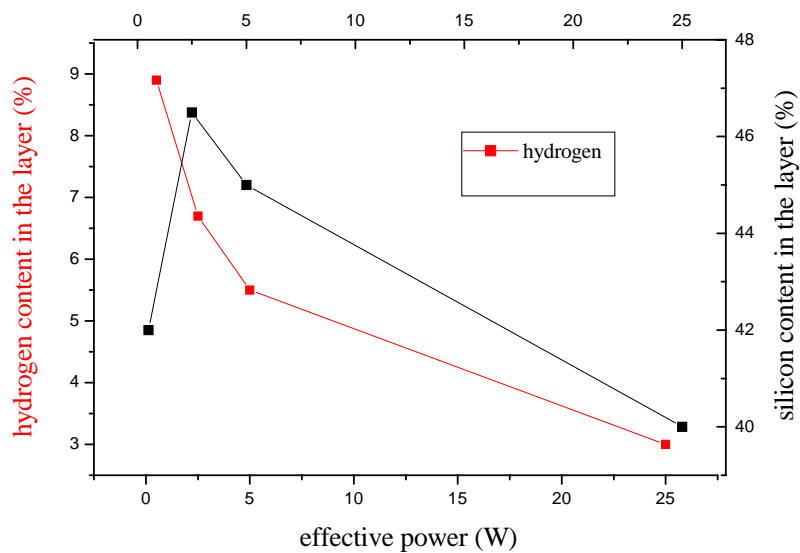


Figure 63: Content of the main significant elements in the *pp* layers as a function of the effective power, $Q_{VTEO} = 0.5$ sccm.

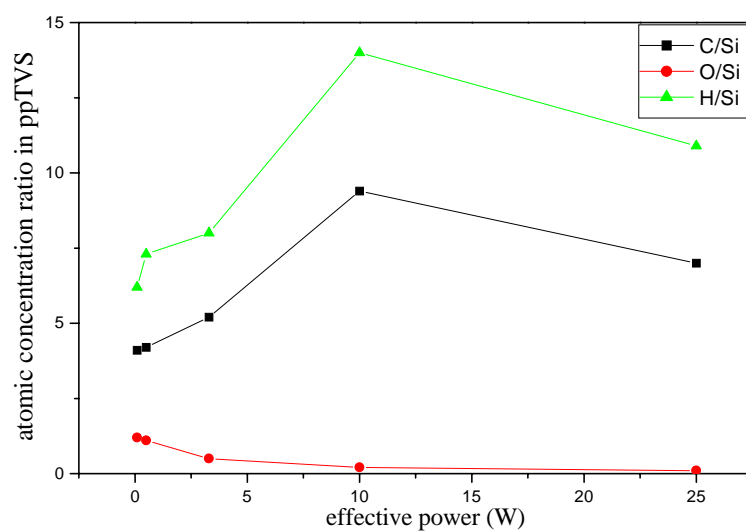


Figure 64: Dependence of the atomic concentration ratio in the *ppTVS* thin film on the effective power, $Q_{TVS} = 0.5$ sccm.

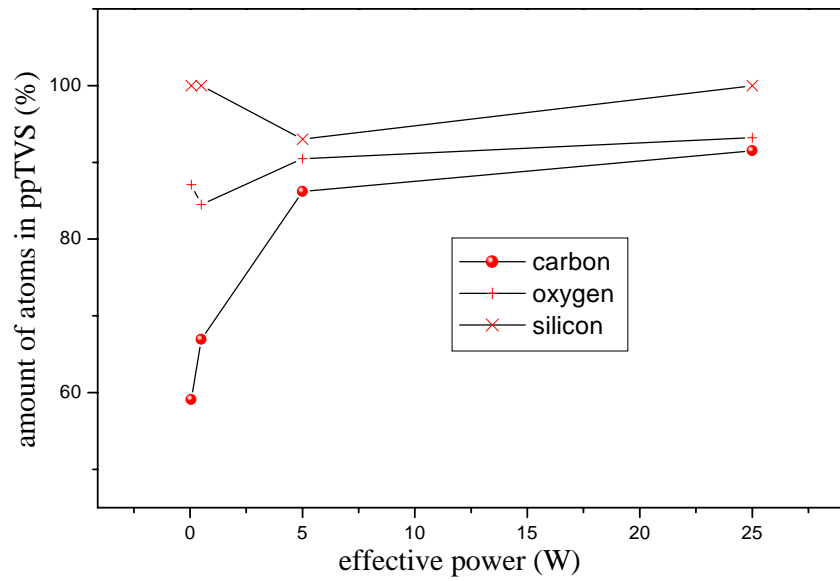


Figure 65: Content of the elements in the ppTVS film prepared from TVS with the oxygen addition of 6 % as a function of the effective power, $Q_{TVS} = 0.5$ sccm.

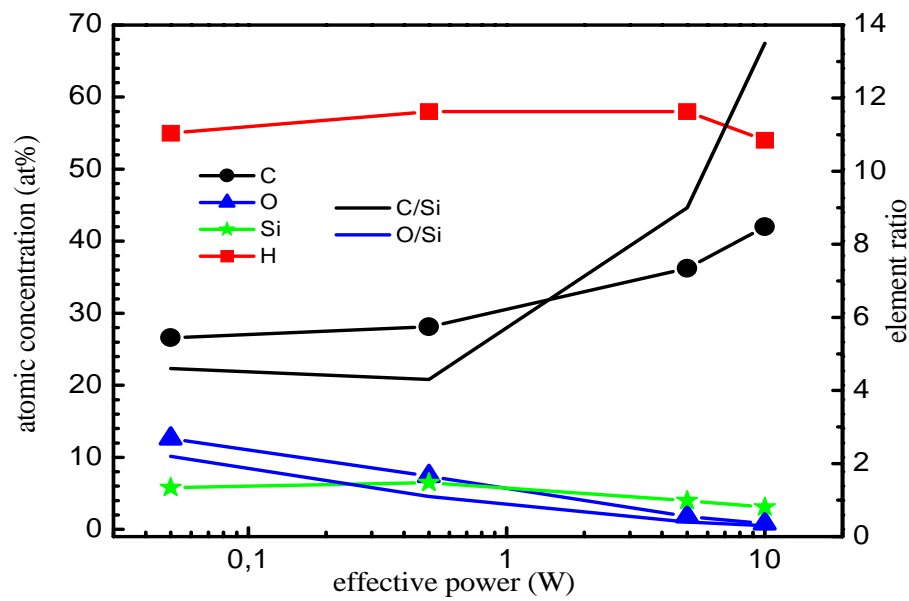


Figure 66: Content of the elements in the ppTVS film prepared from the pure monomer without the oxygen addition as a function of the effective power, $Q_{TVS} = 0.5$ sccm [64].

4 Kinetics of the deposition processes

This section deals with the estimation of the probable kinetic model of the plasma polymerisation using HMDSO, VTEO and TVS as the precursors. The term *polymerisation* is not fully correct. There are not classical polymerisation processes at the plasma conditions. The polymer growth is provided by progressive recombination of the reactive species. It is very complex process where the various fragments are binded more or less accidentally.

Plasma polymerisation is very complex process that consider a lot of particular processes with different reaction channels. In the literature it is possible to find the kinetics of the particular processes and "simple" reactions during the depositions using for example the pure methane or hydrogen with methane. The real polymerisation process using organosilicon compounds as precursors it not fully described up to now. To create the clear model of the plasma polymer creation, the information about particles which are present in the gas phase is required, as well as the plasma polymer diagnostics is needed. It would be very useful to know how the plasma polymers grow to control their properties by plasma conditions changing. On the basis of the results from mass spectrometry (MS), gas chromatography-mass spectrometry (GC-MS) and optical emission spectrometry (OES), we have tried to suggest the pictures of the monomers fragmentation. Moreover, with combination of gas phase diagnostics and thin film diagnostics, the probable structures of the plasma polymers are presented in this part of the work.

From the dissociation products, the plasma chemistry develops to create more complex molecules such as CH₄, CH₂O, CO₂H₂. Thus, the numerical model could take into account at least about 60 chemical reaction describing the kinetics of about 10 - 30 different chemical species [62].

To create the kinetic model, we should consider all types of the possible reactions including the particle diffusion and their recombination on the electrodes or on the reactor walls. If the absolute intensity value of the emission spectrum continuum is known it is possible to estimate the rate of electron impact dissociation. This intensity is directly connected with the rate via spontaneous emission to the repulsive states. If the total continuum emission intensity of the transition for example a - b is expressed in number of photons per cm³ and second and it is integrated over the entire wavelength range we can use the relation:

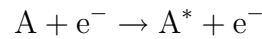
$$\left(\frac{d[X]}{dt}\right) = \int_0^\infty I_{ab}\lambda d\lambda = \sum_{v'=0}^{v'=max} \frac{N_{av'}}{t_{av'}}$$

where $\frac{d[X]}{dt}$ is the rate of radiative process, I_{ab} is the intensity of the a - b transition, $N_{av'}$ is the a-state population at higher vibrational level and $t_{av'}$ is the lifetime of this state.

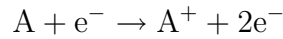
The kinetic model is difficult to calculate even if we have only small particles disposable. It is relatively easy when we have only hydrogen or hydrogen and argon or methane and argon in the reactor.

There are many possible inelastic collisions between electron and gas species in a glow discharge. Examples of those important processes in PECVD are listed bellow:

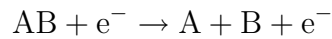
- excitation



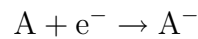
- ionisation



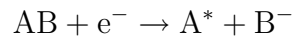
- dissociation



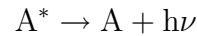
- electron attachment



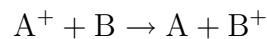
- dissociative attachment



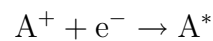
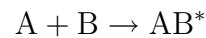
- photoemission



- charge transfer

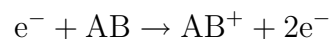


- recombination

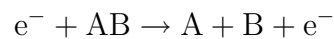


Gas and surface-phase chemical reactions play a critical role in PECVD. The general chemical reactions are following:

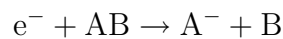
- electron-ion pair production



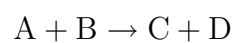
- radical production



- negative ion production



- gas-phase chemical reaction



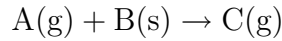
- ion transport to surface

$$\Gamma_i = -D_A \nabla n_i$$

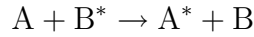
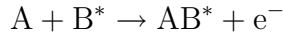
- radical transport

$$\Gamma_i A = -D_A \nabla n_A$$

- surface-phase reactions



- transport of excitation



chemical bond	binding energy [eV]
<i>methane decomposition</i>	
H – CH ₃	4.5
H – CH ₂	4.8
H – CH	4.4
H-C	3.5
<i>silane decomposition</i>	
H – SiH ₃	3.9
SiH ₂	2.8
H – SiH	3.6
H – Si	≤ 3.1
<i>water decomposition</i>	
H – OH	5.2
H – O	4.4
others	
O = CO	5.5
O – C	11.2
O – N ₂	1.7
O – NO	3.2
O – N	6.5

Table 7: Selected binding energies of the compounds playing an important role during the plasma polymerisation.

To estimate the reaction rates, we should know their rate constant k_i .

$$k_i = \int_0^\infty \left(\frac{2E}{m_e}\right)^{1/2} \sigma(E) f(E) dE,$$

where m_e is the electron mass, E is electron energy and σ is the differential collision cross sections. Some collision cross section can be found in literature [14, 28, 35, 68]. However, most of them are not known, and thus, it is difficult to calculate reaction rates.

Using only the mixture of hydrogen and silane or methane, in the first step, free electrons caused fragmentation of the precursors of the plasma polymer. The fragments can form a powder on the surface or undergo the homogeneous oxidation reactions in the gas phase and consequently they can react on the substrate surface to create the bonds or they can only activate the surface and "prepare" it for the film creation. The oxygen

addition has a negligible effect on a monomer activation [22, 46, 70], on the contrary, it plays an important role in plasma chemistry. Oxygen influences the concentration of the organosilicons formed by recombination in the gas phase. Near the substrate, dust particles collect more electrons, depending on the dust particles concentration. The clusters, and later even nanoparticles are created. A rapid agglomeration takes place, too. In the second phase, particles grow by deposition of the plasma generated species on the surface.

chemical bond	energy [eV]
C – C	6.3
C – Si	4.7
H – H	4.5
N – N	9.8
N – Si	4.6
O – O	5.2
O – Si	8.3
Si – Si	3.4

Table 8: *Selected binding energies of the bonds that are present in common organosilicon monomers.*

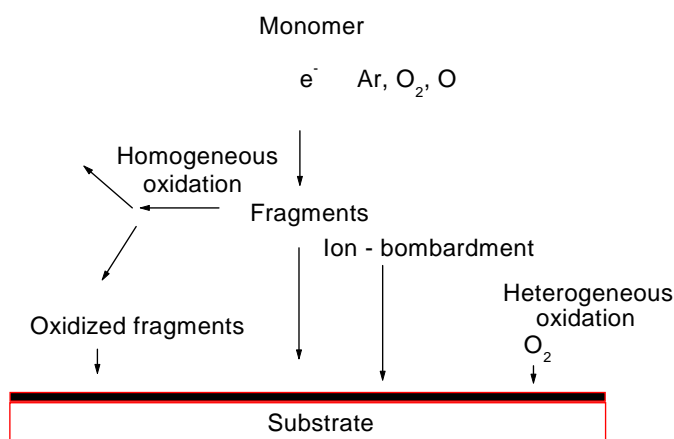


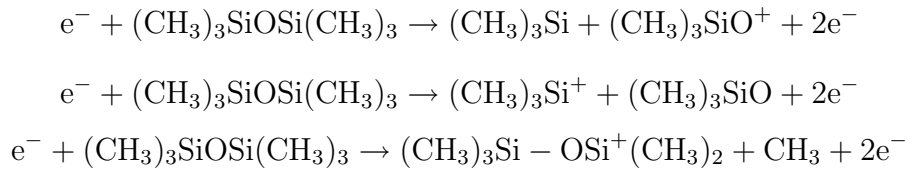
Figure 67: *Scheme of the general deposition in organosilicon plasma with the oxygen and argon addition.*

A scheme of the general deposition process in organosilicon plasma is given in Fig. 67. At the beginning of our experiment, it was solved the problem if the polymerisation proceed by ion or radical mechanism. It is well known that the ion bombardment has

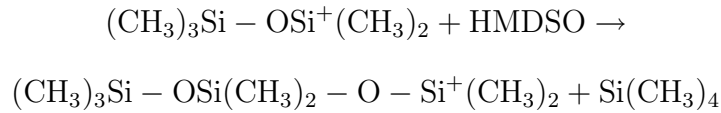
an important role during the deposition [45, 62, 70]. The fragmentation of the molecules used as monomers during the deposition was studied by MS and GC-MS, see sections *Analysis by mass spectrometry* and *Analysis by GC-MS*. Based on these results including the results obtained by the OES of plasma during the deposition, the following kinetic schemes are proposed.

4.1 Hexamethyldisiloxane

The suggested probable fragmentation of HMDSO is given in the Fig. 68. In case of the ionic polymerisation using HMDSO, we can suppose following mechanisms:



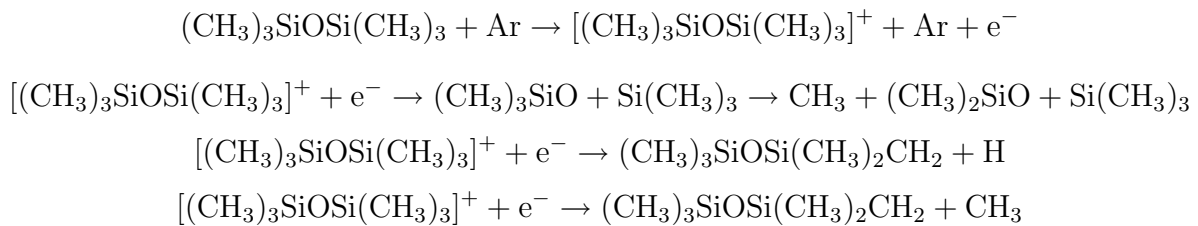
These equations suggest the most probable fragmentation with the three different ions creation. One of the possible ionic polymerisation reaction of these ions is marked bellow:



The CH_3 can be eliminated, and after, the Si-O-Si bond can be created by the reaction with the HMDSO molecule. So, $\text{Si}(\text{CH}_3)_4$ is eliminated from HMDSO.

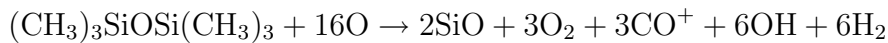
At the plasma conditions, the ion-radical and radical creation is more probable [], thus, we could suppose a radical mechanism of the polymerisation for HMDSO, too.

In many cases, the monomer is activated by argon atoms. An example of the HMDSO fragmentation by argon atom is given bellow, with the possible consequent reactions.



These fragmentations are probable at low effective power, as it is clear from MS and OES analyses. Many smaller fragments are formed at the higher power, and the polymerisation goes by another way.

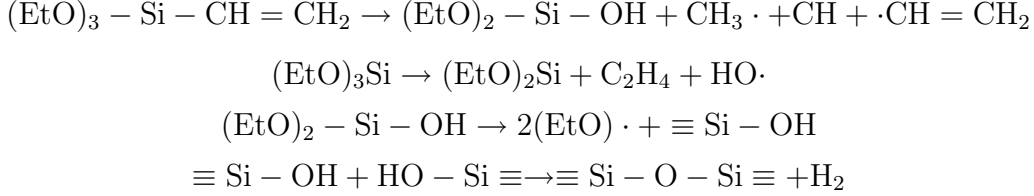
When oxygen is added to HMDSO, the molecule undergoes oxidising reactions. At high effective power and high oxygen flow rate we could complete up to following fragmentation reaction:



Most of these particles were observed mainly by OES, thus, in our case such a high fragmentation could be not neglected.

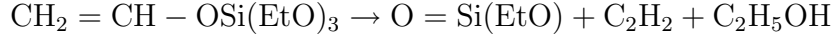
4.2 Vinyltriethoxysilane

When the VTEO is used, we suppose that the main reactions could be as following:



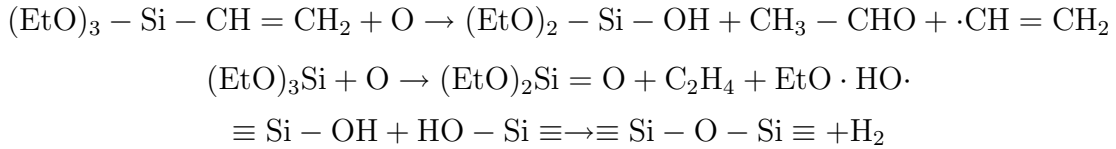
The EtO indicates the ethoxy $\text{CH}_3\text{CH}_2\text{O}$ group. Initially, we solved the problem if the ethoxy or vinyl group is eliminated as the first. With respect to the fact that many C_2 bands are visible in the OE spectrum, we supposed that the C_2 comes from the vinyl group and thus, the vinyl group is supposed to eliminate easier.

In the literature [65], the reaction kinetics of VTEO decomposition is studied. The following reaction is suggested:



Its rate coefficient was calculated $k = 6.1 \cdot 10^{10} \exp(-61500/RT) \text{ s}^{-1}$ But this constant was calculated for the reactions which are more probable during common CVD [37]. In the plasma, more complex reaction mechanism is expected.

When the oxygen is added, the fragmentation way is probably similar like in the previous case.



The kinetics of VTEO dissociation was studied also in literature [70]. Some of reactions you can find in the following table 9. The example of VTEO fragmentation you can see in Fig. 69.

Dissociative enthalpy	
reaction product	ΔH [kJ/mol]
$\rightarrow \text{CH}_2 = \text{CH} - \text{Si}(\text{OC}_2\text{H}_5)_2 + \text{OC}_2\text{H}_5$	32.5
$\rightarrow \text{OSi}(\text{OC}_2\text{H}_5)_2 + \text{C}_2\text{H}_5 + \text{CH}_2 + \text{CH}$	26.1
$\rightarrow \text{O} = \text{Si}(\text{OC}_2\text{H}_5) + \text{C}_2\text{H}_4 + \text{C}_2\text{H}_5\text{OH} + \text{CH}_2 + \text{CH}$	20.4
$\rightarrow \text{O} = \text{Si}(\text{OC}_2\text{H}_5) + \text{CH}_3\text{CHO} + 2\text{C}_2\text{H}_5$	17.7
$\rightarrow \text{Si}(\text{OC}_2\text{H}_5)_2 + \text{C}_2\text{H}_5\text{OC}_2\text{H}_5 + \text{CH}_2\text{O} + \text{CH}$	16.5
$\rightarrow \text{HSi}(\text{OC}_2\text{H}_5)_2 + \text{CH}_3\text{CHO} + \text{CH} + \text{CH}_2$	8.6
$\rightarrow \text{Si}(\text{OC}_2\text{H}_5)_3\text{OH} + \text{C}_2\text{H}_4 + \text{C}_2 + 3\text{H}$	2.5

Table 9: *Dissociative enthalpies of the VTEO $\text{CH}_2 = \text{CH} - \text{Si}(\text{OC}_2\text{H}_5)_3$ selected fragmentation [27].*

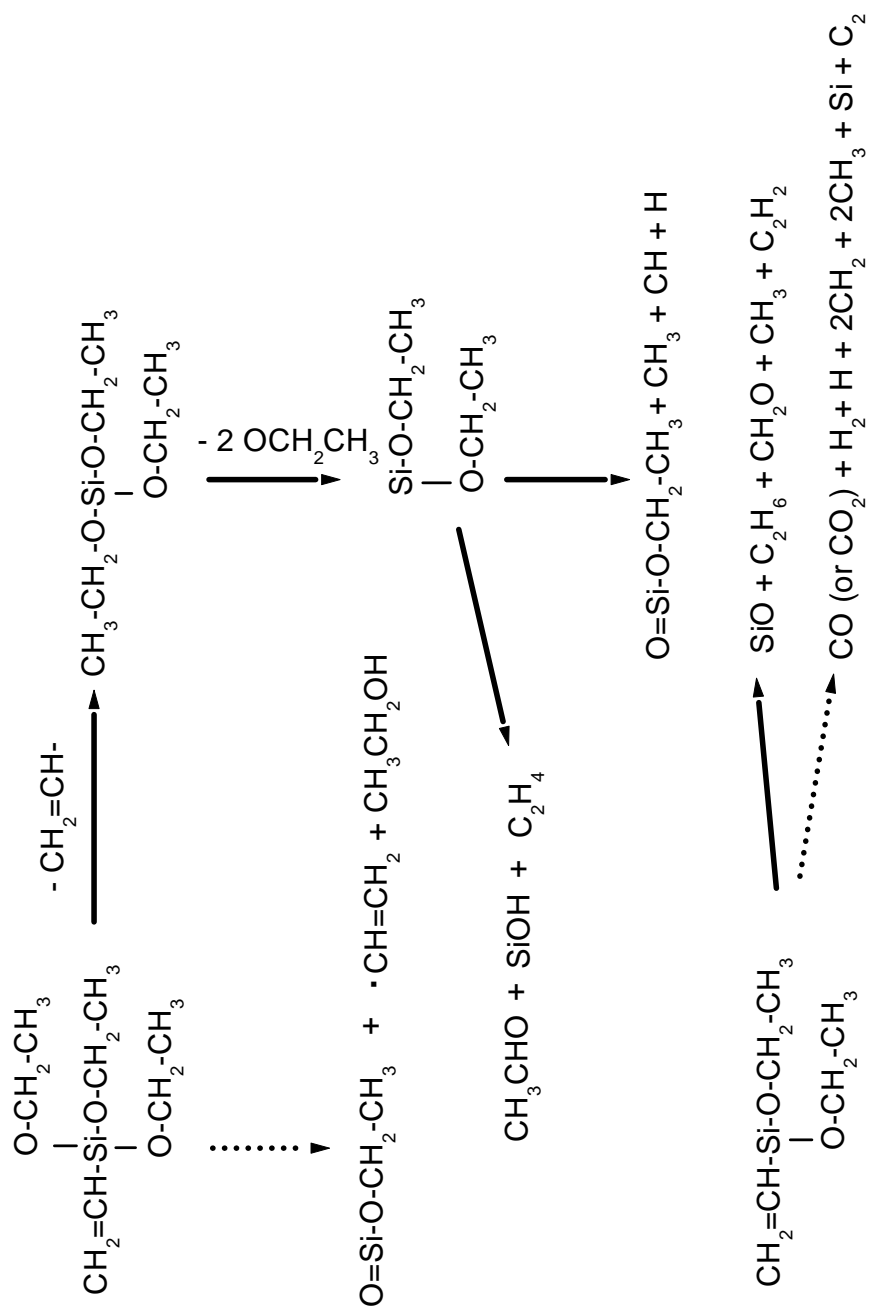
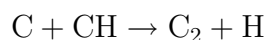
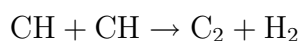
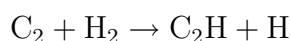
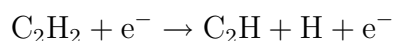
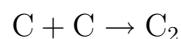
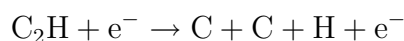
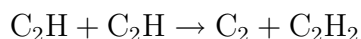
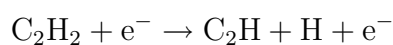
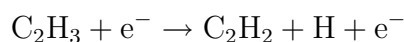


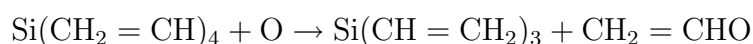
Figure 69: Scheme of the probable VTEO fragmentation. The dotted lines mean the incomplete equation.

4.3 Tetravinylsilane

By using the TVS, the main advantage is that the amount of oxygen can be controlled. The scheme of the TVS fragmentation is given in the Fig. 70. First, the sequential elimination of vinyl groups is expected. Then SiH, SiH₂, CH₃, CH₂, CH and SiR (R is rest of hydrocarbon) could be created and they could form the layer on the substrate. Dissociation of the CH bounds need the higher electron energy (higher effective power or lower pressure). After elimination of vinyl group, we can suppose for example following reactions in plasma volume:



Besides the other species, those mentioned in the equations above appeared in OE spectra in very high intensity. When the oxygen is added, we can suppose for example following fragmentations, too:



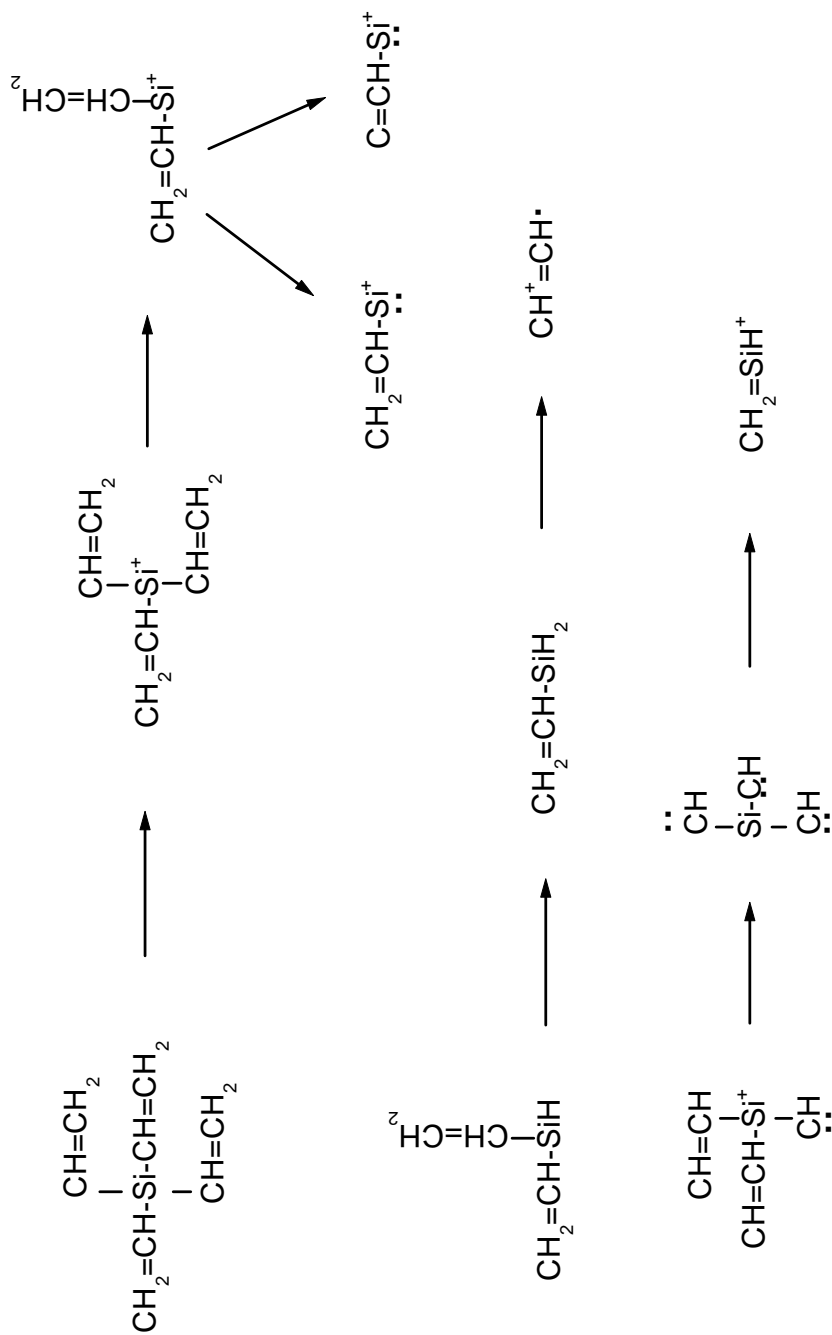


Figure 70: Scheme of the probable TVS fragmentation.

4.4 Structure of plasma polymers

Generally, in a contrast to the common polymers, the content of elements in the plasma polymers differs from the content of elements in the monomer. For example, amount of carbon and hydrogen is lower than in the monomer, in case of the TVS. Furthermore, the oxygen appears in the polymer even if there is no oxygen in the monomer structure. It occurs only at very low effective power. The oxygen comes probably from the atmosphere as impurity. The dissociation degree is high at the high effective power (higher than 10 W in our reactor configuration), and the CO is created in preference. As it was mentioned above, CO is probably not taking place in the polymerisation process.

It was found that the density of plasma polymers is much higher than the density of polymers formed by the classical polymerisation [7]. In the case of the polymer based on HMDSO the density is about 70 % higher than the polydimethylsiloxane. It is caused by crosslinking and by diffusion of the fragments into the substrate. Detailed description is given in the previous work of Jan Vaněk [66, 67].

Based on our results, the probable structures of plasma polymers were suggested. When HMDSO was used for the deposition, the Si – O – Si bonds are built in the plasma polymer. On the other hand, the TVS was evaluated as better precursor for the following plasma polymer that should serve as a polymer interphase in the composites. TVS was suggested due to the double bond in its structure. Those were expected in the plasma polymer too. The Fig. 74 presents the structure of the plasma polymer that was prepared at the effective power of $W_{\text{eff}} = 0.5$ W. We are interested in the structure of ppTVS at this effective power, because it contains enough of hydrogen, carbon, optimum silicon content and also oxygen, therefore it has good adhesivity to the matrix and good physico-chemical properties to be a good interphase for the resin composites. When the VTEO and HMDSO are used as the monomers, the effective power of 5 W is the most interesting for our purpose. To compare the effect of the highest effective power in a pulse mode, the structures of ppVTEO, ppHMDSO and ppTVS created at the effective power of 25 W were studied.

Mostly, the effective power of 5 W was set for the deposition process because the highest deposition rate was reached.

But for our experiments, the whole scale of possible effective powers was tried. As we expected, higher effective power leads to the higher fragmentation degree. The effective power of about 25 W leads to higher substrate temperature what cause the polymer decomposition.

By OES and MS, only the flowing-out particles were measured. To observe the particles taking part into the polymerisation, the optical fibre should be very close to the substrate surface. But that position would increase the fibre coverage by the created film and thus the correct interpretation is really complicated. The absorption diagnostic technique could be very useful too. Anyway, on the basis of OES and additional FTIR and ERDA with RBS analysis it was possible to obtain the estimative picture of monomer fragmentation at different effective powers and the polymer structures could be suggested.

As it was mentioned in the section *Results and discussion*, at high effective power, higher content of carbon and less of oxygen and hydrogen were determined in the pp layers. At the same time, more Si – O – Si bands appear as well as, the crosslinking degree is higher than in the layers prepared at lower effective powers. In the case of ppTVS, the FTIR and NMR analyses indicated that the cyclic structures could be present, too.

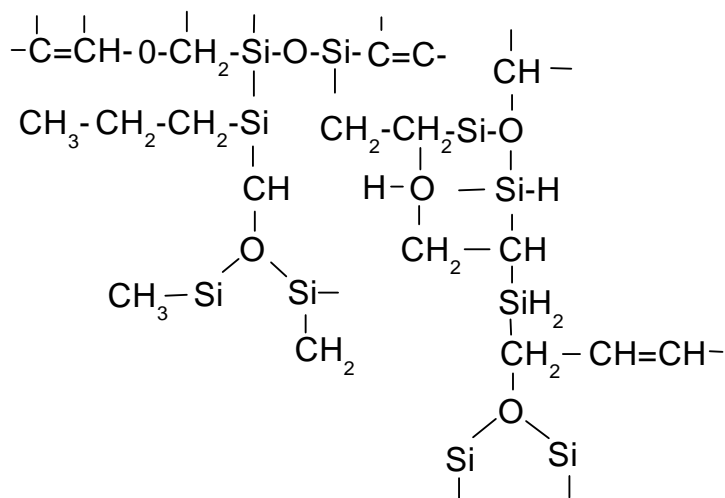


Figure 71: Probable structure of the plasma polymer formed during the deposition with HMDSO, $W_{\text{eff}} = 5 \text{ W}$.

The vinyl group vibration appears in the IR spectra and the wavenumber of its position indicates that it is linked to the cyclic hydrocarbon. The Si – H and Si – C bonds were indicated near the cyclic part, too. At the effective power of 0.5 W, the oxygen is present in the layers, so, we supposed that the Si – O – Si and also C = O bonds are created. But the FTIR analysis indicated only long chain molecule. By the GC-MS analysis, we have identified the similar chain and at lower effective power, the oxygen content was indicated, too. Fragments of TVS can react with oxygen from the leakage very easy at the low effective powers. The oxidised fragments "have time" to create the pp film on the substrate while at the higher effective power, mainly the CO or CO₂ are created and they flow out from the reactor. They were detected as an exhaust gas and also by OES in very high intensity. Similar effect was observed in the case of VTEO. In Fig. 73, a scheme of the probable structure of ppVTEO created at the effective power 25 W is shown and in Fig. 71 you can see the drawing of the ppVTEO created at the effective power of 5 W. In the case of ppHMDSO created at the effective power of 25 W, we supposed that the structure is similar like structure of ppVTEO at the same effective power. In the case of ppHMDSO deposited at the effective power of 5 W, more of Si – O – Si bonds are supposed in comparison with ppVTEO at the same effective power. It is probably caused by the preferential elimination of methyl groups while Si – O – Si could be sustained. In the case of VTEO, ethoxy groups are eliminated during the monomer fragmentation, thus, the SiC and SiH can be formed and of course SiO, too.

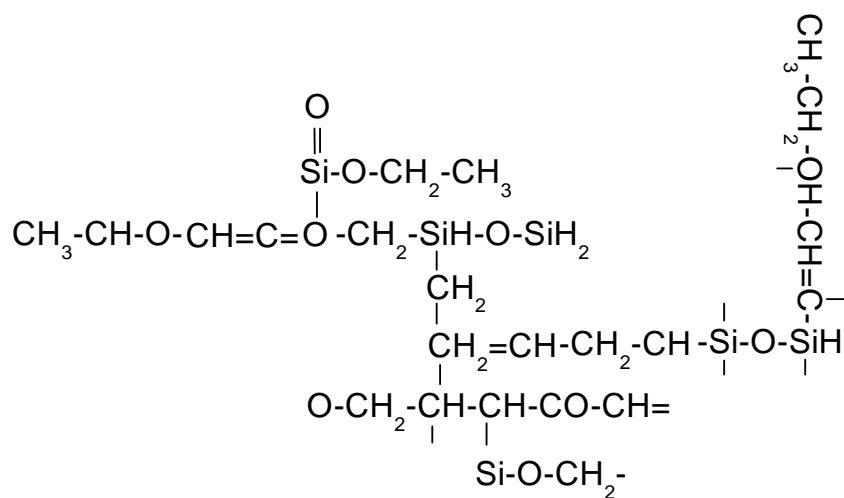


Figure 72: Probable structure of the plasma polymer formed during the deposition with VTEO, $W_{\text{eff}} = 5$ W.

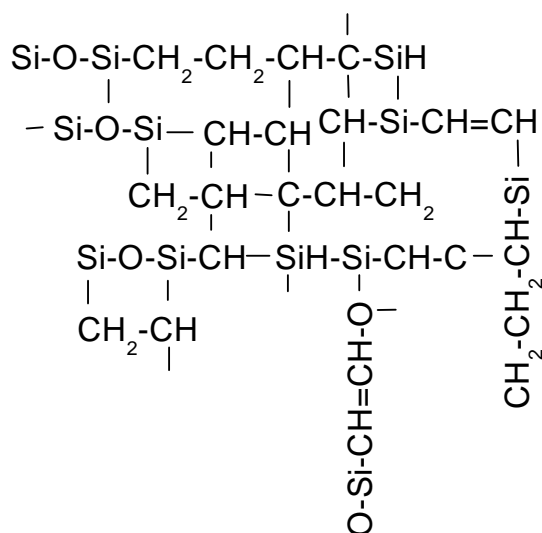


Figure 73: Probable structure of the plasma polymer formed during the deposition with VTEO, $W_{\text{eff}} = 25$ W.

5 Conclusion

The objective of this work was characterisation of the processes during the organosilicon thin films depositions. The important task of this work was the estimation of deposition process mechanism during the searching for the suitable interphase for the application in a composite materials based on glass fibres and polyester matrix. The ideal interphase for composite materials requires content of silicon and high degree of crosslinking because of mechanical resistance and hardness of SiO₂-like thin films. On the other hand, the interphase should content the carbon and oxygen in its structure. It could be controlled mainly by means of the effective power changing. This problem solution is still opened.

By means of PECVD method under various different deposition conditions, the wide set of thin films was prepared on the glass fibres and for better diagnostic conditions on the silicon wafers, too. The hexamethyldisiloxane (HMDSO), the vinyltriethoxysilane (VTEO) and the tetravinylsilane (TVS) were used as monomers for the depositions. The depositions were carried out mainly in the RF inductively coupled device. The thin films were deposited in the continuous mode, at the beginning. The continuous mode was applied especially for a fibre treatment using HMDSO. In the continuous regime, the plasma polymer films based on VTEO were deposited on the plate substrates. But good-property thin films useful for our purpose were obtained by the deposition in the pulse mode.

To compare the deposition condition effect on the pp film properties, the depositions were provided in the four different devices. In two of them the RF-inductively coupled plasma was used, the other one was based on microwave generated plasma. This device was used only as a model apparatus. The last part of our experiments was aimed at comparative spectroscopic measurements during the depositions of diamond-like coatings (DLC) which were carried out in the capacitively coupled RF discharge in the reactor with parallel stainless steel electrodes, at the Department of Physical Electronics at Masaryk University. These DLC thin films were already well known regarding their mechanical properties. Our aim in this case was the emission spectra comparison, in term of emitted bands and lines appearance at different operating conditions.

The work consider the diagnostics during the deposition processes in the devices that were dominantly designed at Institute of the Material Science at Faculty of Chemistry. The thin films were characterised by means of all available methods. The information about the deposition rate was acquired by ellipsometric measurements. The films were analysed extensively by microscopic and spectroscopic techniques to evaluate surface morphology. Moreover, the elemental composition and chemical structure were studied by RBS, ERDA and FTIR. This work was closely connected to the previous works [49, 66] and to the contemporary work [64].

Presented work was focused on the gas-phase diagnostics and on the comparing of results from gas phase diagnostics with the results from the thin film diagnostics. The plasma diagnostics during the thin film deposition was provided by mass spectrometry, optical emission spectroscopy and in the case of using TVS, the GC-MS analysis were carried out. On occasion, the deposition conditions were only simulated. The simulation was necessary when only the short deposition time was required. The combination of these diagnostic techniques allowed the explication of some questions that were put at the beginning of our experiments.

We have tried to create the kinetic model of the depositions that were done. For

example, the preferential elimination of the groups from the monomer was studied. The optimum deposition conditions such as monomer or/and oxygen flow rate, and the effective power were found during our experiments.

First, when the continuous mode was used, the MS and OES diagnostics were difficult. The spectra were very complicated. It was not possible to distinguish emitting particles from optical emission spectrum. And also it was not easy to identify the peaks from the mass spectrum during the measurements by MS as well as by GC-MS. The information about the created compounds and fragments were often not available in the data library. The FTIR analysis showed that the thin films deposited at high effective powers, mainly in a continuous mode, have not required properties to be a suitable interphase. It was idea to use the other monomers. But the results showed, that the lower electron energy and lower deposition rate should be used for the deposition.

So, the generator working in pulse regime was used. In the pulse mode, the effective power was changed slightly from 0.5 to 25 W and the optimum effective power was searched. Between the effective powers of 1.66 and 5 W (or 10 W for TVS) it exists the special range when the properties of the deposited films and the character of the optical emission spectra are changed sharply.

This "step" observed in the OE spectra could be caused by the other fragmentation degree and fragmentation way of the monomers.

In the literature, it is often mentioned that by OE measurements it is possible to monitor the particles that take part in the deposition process. What is important is the fact that in our case, especially the particles which are not participating in the deposition process (plasma polymer formation) were recorded by OES. The H_2 , H, CO, CH, C_2 are particles with the most intensive spectra. But just these particles probably do not attend the main polymerisation process. These particles are created from the eliminated fragments of monomer and they form thin film on the reactor walls or they flow out from the reactor. Therefore it is possible to estimate the plasma polymerisation process depending on these eliminated particles density in the volume. For example, with high effective power, the density of H, CH or CO increases while the content of these groups or atoms in the substrate surface decreases. Furthermore, it was found that oxygen content in the layer is higher at low effective power even if at high effective power sufficient oxygen flow rate is applied. At lower effective power, plasma polymers based on TVS contain oxygen even if no oxygen is added to TVS during the deposition. The fragments react with oxygen from the leakage and the power is not sufficient to dissociate this created bonds. Therefore, the fragments takes part in growing of the polymer thin film.

The significant part of this work is concentrated on the calculations of plasma parameters from OES and MS measurements. The evolution of electron temperature and electron density was plotted as a function of the effective power and as a function of substrate position in the reactor. It was found that the highest electron density is not in the discharge centre but it is shifted down stream probably due to the local electric field of the surrounding negatively and positively charged particles. Electron temperature is the highest in the discharge centre, as we expected and it is in the range of 1 - 4 eV, depending on the position and on the used monomer. For the TVS the highest temperatures were calculated. For the vibrational and rotational temperature calculation by using the special program, the emission of the CH and nitrogen bands were used. The relative densities of selected most intensive particles were calculated. From the actinometric measurements, the concentration estimations of oxygen, hydrogen and CH in the plasma volume were

obtained. Regarding the particle density evolution with the increasing effective power, the results correspond with those from MS measurements during the deposition and also the FTIR analysis of thin film surface sustain our results from OES.

Furthermore, at the beginning of our experiments it was found that oxygen plays very important role in plasma chemistry. So, many experiments with oxygen addition to the monomer were provided. It is known that Si – O – Si and Si – OH bonds in the films are responsible for their hydrophilic character. It was found that high power leads to decrease of these group presence in the layer.

Relative densities of the selected particles were plotted as a function of the effective power and/or oxygen or monomer flow rate. Moreover, the content of elements in the pp films was plotted as a function of the effective power, too. The results from the gas-phase diagnostics were confronted with the results from thin layer diagnostics. On the basis of these results, probable models of fragmentation and deposition mechanisms were suggested for each monomer. Furthermore, probable plasma polymer structures were drawn out for all monomers and for the different effective powers.

At lower effective power, the monomer is not completely dissociated, thus, the plasma polymer contains larger parts of monomer and the plasma polymer structure has a parts similar to the polymer created by the classical polymerisation. With increasing an effective power (off period of pulse mode is shorter), the content of Si in the layer also increases. Inert gas (argon) was used for the energy transfer to ionisation and fragmentation of the monomer, in some cases. Reactive gases (monomer, oxygen) were used for the chemical modification of the substrate. The deposition of thin films in the oxygen atmosphere leads to the increasing of the Si – O – Si bonds amount in the plasma polymer.

Corresponding measurements by mass spectrometry and optical emission spectroscopy shows that in the case of higher effective powers, the fragmentation degree increases as well as the degree of crosslinking. With increasing Si content in the layer, the mechanically resistant films are created, therefore, the OES were tried to detect of Si atoms in the plasma volume. It would be useful to control the silicon content by observation its concentration in the gas phase. But only SiH band emission was possible to observe at low effective powers and high integration time, so, the use of these species for the process monitoring is strongly limited. Si – H bonds were identified in the pp thin films, too.

Significant part of this work was focused on the experiments with TVS. It was found that TVS is very useful monomer for the pp deposition. High reactivity of the vinyl group is the reason why the deposition rate is higher than in the case of the other monomers. It is possible to control oxygen content in the pp films by deposition condition. The pp properties such as the module of elasticity, hardness and surface energy were changed by means of the effective power changing. Thus, the spectroscopic measurements were provided during the depositions at different effective power that was changed by smaller steps than in the case of the other monomers. This monomer is very promising as a precursor for good interphase for the composites and the research is not finished.

In this work, the spectra identifications were provided, the plasma conditions during the depositions were characterised and the density of the most important particles in the gas phase was determined. The schemes of probable fragmentation were suggested and consequently the plasma polymer structures were estimated. The results are corresponding to each other and they are complementary to the results from the thin film analyses. However, this work is only the beginning of the further studies. The next research will be focused on the most important effective power range during the deposition.

The deposition conditions improvement is an important task for the future work. Simultaneously, the research will be carried out also in the fields of the deposition, absorption and emission spectroscopy the monomer fragmentation study and also of the consequent polymerisation.

References

- [1] Aumaille K., Granier A., Schmidt M., Grolleau B., Vallee C.: Study of oxygen/tetraethoxysilane plasmas in a helicon reactor using optical emission spectroscopy and mass spectrometry, *Plasma Sources Sci. Technol.*, **14** 331 (2000)
- [2] Bálková R., Příklad R., Grycová A., Vaněk J., Čech V.: Plasma Polymerized Film of Vinyltriethoxysilane as Adhesion Interlayer between Glass Fiber and Polyester Resin, *Czech. J. Phys.*, **54**, 578 (2002)
- [3] Bernshtam V.A., Ralchenko Y., Maron Y.: Empirical formula for cross section of direct electron-impact ionization of ions, *J. Phys. B: At. Mol. Opt. Phys.*, **33**, 5025 (2000)
- [4] Brandejs K.: Diagnostics of Plasma Used for Plasmachemical Thin Film Deposition, Diploma thesis, Faculty of Chemistry, Brno University of Technology, Brno (2004)
- [5] Brinkman A., Raiche G.A., Brown M.S., Jeffries J.B.: Optical diagnostics for temperature measurement on a DC arcjet reactor used for diamond deposition, *Appl. Phys.* **64**, 689 (1997)
- [6] Čech V., Studýnka J., Conte N., Peřina V.: Physico-chemical properties of plasma-polymerized tetravinylsilane, *Surf. Coat. Technol.*, in print, 2005
- [7] Coltrin E., Ho P., Moffat H., Buss R.: Chemical kinetics in chemical vapor deposition: growth of silicon dioxide from tetraethoxysilane, *Thin Solid Films*, 251 (2000)
- [8] Cunge G., Kogelschatz M., Joubert O., Sadeghi N.: Plasma-wall interaction during silicon etching processes in high-density plasmas, *Plasma Source Sci. Technol.*, **14**, 42 (2005)
- [9] Cunge G., Kogelschatz M., Sadeghi N.: Influence of reactor walls on plasma chemistry and silicon etch product densities during silicon etching in halogen-based plasmas, *Plasma Sources Sci. Technol.*, **13**, 524 (2004)
- [10] Dvořák P.: Komplexní diagnostika reaktivního plazmatu doutnavého výboje, Dissertation thesis, Department of Physical Electronics, Masaryk University, Brno (2005)
- [11] Engel, A.H.: Ionised Gasses, Oxford University Press, 2nd edit., Oxford (1994)
- [12] Eufinger S., van Oij W.J., Connors K.D.: Surface and interface analysis *Thin Solid Films* **24**, 841 (1996)
- [13] Feitknecht L., Meier J., Torres P., Zürcher J., Shah A.: Plasma deposition of thin film silicon: Kinetic monitored by optical emission spectroscopy, *Solar Energy Mater. Solar Cells*, **74**, 539 (2002)
- [14] Gherman T., Eslami E., Romanini D., Kassi S., Vial J.C., Sadeghi N.: High sensitivity broad-band mode-locked cavity-enhanced absorption spectroscopy: measurement of $\text{Ar}^*(P - 3(2))$ and N_2^+ density, *J. Phys. Appl.* **37**, 2408 (2004)
- [15] Gilmore, F.R., Laher R.R., Espy P.J.: *J. Phys. Chem. Ref. Data*, **21**, 1005 (1992)

- [16] Good J.R.: Contact angle, wettability and adhesion, *Adv. in Chem. Series*, **43**, 136 (1993)
- [17] Goujon M., Henrion G., Belmonte T., Choquet P., Michel H.: Influence of the process parameters on both the plasma and silicon oxide film properties in an O₂/HMDSO PACVD process, *Thin Solid Film*, **475**, 23 (2002)
- [18] Griem H.R.: Spectral line broadening by plasmas, Academic Press, 4th edit., New York (1974)
- [19] Griem, H.R., Kolb A.C., Shen K.Y.: *Phys. Rev.*, **21**, 116 (1996)
- [20] Günzler, H., Gremlich H.U.: IR Spectroscopy, VCH Publishing, 2nd edit., Weinheim (2002)
- [21] Hamers, E.A.G.: The Effect of Ions on the Growth of Amorphous Microcrystalline Silicon, *Acta Phys. Slov.*, **50**, 123 (2000)
- [22] Hatakeyama, S., Saga, T., Hiromo, H.: *Surf. Eng.*, **4**, 546 (1988)
- [23] Herzberg, G.: Molecular Spectra and Molecular Structure: Spectra of the Diatomic Molecules, D. Van Nostrand Co., New York, 1.edit. (1950)
- [24] Hollahan, J.: Techniques and Application of Plasma Chemistry, John Wiley, Richmond (1996)
- [25] Huber, K. P., Herzberg G.: Constants of Diatomic Molecules, Van Nostrand Reinhold, 4th edit., New York (1979)
- [26] <http://www.physics.nist.gov>
- [27] <http://www.lpgp.u-psud.fr/gaphyor/gaphyor.html>
- [28] Irene, E.A.: Models for the oxidation of silicon, *CRC Critic. Rev. in Solid St. and Mat. Sci.*, edit. J.E. Green, **14**, 175 (1988)
- [29] Jobin Yvon: Triax user manual, Horiba group, Longjumeau (1999)
- [30] Kawahara, T., Yuuki A. Matsui Y.: Reaction Mechanism of Chemical Vapor Deposition Using TEOS and Ozone at Atmospheric Pressure, *Jpn. J. Appl. Phys.*, **31**, 552 (1992)
- [31] Kessels, W.M.M. *et al.*: Hydrogenated Amorphous Silicon Deposited by an Expanding ArH₂SiH₄ plasma, *J. Appl. Phys.*, **89**, 534 (2001)
- [32] Keudell A., Möler W., Hytry R.: Deposition of dense hydrocarbon films from a nonbiased microwave plasma, *Appl. Phys. Lett.*, **62**, 288 (1993)
- [33] Kousal J.: Atmosférické výboje duté katody, Diploma thesis, Department of Physical Electronics, Masaryk University, Brno (2002)
- [34] Kovacs, I.: Rotational Structure in the Spectra of diatomic Molecules, Hilger, Budapest (1969)

- [35] Lang N., Lavrov B.P., Röpcke J.: Spectroscopic determination of the dissociation degree in pulsed plasmas containing hydrogen, *Proc. FLTPD IV* (2001)
- [36] Lavrov B., Melnikov A., Käning M., Röpcke J.: UV continuum emission and diagnostics of hydrogen-containing nonequilibrium plasmas, *Phys. rev.*, **59**, 3527 (1999)
- [37] Lavrov B.P., Pipa A.: Account of the fine structure of hydrogen atom levels in the effective emission cross sections of balmer lines excited by electron impact in gases and plasma, *Opt. and Spectr.*, **92**, 709 (2002)
- [38] Lawrence G.M.: Dissociative excitation of some oxygen-containing molecules: Lifetime and electron impact cross sections, *J. Chem. Phys.*, **47**, 12 (1970)
- [39] Lee H.J., Oh K.S., Choi C.K.: Surface and Coating technology, **13** 171 (2003)
- [40] Lieberman M.A, Lichtenberg A.J.: Principles of plasma discharges and materials processing, John Wiley and sons, 2nd edit., New York (1994)
- [41] Lombardi G., Stancu G., Hempel F., Gicquel A.: Quantitative detection of methyl radicals in non-equilibrium plasmas, *Plasma Sources Sci. Technol.*, **13**, 27 (2004)
- [42] Lunge J., Juchmann W., Jeffries J.B.: Spatial density distribution of C₂, C₃ and CH radicals by laser-induced fluorescence in a diamond depositing DC-arcjet, *J. Appl. Phys.* **82**, 2072 (1997)
- [43] Luque J., Juchmann W., Brinkman E.A., Jeffries J.B.: Excited state density distributions of H, C, C₂ and CH by spatially resolved optical emission, California (1997)
- [44] Macko P., Sadeghi N.: Determination of the non-relaxing (reflection) probability of metastable Ar(P-3(2)) atoms on a Pyrex surface *Plasma Source Sci. Technol.*, **13**, 303 (2004)
- [45] Melius, C.F.: Theoretical Study of the Thermochemistry of Molecules in the Si-O-H-C System, *J. Phys. Chem.*, **99**, 205 (1995)
- [46] Navrátil Z., Buršíková V., Šťáhel P., Šíra M., Zvěřina P.: On the analysis of surface free energy of DLC Coatings Deposited in low pressure RF discharge, *Czech. J. Phys.*, **54**, 328 (2004)
- [47] Pearse R. W. B., Gaydon A. G.: The Identification of Molecular Spectra, John Wiley, 4th edit., London (1976)
- [48] Příkryl R.: Plazmové polymery na bázi Si, Thesis report, Brno (2001)
- [49] Příkryl R.: Depozice polymerních vrstev v nízkoteplotním plazmatu, Dissertation thesis, Brno (2003)
- [50] Příkryl R., Salyk O., Vaněk J., Studýnka J., Čech V.: Surface processing of continuously moving fiber bundle using new helicalcoupled plasma system, *Czech. J. Phys.*, **52**, D816 (2002)
- [51] Raizer, Y.P.: Gas Discharge Physics, Springer Verlag, 4.edit., New York (1991)

- [52] Ricard, A.: Reactive plasmas, Paris, SFV, 4. edit. (1996)
- [53] Roth, J. R.: Industrial Plasma Engineering, The Institute of Physics, 1st edit., London (2001)
- [54] Rossangel S.M., Cuomo J., Westwood W.D: Handbook of plasma processing technology: Fundamentals, etching, deposition and surface interactions, New York (1990)
- [55] Sa P.A., Guerra V., Loureiro J., Sadeghi N.: Self-consistent kinetic model of the short-lived afterglow in flowing nitrogen *J. Phys. D, Appl. Phys*, **37**, 221 (2004)
- [56] Sanogo, O., Zachariah M.R.: Kinetic Studies of the Refraction of Tetraethoxysilane with Oxygen Atoms, *Elektrochem. Soc.*, **8**, 144 (1997)
- [57] Shul, R.J., Pearton, S.J.: Handbook of Advanced Plasma Processing Techniques, Springer Verlag, Heidelberg (2000)
- [58] Šimek, M., Dilecce G., DeBenedictis S.: *Plasma Chem. Plasma Proces.* **15**, 427 (1997)
- [59] Šmíd R., Zajíčková L., Janča J.: Spatially resolved measurements in rf capacitive discharges in argon and nitrogen, *Czech. J. Phys.*, **54**, 592 (2004)
- [60] Sneep M., Ubachs W.: Direct measurements of the Rayleigh scattering cross section in various gases, *Elsevier*, **34**, 741 (2004)
- [61] Šormová H.: Numerical Simulations of Diatomic Molecular Optical Spectra, Dissertation Thesis, Faculty of Chemistry, Brno University of Technology, Brno (2005)
- [62] Sorokin M.: Dust Particle Formation in Silane Plasmas, Disertation thesis, Technische Universiteit Eindhoven (2005)
- [63] Špatenka P. Petig K., Wiesemenn K., Suhr H.: Langmuir probe measurements PACVD in the system argon/hydrogen/ cyclopentadienyl/dimethyl hafnium, *Plasma Chem. Plasma Process*, **15**, 371 (1995)
- [64] Studýnka J.: Vliv depozičních podmínek na složení, strukturu a vlastnosti plazmových polymerů připravených z organosilanů, Diploma thesis, Masaryk University Brno (2004)
- [65] Vallee, C., Aumaille K., Goullet A., Granier A., Turban G.: In Situ Control of the Growth of Thin Films in Oxygen/Organosilicon Plasmas by Optical Emission Spectroscopy and Elipsometry, *J. Phys. Chem*, **7**, 99 (1995)
- [66] Vaněk J.: Příprava tenkých vrstev v nízkoteplotním plazmatu, Dissertation thesis, Brno University of Technology, Brno (2005)
- [67] Vaněk J., Grycová A., Přikryl R., Studýnka J.: Thin films of organosilicon monomers prepared by plasma polymerization and wet-chemical process, *Chem. Pap. Symp.*, **96**, S225 (2002)
- [68] Wiere, W. L., Smith, M. W., Glenon, B. M.: Atomic Transition Probabilities, NSRDS-NBS4, 2nd edit. (1996)

- [69] Welzel T., Dani I., Richter F.: Determination of radical densities by optical emission spectroscopy during the ECR plasma deposition of Si-C-N:H films using TMS as a precursor, *Plasma Sources Sci. Technol.*, **11**, 351 (2002)
- [70] Wr obel, A.M.: Mechanism of Initiation Step in Remote Oxygen PCVD of Silica Films from Tetraethoxysilane, *J. Phys. Chem*, **99**, 337 (2001)
- [71] Zajíčková L., Buršíková V., Franta D.: The influence of substrate emissivity on plasma enhanced CVD of diamond-like carbon films, *Czech. J. Phys.*, **49**, 1213, (1999)
- [72] Зайдель, А.Н., Прокофьев, В.К., Райский, Ц.М., Шрейдер, Е.Я.: Таблицы спектральных линий
- [73] Zellner M.: Comparison of Stark broadening and Doppler broadening of spectral lines in dense hot plasmas, Millersville University (1992)

Appendices